STUDIA

UNIVERSITATIS BABEŞ-BOLYAI

PHYSICA

2

1987

CLUJ-NAPOCA

REDACTOR-ŞEF: **Prof. A. NEGUCIOIU**

REDACTORI-ŞEFI ADJUNCŢI: **Prof. A. PÁL, conf. N. EDROIU, conf. L. GHERGARI**

COMITETUL DE REDACŢIE FIZICĂ: **Prof. Z. GÁBOS, prof. V. MERCEA (membru corespondent al Academiei), prof. AL. NICULA, prof. I. POP (redactor-responsabil), conf. M. VASIU, lect. O. COZAR (secretar de redacţie)**

TEHNOREDACTOR: **C. Tomoaia-COTIŞEL**

ANUL XXXII 1987

STUDIA

UNIVERSITATIS BABEŞ-BOLYAI

PHYSICA

2

Redacţia: 3400 CLUJ-NAPOCA, str M. Kogălniceanu, 1 Telefon ● 1 61 01

SUMAR — CONTENTS

AL. NICULA, S. AŞTILEAN, S. NICULA, Theory of One-Dimensional Magnetic Resonance Imaging 3

O. COZAR, I. MILEA, I ARDELEAN, T FIAT, P SIMONFI, EPR and Diffuse Reflectance Studies on Coloured Quartz Samples Impurified with Copper Oxide 10

L. POP, M. CRISTEA, O. POP, I. POP, Magnetic Behaviour of the Thernary Oxidic Semiconducting α-(Fe_2O_3—Al_2O_3—Cr_2O_3) System 12

Z. GÁBOS, G FULÖP, On the Principle of Generalized Equivalence 20

V. CRIŞAN, C. HĂGAN, I. POP, Structure Study of the Intermetallic Compounds $Tb_2Ni_{17-x}Al_x$ by X-Rays 24

I. GH POP, I. POP, Effect of Crystalline Field on the Magnetic Properties of Diamagnetic Ionic Crystals 30

AL. NICULA, S AŞTILEAN, M TODICĂ, S NICULA, Obtainment of Magnetic Field Gradients and Analysis of Spatial Resolution in EPR Imaging 35

I ARDELEAN, GH ILONCA, O COZAR, I ARDELEAN, Magnetic Susceptibility Studies of $x\overline{Cr_2O_3} \cdot (1-x)[2P_2O_5 \cdot Na_2O]$ Glasses 41

L. POP, I POP, Magnetic Behaviour of the α-Fe_2O_3 Oxide 44

C. COSMA, K. KOVÁCS, T FIAT, F COSMA, L MÂNZAT, In Situ Experiments on Eggs Radioactivity between 1-st to 30-th of May 1986 47

O. CRISTEA, Quantum Mechanic Effects in High-Speed Rotating Frames 52

H. SZŐCS, On the Possibility of Determining a Magnetical Field From its Hypothetical Sources 58

O. POP, The Design of a Syntactical Analyser for an 8-Bit Microcomputer Using the k-Code Algorithm 63

D. CIURCHEA, An X-Ray Diffraction Line Profile Analysis Computer Code Using Fast Fourier Transform and Tikhonov Regularisation 68

D. DĂDÂRLAT, R TURCU, M CHIRTOC, R M CÂNDEA, C FULEA, On the Photoconductivity of PbSe Films Obtained by Chemical "Anorganic" Deposition . 74

V. CRISTEA, E TRIF, N IUGA, D STRUGARU, Temperature Dependence of the Electrical Resistance of Y-Type Synthetic Zeolites 78

V. TOŞA, M GULÁCSI, ZS GULÁCSI, Rotational Splitting of CH_4 Analysed With Irreducible Invariant Tensor Operator Combintions 82

M. GULÁCSI, ZS. GULÁCSI, V. TOŞA, Anharmonic Force Field Constants for UF_6 Molecule 85
ZS. GULÁCSI, V. TOŞA, M. GULÁCSI, Tabulated T^8 Eigenvalues for Cubic Symmetry 88
C. CUNA, Electric Prism-Homogeneous Magnet Double Focusing Mass Spectrometer Experimental Set-Up and Preliminary Tests 91
I. COSMA, Magnetic Moment in Ni-Rich Ni-Cu-Zn Alloys 93
S. SIMON, I. BARBUR, I ARDELEAN, EPR on Some Superconducting Oxide Ceramics 96

Recenzii — Book Reviews

D. Chowdhury, **Spin Glasses and Other Frustrated Systems** (M. CRIŞAN) . . . 100
P. C. W. Davies, **The Forces of the Nature** (L. MÂNZAT) 100
W. Ebeling, Y. L. Klimontovich, **Selforganization and Turbulence in Liquids** (S. CORDEANU) 101
W. Schultz—Piszachich, **Nonlinear Models of Flow, Diffusion and Turbulence** (S. CODREANU) 101
Jean — Louis Basdevant, **Mécanique quantique** (S. CODREANU) 101
Martin Hartley Jones, **A Practical Introductinn to Electronic Circuits** (E. TĂTARU 102
H. E. Duckworth, R. C. Barber and, V. S. Venkatasubramanian, **Mass Spectroscopy** V. ZNAMIROVSCHI) 102

STUDIA UNIV BABEŞ—BOLYAI, PHYSICA, XXXII, 2, 1987

THEORY OF ONE-DIMENSIONAL MAGNETIC RESONANCE IMAGING

AL. NICULA*, S. AŞTILEAN* and S. NICULA*

Received September 21, 1987

ABSTRACT. — A method for obtaining one-dimensional images of the spin density distribution using magnetic resonance is described. The observed image can be written as a convolution of the sample magnetization with a resolution function.

Introduction. In recent years, Lauterbur [1], Mansfield [2], and others independently demonstrated nuclear magnetic resonance as a means of imaging In NMR imaging, there exist two principal methods of image formation namely the projection reconstruction method [1, 3] and the Fourier transformation method [4, 5, 6] In both methods the basic principle of measurment is to project a spin distribution in a direction in real space Since the published paper on EPR imaging (EPRI), several research groups have reported their efforts to obtain spin mapping, as well as spectral information to a particular spatial site [7, 8, 9] Magnetic resonance imaging (MRI) has become an important technique in biological and medical studies [10, 11].

The most methods of MR imaging require the preselection of a desired spatial region. By the application of magnetic field gradients and suitably shaped r. f. pulses, it is possible to restrict interaction to a selected portion of the total spin system The method now usually adopted is the selective excitation.

The present paper relates the theory for producing a one-dimensional image of relative spin densities insides an object by subjecting the sample to an initial magnetic field gradient together with a 90° selective r. f. pulse. The motion of the spin magnetization is described by solutions of the Bloch equations in matrix form [12]

Thus we obtain the components of the normalized elemental spin, which constitutes the initial conditions for FID. The image of the spin density can be extracted from FID. By introducing a resolution function, the FT of the FID is seen to be the convolution of real spin density with the resolution function. Since this procedure is central to the practical generation of NMR images nowadays, we should examine the process in more detail.

1. *Selective irradiation* We assume that an initial magnetic field gradient G_x together with a static main field is applied to a one-dimensional system containing a distribution of magnetic moments.

* *University of Cluj-Napoca, Faculty of Mathematics and Physics, 3400 Cluj-Napoca, Romania*

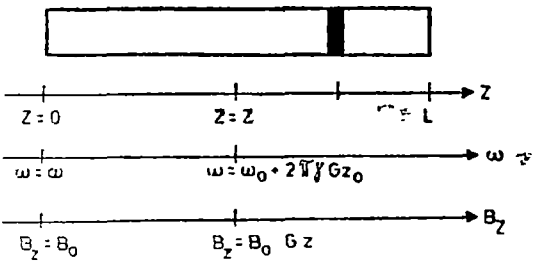

Fig. 1 A sample of lenght L is placed in a magnetic field $B_z = B_0 + Gz$. The angular frequency $\omega_0 = \gamma B_0$ establishes the reference resonant frame so that the element at $z = z_0$ is at angular-frequency $2\pi\gamma G z_0$ relative to $z = 0$.

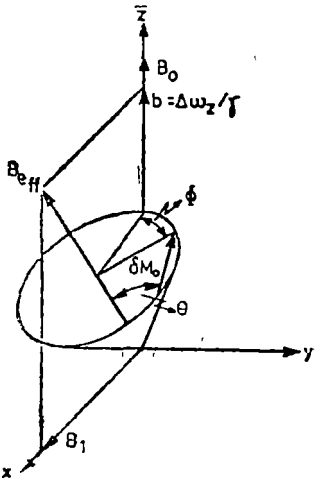

Fig. 2. Precession of elemental spin magnetization $\vec{\delta M}$ in the tilted rotating reference frame

In the initial equilibrium state a magnetization/unit lengh is $m_0(z)$ and the total equilibrium spin magnetization is therefore·

$$M_0 = \int_0^L m_0(z)\, dz \tag{1}$$

We shall apply a *rf* pulse If the sample is of lenght L and if the spin system are resonant at the sample position (z_0) as shown by Fig. 1, in this case $\omega_0 = \gamma(B_0 + G_z \; z_0)$ and in a reference frame rotating with angular frequency ω_0 the *rf* pulse is stationary and has a constant amplitude iB_1 Spins which lie in the plane z_0 are therefore at exact resonance and interact strongly with the *rf* pulse Spins of either side of this plane will be progressively less affected the further thay lie from the isochromatic plane The presice behaviour of the spin system is best calculated by considering spins displaced $\Delta z = z - z_0$ from z_0 which are then off resonance with respect to the pulse by:

$$\Delta\omega = \omega - \omega_0 = \gamma\, \Delta z G_z$$

where b is the component of the magnetic field directed after the axe Oz in reference frame rotating The motion of the spin magnetization in the plane sheet of thickness dz is shown in Fig 2 and is describet by solutions of the Bloch equations in matrix form·

$$\delta\widetilde{M}(t) = e^{\widetilde{A}t} e^{\widetilde{T}t} \delta\widetilde{M}(0) + \delta M_0 (1 - e^{-t/T_1}) \tag{2}$$

in which·

$$\widetilde{A} = \begin{bmatrix} 0 & \Delta\omega_z & 0 \\ -\Delta\omega_z & 0 & \omega_1 \\ 0 & -\omega_1 & 0 \end{bmatrix} \text{ and } e^{\widetilde{T}t} = \begin{bmatrix} e^{-t/T_1} & 0 & 0 \\ 0 & e^{-t/T_1} & 0 \\ 0 & 0 & e^{-t/T_1} \end{bmatrix}$$

where $\omega_1 = \gamma B_1$ and where T_1 and T_2 are the spin-latice and spin-spin relaxations times, respectively
In this analysis we shall assume that *rf* pulse is always applied for time less than T_1 so that $e^{-t/T_1} = 1$

In our case the precession of elemental spin magnetization $\delta\vec{M}_0$ is in a tilted rotating reference frame, follows a cone of precession about an efective field $\vec{B}_{eff} = B_1\vec{i} + b\vec{k}$ This field. makes a non-Euler angle $\theta = \tan^{-1}(B_1/b)$ with the z axis Thus referred to the tilted frame (where the tilted axis $\vec{B}_{eff}$ is itself a positiv non-Euler rotation about y) we see that:

$\tilde{A}' = R_y^{-1}(\theta)\,\tilde{A}R_y(\theta)$ A non-Euler rotation through angle θ about the y axis is represented by

$$R_y(\theta) = \begin{bmatrix} \cos\theta & 0 & \sin\theta \\ 0 & 1 & 0 \\ -\sin\theta & 0 & \cos\theta \end{bmatrix},$$

Straightforward multiplication of the matrices gives

$$\tilde{A}' = \begin{bmatrix} 0 & \omega_{ef} & 0 \\ -\omega_{ef} & 0 & 0 \\ 0 & 0 & 0 \end{bmatrix} \text{ where } \omega_{\text{eff}}^2 = \omega_1^2 + \Delta\omega_z^2$$

We notice that under this case is easy to prove that the propagator matrix $e^{\tilde{A}'t} = Rl^{-1}(\Phi)$ (the rotation matrix, where l is the axis along which $\vec{B}_{\text{eff}}$ is applied and $\Phi = \omega_{ef}t$ is the precessional Euler angle Φ of the spins).
Therefore, if we now include the relaxation matrix $e^{\tilde{T}'t} = E'(t)$ in the tilted frame, with the plausible assuption that T_2' in this frame is offset independent, we obtain for the propagator matrix in the nontilted frame·

$$e^{\tilde{A}t}e^{\tilde{T}t} = R_y(\theta)\,[R_1^{-1}(\Phi)\,E'(t)]\,R_y^{-1}(\theta) = \tag{3}$$

$$= \begin{bmatrix} \cos\theta & 0 & \sin\theta \\ 0 & 1 & 0 \\ -\sin\theta & 0 & \cos\theta \end{bmatrix} \cdot \begin{bmatrix} \cos\Phi & \sin\Phi & 0 \\ -\sin\Phi & \cos\Phi & 0 \\ 0 & 0 & 1 \end{bmatrix} \cdot \begin{bmatrix} e^{-t/T_2} & 0 & 0 \\ 0 & e^{-t/T_2} & 0 \\ 0 & 0 & 0 \end{bmatrix} \cdot$$

$$\cdot \begin{bmatrix} \cos\theta & 0 & -\sin\theta \\ 0 & 1 & 0 \\ \sin\theta & 0 & \cos\theta \end{bmatrix} =$$

$$= \begin{bmatrix} E_2'\cos^2\theta\cos\Phi + \sin^2\theta & \cos\theta\sin\Phi E_2' & \sin\theta\cos\theta(1 - E_2'\cos\Phi) \\ -E_2'\sin\Phi\cos\theta & \cos\Phi & \sin\theta\sin\Phi E_2' \\ \cos\theta\sin\theta(1 - E_2'\cos\Phi) & -\sin\theta\sin\Phi E_2' & \cos^2\theta + \sin^2\theta\cos\Phi E_2' \end{bmatrix}$$

when $E_2' = e^{-t/T_2'} = 1$, this rotation matrix thus constitues first a negative otation about y through θ to bring the l axis of B_{eff} along the z axis, an

Euler rotation through-Φ about z and finally a positive rotation about y to take z back to l.
Taking

$$\delta\widetilde{M}(0) = \begin{bmatrix} 0 \\ 0 \\ m_0 dz \end{bmatrix} \text{ and } \delta\widetilde{M}(t) = \begin{bmatrix} \delta M_x(t) \\ \delta M_y(t) \\ \delta M_z(t) \end{bmatrix}$$

we obtain the following components of the elemental spin

$$\delta M_x(t) = m_x dz = \sin\theta\cos\theta\,(1 - \cos\Phi)\,m_0 dz =$$

$$= \frac{B_1 b}{B_1^2 + b_2}\,(1 - \cos\gamma(B_1^2 + b^2)^{1/2}t)\,m_0 dz \tag{4 a}$$

$$\delta M_y(t) = m_y dz = \sin\theta\sin\Phi\, m_0 dz = \frac{B_1}{\sqrt{B_1^2 + b^2}} \cdot \sin(\gamma(B_1^2 + b^2)^{1/2}t)\, m_0 dz \tag{4 b}$$

$$\delta M_z(t) = m_z dz = \cos^2\theta + \sin^2\theta\cos\Phi\, m_0 dz =$$

$$= \frac{b^2}{B_1^2 + b^2} + \frac{B_1^2}{B_1^2 + b^2}\cos\gamma(B_1^2 + b^2)^{1/2}\, t m_0 dz \tag{4 c}$$

A 90° selective pulse with angular frequency $\omega_0 = \gamma(B_0 + G_z \cdot z_0)$ corresponds to the condition $\omega_1 t_w = \gamma B_1 t_w = \pi/2$ Now, the spin components m_x, m_y and m_z may be plotted as a function of offset b following a 90° selective pulse applied along x and yield to nonequilibrium spin components existing at time t_w
The normalized components m_x/m_0, m_y/m_0 and m_z/m_0 are displayed graphically on colour display of the personal computer HC—85 and in this paper there are in Fig. 3 *a, b, c*
These show a depletion of magnetization m_z/m_0 and a maximum in m_y/m_0 as expected on resonance when $b = 0$.
The actual values of the total transverse magnetization components $M_x(t_w)$ and $M_y(t_w)$ immediately following the selective pulse at t_w may be obtained by integrating

$$M_x(t_w) = \int \delta M_x dz = \frac{m_0 B_1}{G_z} \int_{-\infty}^{+\infty} \frac{b(1 - \cos\gamma t_w (B_1^2 + b^2)^{1/2})}{B_1^2 + b^2}\, db = 0 \tag{5}$$

for all t_w because m_x/m_0 is an antisymmetric distribution

$$M_y(t_w) = \int \delta M_y dz = \frac{m_0}{G_z} \int_{-\infty}^{+\infty} \frac{B_1}{(B_1^2 + b^2)^{1/2}} \sin\gamma t_w (B_1^2 + b^2)^{1/2} db \tag{6}$$

which may be summed analytically to give

$$M_y(t_w) = \frac{\pi B_1 m_0}{G_z} \mathfrak{J}_0(\gamma B_1 t_w) \tag{7}$$

where $\mathfrak{J}_0(\gamma B_1 t_w)$ is the zero-order Bessel function
Thus a 90° selective pulse produces quite a large M component.

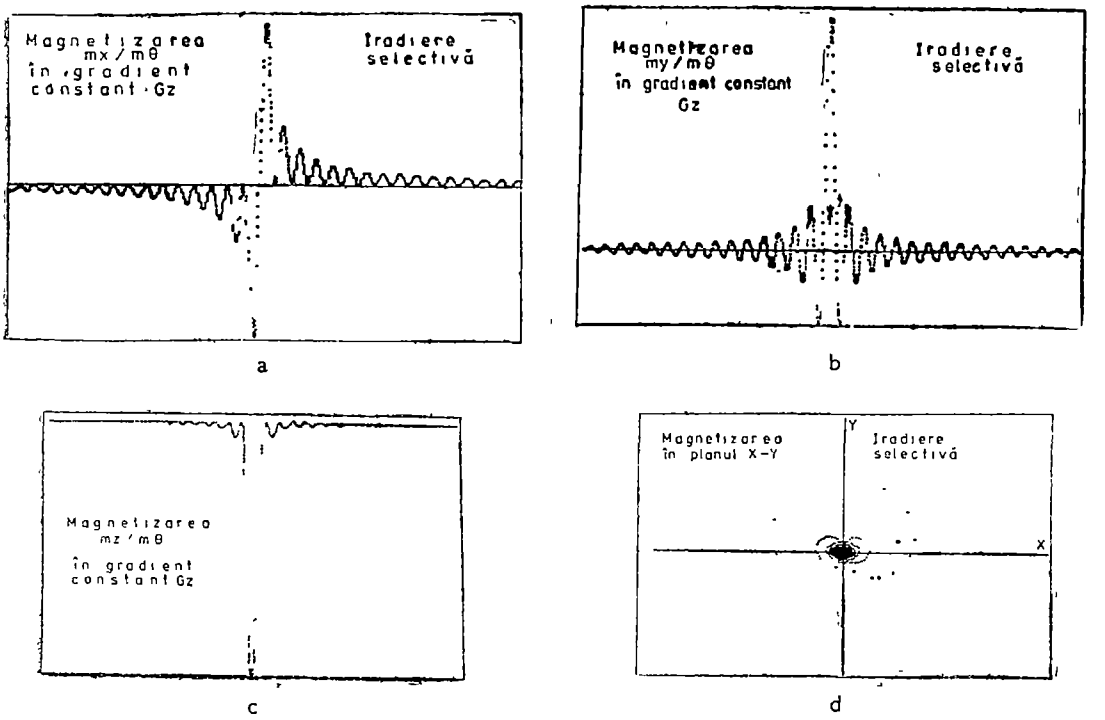

Fig. 3. *a, b, c, d*: Computed magnetization cmoponents $m_x(t_w)$, $m_y(t_w)$ and $m_z(t_w)$ using rectangular 90° selection pusle a one-dimensional spin distribution.

The theory presented shows that following a single *rf* pulse, of lenght t_w, applied to a homogeneous spin distribution in a linear magnetic field, and m_x and m_y spin distribution exists which constitutes *the initial conditions* for free precession (FID) in the field gradient.
The FID response is a point-start in all MR imaging methods.

2. *Mathematical analysis of the one-dimensional image.* The evolution of the x, y magnetization in a constant gradient field following a 90° *rf* pulse is given by Bloch equation. Thus, if the sample is of lenght L and if the spin are resonant at the sample center ($z = z_0$) as shown in Fig. 1, the magnetization in the laboratory frame at $z \neq z_0$ following a $\pi/2$ pulse will be given by complex expresion:

$$m(z, t) = m_0(z)\, exp(-t/T_2(z)\, exp(-2\pi\, i\gamma G_z z t) \quad exp(-i\omega_0 t) \tag{8}$$

where $m_0(z)$ constitutes the initial conditions for free precesion after a $\pi/2$ pulse and whose contribution to the time dependent magnetization $m(z, t)$ is modified explicitly by the spin-spin relaxation time $T_2(z)$ and implicity by the spin-latice relaxation time $T_1(z)$. Here $m(z, t) = m_x(z, t) + im_y(z, t)$ is the complex time dependent magnetization.

Since the sample is of lenght L, the total signal $S(t)$ or the FID obtained after an excitation pulse will be the sum of the contributions from each spatial element. The total magnetic signal in the rotating frame ($\omega_0 = 0$) is given by:

$$S(t) = \int_0^L m_0(z) e^{-t/T_2(z)} \quad e^{-i\alpha z} \cdot dz \tag{9}$$

where we have introduce $\alpha = 2\pi\gamma G_z$ for convenience. *The image* of $m_0(z) = \rho(z) m_0$ (the spin density) can be extracted from FID or $S(t)$ by considering only the Fourier components that do not rotate in time
The observed image $S(z)$ is the Fourier transform of Eq 9 given by

$$S(z) = Re \frac{\alpha}{\pi} \int_0^T S(t) e^{i\alpha z t} dt = \frac{\alpha}{\pi} Re \int_0^T e^{i\alpha z t} dt \int_0^L m_0(z')\, e^{-t/T_2} e^{-i\alpha z' t} dz' =$$

$$= \frac{\alpha}{\pi} \int_0^L m_0(z') dz' \quad Re \int_0^T e^{-t/T_2(z')} e^{i\alpha(z-z')t} dt \tag{10}$$

Eq. 10 is similar to a Fourier tranform pair, but differs in several respects: first, exp $(-t/T_2(z))$ is included in the integrand and this line-broadening term produces a Lorentz lineshape rather than a delta function A second differences is the finite limits $[0, L]$ on the spatial integral imposed by finite lenght of the sample. Finally, in many cases, we will be interested in a finite sampling time intervals from $t=0$ to $t = T$ where $T \ll T_2(z)$

By introducing a new variable $u = z' - z$ and defining a resolution function $f(u)$ such that:

$$f(u) = \frac{\alpha}{\pi} Re \int_0^T e^{-t/T_2(z+u)} e^{-i\alpha u} dt \tag{11}$$

we can rewrite Eq. 10 into the form

$$S(z) = \int_{-z}^{L-z} m_0(z + u) f(u)\, du \tag{12}$$

where the observed *image* $S(z)$ is then seen to be the convolution of the sample magnetization or of the spin density with the resolution function In general $f(u)$ will be a peaked function whose width depends on T and T_2, for $T \to \infty$. Eq. 11 is the FT an exponential, which is a Lorentzian

Conclusions. In this paper we contributed to a theoretical study of MRI using, as aditional magnetic field, a linear gradient field for a one-dimensional spin distribution. This study can be generalised for two and there dimensional distribution [4, 10]. The same procedure may be applied for obtaining the spin imaging in a dipolar spatial field Other experimental and theoretical results of ours are already published [13, 14] or will be published

REFERENCES

1. P C. Lauterbur, *Nature (London)*, **242,** 190 (1973)
2. P. Mansfield, P K. Grannell, *Phys Rev.*, **B12,** 3618 (1975)
3. A E Stillman, D N. Levin, B D Yang, P C Lauterbur, *J Magh Reson*, **69,** 168 (1986)
4. A Kumar, D Welti, R. R Ernst, *J Magn Reson*, **18,** 69 (1975).
5. P J McDonald, I I Attard, D G Taylor, *J. Magn Reson*, **72,** 224 (1987)
6. T C Farrar, E D Becker, "Pulse and Fourier Transform NMR", Acad Press, New York and London, 1971
7. M M Maltempo, *J. Magn Reson*, **69,** 156 (1986)
8. L J Beliner, *Magn Resonance in Medicine*, **4** 380 (1987)
9. Al Nicula, S. Nicula, L. Giurgiu, I Ursu, *Studia*, **XXXI** (1), 1986
10. P Manfsfield; P G Morris; "Advances in Magnetic Resonance", *Supplement* 2, "NMR Imaging in Biomedicine", Academic Press, New York — London (1982)
11. E R Andrew, *Conferința internațională Ampère*, București, (1985)
12. Al Nicula, S Nicula, *Studia*, **XXXI** (2), 1986
13. Al Nicula, S Aștilean, S. Nicula, „Progrese în fizică", *Sesiunea anuală ICEFIZ* București, *R*1987.
14. Al Nicula, S Aștilean *Studia*, **XXXII** (1), 1987

STUDIA UNIV BABEŞ—BOLYAI, PHYSICA, XXXII, 2, 1987

EPR AND DIFFUSE REFLECTANCE STUDIES ON COLOURED QUARTZ SAMPLES IMPURIFIED WITH COPPER OXIDE

O. COZAR*, I. MILEA, I. ARDELEAN*, T. FIAT* and P. SIMONFI*****

Received September 18, 1987

ABSTRACT. — We investigated the distribution mode of the metallic ions in the coloured quartz samples impurified with copper oxide using EPR and diffuse reflectance measurements. Both EPR and diffuse reflectance data suggest that the copper atoms are present in majority as metallic microparticle sizes.

The results obtained by EPR and diffuse reflectance measurements on some coloured quartz samples impurified with cooper oxide are reported. We investigate the distribution mode of metallic ions in the quartz matrix, the reddish colour of this being attributed to the presence in majority of cooper as metallic microparticle sizes. Because of the high melting temperature (~2700°C) the Cu^{2+} ions are reduced succesively to Cu^{+} and Cu^{0}, which are associated as metallic microparticle sizes. Both Cu^{+} and Cu^{0} do not give EPR signals and $d-d$ electronic absorption bands characteristic for Cu^{2+} ions in a distorted-octahedral coordination [1]. The number of Cu^{2+} ions is very small in the studied samples This fact is suggested by both EPR and diffuse reflectance measurements

The diffuse reflectance spectra were obtained with a VSU—2P spectrophotometer in the visible range using the 0/r dispozitive which allowes a normal lighting and a collection of the reflected light by the sample between 35°—45°. The typical diffuse reflectance spectrum is shown in Fig. 1, which contains the reflection coefficient versus wavelenght Five weak absorbtion bands at 675 nm (14800 cm^{-1}), 560 nm (17850 cm^{-1}), 500 nm (20000 cm^{-1}), 420 nm (23800 cm^{-1}) and 355 nm (28170 cm^{-1}) can be observed on the general shape of the diffuse reflectance spectrum. The bands I—IV are characteristic for $d-d$ transitions of Cu^{2+} ions in a rhombic distortion of the coordination octahedron The last band may by ascribet to the metal-ligand charge transfer transition [2—4].

The presence of the inclusions of metallic copper microparticle sizes in the quartz matrix suggest the fact that the refractive index is complex, $n = n_r - i\chi$ [5—7]. For the low frequancy range, the real part of this is greater than the imaginary part, this fact leading to a strong reflection as can be shown in Fig. 1. At the high frequency, the imaginary part decreases to zero together with the refractive index and the sample becames transparent. However, as can be seen from Fig 1 in the case of studied samples a great reflectance appears in this frequency range, which may be explained by the presence

* *University of Cluj-Napoca, Department of Physics, 3400 Cluj-Napoca, Romania*
** *Politechnical Institute of Cluj-Napoca, 3400 Cluj-Napoca, Romania*
*** *ICPTSCF Bucharest, Department of Turda, 3350 Turda, Romania*

of metal-ligand charge transfer fenomena [5, 6].

The complex refractiv index may be calculated from the definition of the reflection coefficient $R = I/I_0 = [(n-1)/(n+1)]^2$ Thus the following values were obtained for the suitable positions of the five peaks from the diffuse reflectance spectrum $n = 1\,650$(I); 1.289(II), 1,280(III), 1 358(IV), 2(V).

By extrapolating the linear region of the reflectance slope to longer wavelenghts we have determined the activation optical energy of the electrical conductivity The value obtained for this energy $h\nu = 1\,95$ eV suggests an isolated dispertion mode of copper metallic microparticle sizes in the quartz matrix.

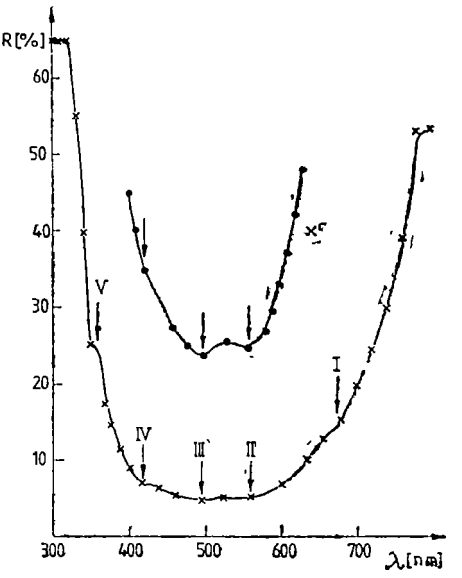

Fig. 1. The diffuse reflectance spectrum of quartz impurified with CuO.

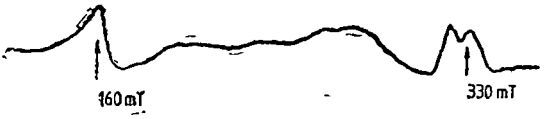

Fig. 2. EPR spectrum of quartz impurified with CuO.

Further informations on the distribution mode of metallic ions were obtained from EPR data. The EPR measurements were performed at 9.4 GHz (X band), using a standard JEOL—JES—3B equipment at the 295 K The weak intensity of the EPR spectra (fig 2) suggests the presence of a small number of Cu^{2+} in the studied samples. Also, the absence of hyperfine structure and the presence of low field signal at $g \simeq 4$ provided evidence for the existence of $Cu^{2+} - Cu^{2+}$ pairs [8—11]. Thus, even the minority copper (II) ions behave as ,,associated'' species and do not are ,,isolated'' dispersed in the quartz matrix. The $Cu^{2+} - Cu^{2+}$ pairs are strongly coupled by superexchange interactions [9—11]. The lines from the $B = 330$ mT region are due to the allowed transitions $\Delta M_S = \pm 1$ from the triplet state ($S = 1$) and that from the $B = 160$ mT region belongs to the forbiden transitions $\Delta M_S = \pm 2$ [8].

The existence of the associations in the case of minority copper (II) ions stress the idea of the presence of majority copper atoms as metallic microparticle sizes in the studied samples. These metallic microparticle sizes confer the reddish colour of the studied impurified quartz matrix.

REFERENCES

1. R Deen, P I Th Scheltus, G de Vries, *J Catal*, **41**, 218 (1976).
2 B J Hathaway, D E Billing, *Coordin Chem Rev*, **5**, 143 (1970)
3 I M Procter, B J Hathaway, P Nicholls, *J Chem Soc*, **A**, 1678 (1968).
4 I Ardelean, W Mieskes, *Phys Stat Sol (a)*, **51**, K 129 (1979)
5 F Wooten, "Optical Properties of Solids", Academic Press, New York, 1972
6 J. Wong, C A. Angell, "Glass Structure by Spectroscopy", Marcel Dekker Inc, New York and Basel, 1976
7. D G Holloway, "The Physical Properties of Glasses", Wikeham Publ Ltd, London and Winchester, 1975
8 J F Boas, R H Dunhill, J R Pilbrow, R C Srivastava, T D. Smith, *J. Chem Soc*, **A**, 94 (1969)
9 G.A Korteweg, L L van Reijen, *J Mag Res*, **44**, 159 (1981)
10 O Cozar, V Znamirovschi, *Czech J Phys*, **B 33**, 1357 (1983)
11 I Ardelean, O Cozar, Gh Ilonca, *J Non-Cryst Solids*, **68**, 33 (1984).

STUDIA UNIV BABEŞ—BOLYAI, PHYSICA, XXXII, 2, 1987

MAGNETIC BEHAVIOUR OF THE THERNARY OXIDIC SEMICONDUCTING α-(Fe_2O_3—Al_2O_3—Cr_2O_3) SYSTEM

LILIANA POP*, MINERVA CRISTEA, OLIVIA POP*** and IULIU POP***

Received October 5, 1987

ABSTRACT. — The temperature dependence of the magnetic susceptibility between 100 and 1300 K was investigated for the α-(Fe_2O_3—Al_2O_3—Cr_2O_3) solid solutions. A large variety of the magnetic properties was pointed out. The system pass from the noncolinear antiferromagnetic state to colinear antiferomagnetic state and then to paramagnetic state, or from colinear antiferomagnetic state to paramagnetic state, depending of the α-Cr_2O_3 concentration.

Introduction. In the previous paper [1] we have reported the interesting magnetic behaviour of the α-(Fe_2O_3-Al_2O_3) semiconducting system in the antiferomagnetic ordering region and also in the paramagnetic region, pointing out the phase diagram, i e the concentration dependence of the Néel temperature, and of the spins reorientation temperature, and also the existence of the temperature independent magnetic susceptibility, between 900 K and 1,100 K.

This peculiar magnetic behaviour determined us to investigate the thernary oxidic system α-(Fe_2O_3-Al_2O_3-Cr_2O_3), belonging to the same crystallographic variety of the corundum type

Samples preparation and experimental technique The starting materials for the preparation of the thernary oxidic system α-(Fe_2O_3-Al_2O_3-Cr_2O_3) were $AlCl_3 \cdot 6H_2O$; $FeCl_3 \cdot 6H_2O$ and $CrCl_3$ $6H_2O$ of p a purity

The thernary oxidic samples were obtained by thermic decomposition of the aluminium, iron and chromium hydroxid coprecipitates The coprecipitates were calcined at 1,523 K and slouly cooled down and final calcined for 7 houres in five cycles

The solid solutions and their homogenity we checked out by X ray analyse, using a TUR—M—61 diffractometer and Cu—K_α radiation [2]

The temperature dependence of the magnetic susceptibility was determined using a Weiss and Forrer magnetic balance type, with 10^{-8} cm^3/g sensitivity in the temperature range 100—1,300K, and 9,200 Gs magnetic field intensity.

Experimental results and dissecutions. The temperature dependence of the magnetic susceptibility was investigated for five samples with constant content of 90 molar % α-Fe_2O_3 [3] and for three samples with 70 molar % α-Fe_2O_3 in comparison with the binar compound 90 molar % α-Fe_2O_3 and 10 molar% α-Al_2O_3. As it can see from the figure 1, where is given the temperature dependence of the magnetic susceptibility in the temperature range 100—1,200 K

* *University of Cluj-Napoca, Faculty of Mathematics and Physics, 3400 Cluj-Napoca, Romania*
** *Timişoara Polytechnical Institute, 1900 Timişoara, Romania*
*** *Cluj-Napoca Polytechnical Institute, 3400 Cluj-Napoca, Romania*

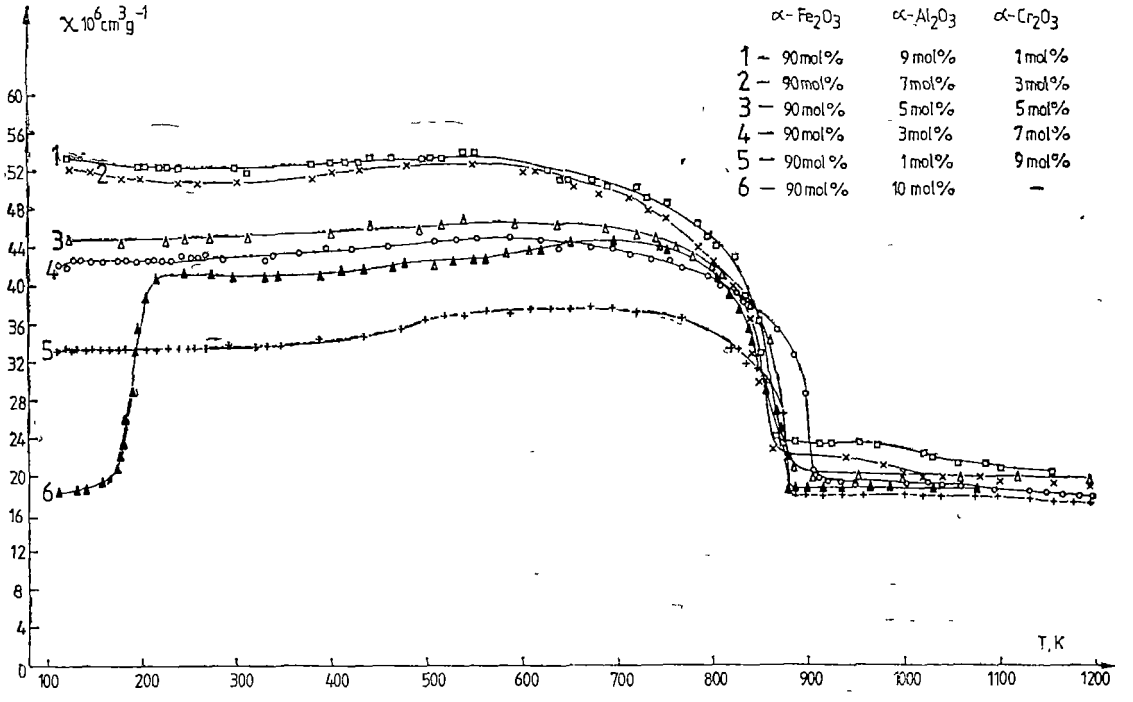

Fig 1 Temperature dependence of the magnetic susceptibility for α-(Fe_2O_3—Al_2O_3—Cr_2O_3) system with 90 mol% α-Fe_2O_3 content.

for the five samples with the constant content of 90 molar % α-Fe_2O_3 of the thernar system α-(Fe_2O_3—Al_2O_3—Cr_2O_3) in comparison with the binar compound the thermal vanation of the magnetic susceptibility is very different. For the binar compound α-(90 mol% Fe_2O_3 —10 mol% Al_2O_3) the magnetic susceptibility fals in three stages, meanwhile for the thernar system fals only in two stages This mean the change in the magnetic spin structure of the thernary system Indeed, the anomaly at low temperature, bellow 200 K, wanishes in the temperature dependence of the magnetic susceptibility for the thernar system So the spin magnetic moments are antiferromagnetically oriented perpendicular to *c* axis from 100 K up to the Néel temperature The presence of α-Cr_2O_3 in the α-(Fe_2O_3—Al_2O_3) lattice less then 1 mol% α-Cr_2O_3 give rise to the increase of the magnetic susceptibility value, but for the more concentrated samples the magnetic susceptibility decreases monotonously with the α-Cr_2O_3 concentration increase, as one can see from the figure 2, where is given the α-Cr_2O_3 concentration dependence of the magnetic susceptibility for the investigated thernar system

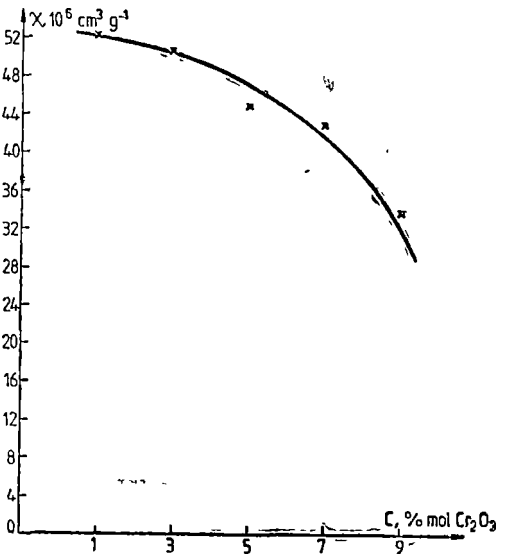

Fig. 2. α-Cr_2O_3 concentration dependence of the α-(Fe_2O_3—Al_2O_3—Cr_2O_3) magnetic susceptibility, with 90 mol% α-Fe_2O_3 content

This concentration dependence indicates on the formation of the Cr^{3+} magnetic sublattice in the thernar system, which determins the change in the spin structure of the system, resulting a more complicated magnetic spin structure than that of the α-(Fe_2O_3—Al_2O_3) system. Indeed, the temperature dependence of the magnetic susceptibility in the so called paramagnetic region, for $T > T_N$, is very unusual The anomaly in the temperature dependence of the magnetic susceptibility at high temperatures, at about 900 *K*, atributed so far to the Néel temperature for α-Fe_2O_3, and for α-(Fe_2O_3—Al_2O_3) is a critical tempetature for order-order transition, but not for order-disorder transition. This fact is confirmed by the temperature dependence of the reciprocal magnetic susceptibility represented in the figure 3, for $T > 870$ K. As one can see from this figure, for the first three samples with 1, 3, and 3 mol% of α-Cr_2O_3, the temperature dependence of the reciprocal magnetic susceptibility is not linear, suggesting a ferrimagnetic spin structure superposed on the antiferromagnetic spin structure, or succeeding the antiferromagnetic spin structure The effect is given more clear for the sample 4, with 7 mol% — α-Cr_2O_3, for which the temperature dependence of the reciprocal magnetic susceptibility is not linear, but has a minimum bellow 1,000 K suggesting a more complicated magnetic spin structure. For the sample-5, with 9 mol% α—Cr_2O_3 the temperature dependence of the reciprocal magnetic susceptibi-

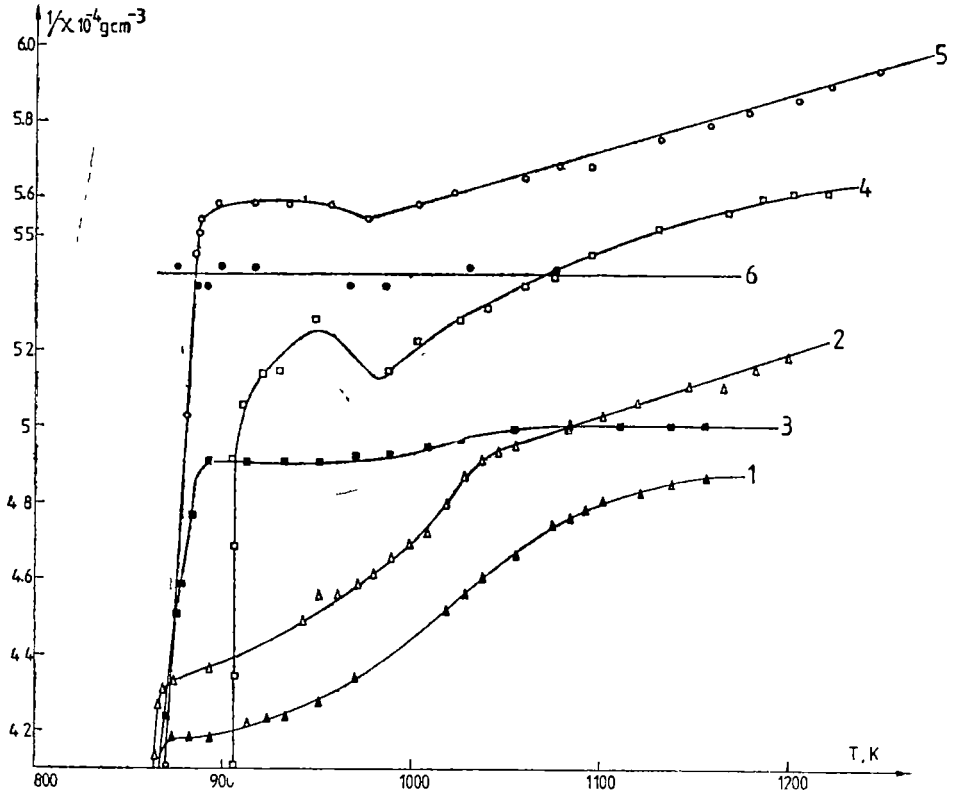

Fig. 3. Temperature dependence of the reciprocal magnetic susceptibility for α-(Fe_2O_3—Al_2O_3—Cr_2O_3) system with 90 mol% α-Fe_2O_3 content.

lity has a minimum, corrseponding to the Néel temperature and then is linear, and obey the Curie—Weiss law. So we have a succession of the second order phase transitions of the order-order and order-disorder type in the α-(Fe_2O_3—Al_2O_3—Cr_2O_3) system, and really the critical temperature atributed so far for the Néel temperature for α-Fe_2O_3 and α-(Fe_2O_3—Al_2O_3) systems is not correct, because for the temperatures higher then so called Néel temperature, in a large temperature range the magnetic susceptibility is practically temperature independent, which is very peculiar for the oxidic systems [1].

The magnetic spin structure of the α-(Fe_2O_3—Al_2O_3—Cr_2O_3) system is strongly dependent of the α-Cr_2O_3 concentration increase So, the shape of the temperature dependence of the magnetic susceptibility curves is modified and the magnetic susceptibility value decreases with α-Cr_2O_3 concentration increasing, as one can see from the figure 4, where is represented the temperature dependence of the magnetic susceptibility for three samples with 70 mol% of α-Fe_2O_3 The system has only one critical temperature of order-disorder type at about 700 K, which is the Néel temperature In the paramagnetic region the magnetic susceptibility decreases when the temperature increases. In the

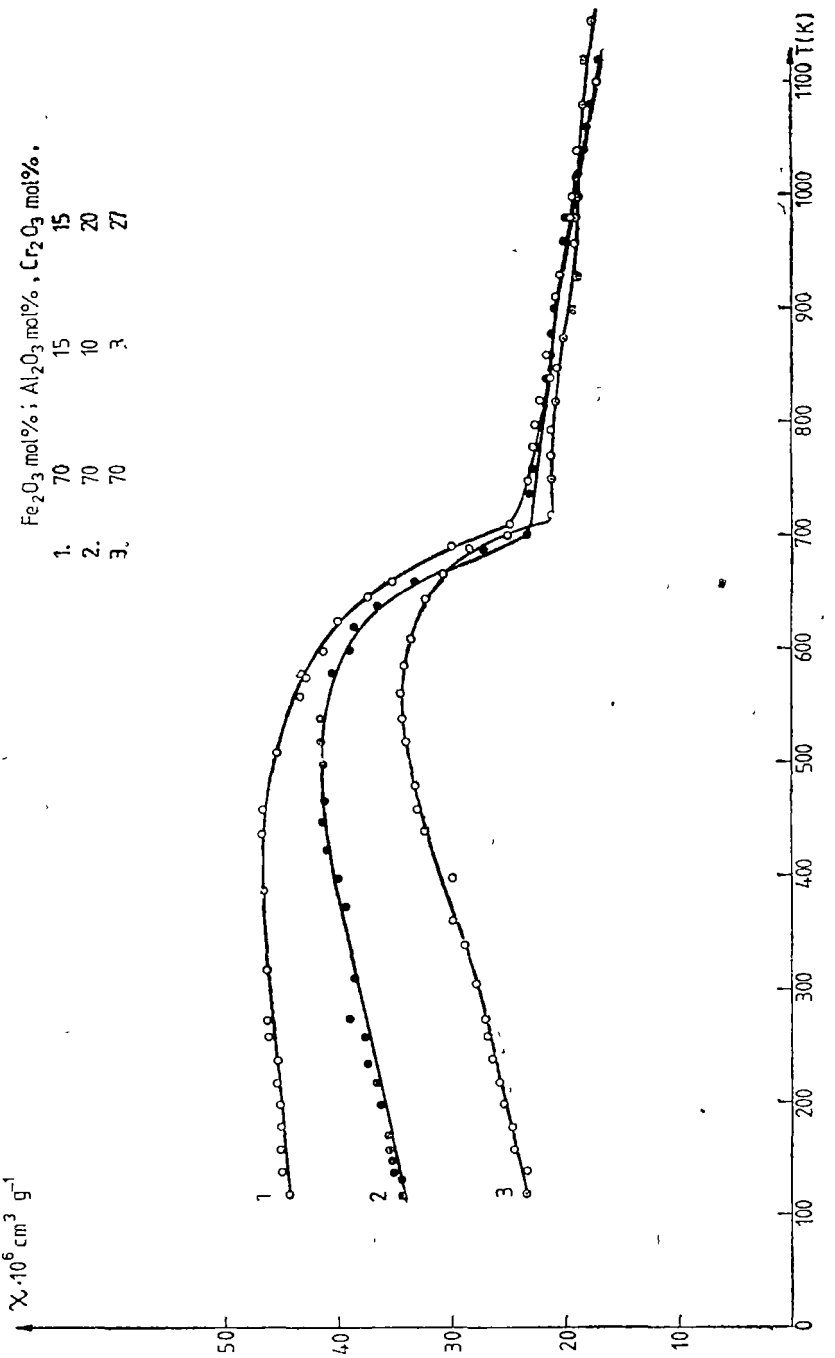

Fig. 4. Temperature dependence of the magnetic susceptibility for α-(Fe_2O_3—Al_2O_3—Cr_2O_3) system with 70 mol% α-Fe_2O_3 content.

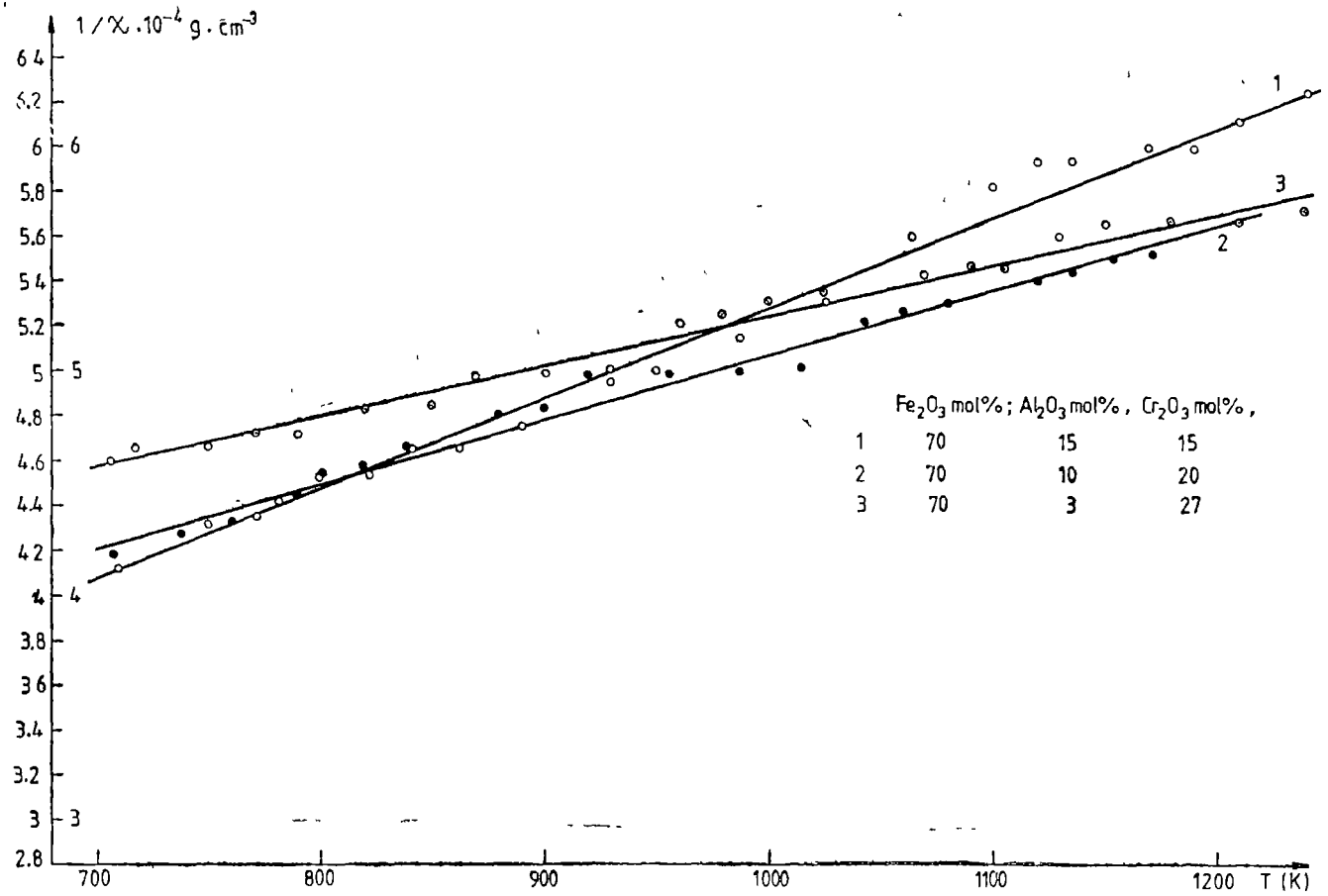

Fig. 5. Temperature dependence of the reciprocal magnetic susceptibility for α-(Fe_2O_3—Al_2O_3—Cr_2O_3) system with 70 mol% α-Fe_2O_3 content.

ordered state the magnetic susceptibility increases passing through the maximum bellow the Néel tempeature with the temperature increase.

The temperature dependence of the reciprocal magnetic susceptibility for $T > T_N$ is linear, as one can see from the figure 5, obeying the Curie—Weiss law, as for the usual paramagnetic with the localized magnetic moments From the slope of the lines we have determined the Curie constant values, and consequently the effective magnetic moment values per formula unit. The obtained values are in good agreement with the calculated values, taking the values 5 92 μ_B/Fe^{3+} and 3 87μ_B/Cr^{3+} in the formula

$$\mu_{eff} = [f_1 \cdot \mu^2_{Fe^{3+}} + f_2 \cdot \mu^2_{Cr^{3+}}]^{1/2},$$

where f_1 and f_2 are the molar fractions of the α-Fe_2O_3 and Cr_2O_3 in the compound

Conclusions. The thernar α-(Fe_2O_3—Al_2O_3—Cr_2O_3) semiconducting oxidic system give rise to a large range of solid solutions From the magnetic point of view this system of solid solutions is very interesting, showing a complicated magnetic spin structure picture Even the simple oxid α-Fe_2O_3 behavs peculiar in the paramagnetic region, the magnetic susceptibility being temperature independent in very large temperature range. This fact points out that the critical temperature accepted so far as Néel temperature, actually is an order-order critical temperature type and not order-disorder critical temperature for the transition from the antiferromagnetic state into paramagnetic state. A similar behaviour was pointed out for the binar system α-(Fe_2O_3—Al_2O_3) [2]

In the thernar α-(Fe_2O_3—Al_2O_3—Cr_2O_3) the anomaly in the temperature dependence of the magnetic susceptibility corresponding to the critical temperature for the spin reorientation, T_{sr}, from the parallel to perpendicular to c-axis direction, vanishes.

In the high temperature region a succesion of the two second order phase transition was pointed out, i e. order-order phase transition type and order-disorder phase transition type, which are connected with the more complicated magnetic spin structure.

For the less α-Fe_2O_3 concentrated samples (70 mol% α-Fe_2O_3) only one critical temperature of order-disorder type was pointed out. This meances that the presence of α-Cr_2O_3 in the lattice of the thernar system plays an important role, and give rise to the large diversity of the magnetic spin structure.

REFERENCES

1. Liliana Pop, Camelia Maraloiu, L Stănescu, Iuliu Pop, *Studia Univ. „Babeş—Bolyai", Physica*, **XXXII**, (1) 1987
2. Minerva Cristea, *Teză de doctorat*, Institutul Politehnic Timişoara (1984)
3. Liliana Pop, Minerva Cristea, Olivia Pop, Iuliu Pop, *Lucrările conferinţei anuale de semiconductoare, CAS'87, Ediţia a 10-a jubiliară, 7—10 octombrie*, 1987, Sinaia, p. 531,

STUDIA UNIV BABEŞ—BOLYAI, PHYSICA, XXXII, 2, 1987

ON THE PRINCIPLE OF GENERALIZED EQUIVALENCE

Z. GÁBOS* and G. FÜLÖP*

Received September 11, 1987

ABSTRACT. — The gravitational action of a central rotating body on a homogeneous, spherical test body, of small radius, is investigated. It is shown that when the rotation of the test body is slow, the motion problem may be geometrized. The movement may be considered as inertial, in a seven-dimensional space, which admits as subspaces the time space ($x^0 = ct$), the ordinary space ($x^1 = x$, $x^2 = y$, $x^3 = z$) and the internal space defined with the aid of the Euler angles ($\alpha^1 = \vartheta$, $\alpha^2 = \varphi$, $\alpha^3 = \psi$). Through geometrization, one automatically respects the requirements imposed by the generalized equivalence principle, which is valid both for the translation and the rotation movement.

1°. We consider the case in which the central body is homogeneous and has spherical shape. Let A be the radius, M_0 the rest mass and $\vec{\Omega}$ the constant angular velocity of this body. For the corresponding data on the test body, we use the small characters $(a, m_0, \vec{\omega})$. We admit the following:

a) the inequality below is respected:

$$\frac{a}{r - A} \ll 1, \text{ where } r = |\vec{x}| \tag{1}$$

(vector $\vec{x}$ specifies the position of the centre of the test body relative to the centre of the central sphere),

b) as the effects are small, a second order approximation is considered as satisfactory (the zero order being the newtonian approximation);

c) the rotational motion of the test body is relatively slow, so that the ratio

$$\frac{a|\vec{\omega}|}{|\vec{v}|} \tag{2}$$

(where $\vec{v}$ is the translational velocity of the test body) is sufficiently small to make (within the approximation used) the terms of the type $a^2\omega^2v^2$, $a^4\omega^4$ negligable as compared to v^4),

d) the lagrangean of the system derives from the Fock — Fichtenholtz lagrangean for a system of material points [2], [5], by taking into account the restrains imposed onto the points of the two spheres (they undergo a rotational movement).

* *University of Cluj-Napoca, Faculty of Mathematics and Physics, 3400 Cluj-Napoca, Romania*

Under the conditions imposed above, one is led to the following lagrangean [9]

$$\frac{L}{m_0} = -c^2 + \frac{1}{2}v^2 + \frac{1}{8c^2}v^4 - \Phi - \frac{1}{2c^2}\Phi^2 - \Psi + c(\vec{\xi}, \vec{v}) + \\ + \frac{1}{5}a^2\omega^2 + a^2(\vec{K}, \vec{\omega}), \tag{3}$$

which contains the quantities

$$\Phi = -\frac{\lambda c^2}{r}, \quad \text{with} \quad \lambda = \frac{kM_0}{c^2}, \tag{4}$$

$$\vec{\xi} = \frac{4\lambda A^2}{5cr}(\vec{x} \times \vec{\Omega}), \tag{5}$$

$$\Psi = -\frac{3\lambda A^2}{5r^3}\Omega^2 - \frac{3\lambda A^4}{70r^5}[r^2\Omega^2 - 3(\vec{\Omega}, \vec{x})^2], \tag{6}$$

$$\vec{K} = \vec{K}_1 + \vec{K}_2, \tag{7}$$

where

$$\vec{K}_1 = -\frac{3\lambda}{r^3}(\vec{x} \times \vec{v}), \tag{8}$$

$$\vec{K}_2 = \frac{4\lambda A^2}{25r^5}[r^2\vec{\Omega} - 3(\vec{\Omega}, \vec{x})\vec{x}]. \tag{9}$$

Using the expressions

$$\omega^1 = \dot{\varphi}\sin\vartheta\sin\psi + \dot{\vartheta}\cos\psi, \\ \omega^2 = -\dot{\varphi}\sin\vartheta\cos\psi + \dot{\vartheta}\sin\psi, \tag{10} \\ \omega^3 = \dot{\varphi}\cos\vartheta + \dot{\psi}$$

for the components of the angular velocity, togather with the relationship

$$\mathrm{d}S^2 = \frac{1}{c^2}\left(\frac{L}{m_0}\right)^2 \mathrm{d}t^2 \tag{11}$$

one is led to the expression

$$\mathrm{d}S^2 = \mathrm{d}s^2 + a^2\mathrm{d}\sigma^2 \tag{12}$$

defined in a seven-dimensional space. Within the approximation used for $\mathrm{d}s^2$ and $\mathrm{d}\sigma^2$, we have:

$$\mathrm{d}s^2 = f(r)(\mathrm{d}x^0)^2 - g(r)\mathrm{d}x^j\mathrm{d}x^j - 2\xi_j\mathrm{d}x^j\mathrm{d}x^0, \tag{13}$$

$$\mathrm{d}\sigma^2 = -\frac{2}{5}\rho_{jk}\mathrm{d}\alpha^j\mathrm{d}\alpha^k + h_{jk}\mathrm{d}x^j\mathrm{d}\alpha^k + s_j\mathrm{d}\alpha^j\mathrm{d}x^0, \tag{14}$$

with

$$f(r) = 1 + \frac{2}{c^2}\left(\Phi + \Psi + \frac{\Phi^2}{c^2}\right), \quad g(r) = 1 - \frac{2}{c^2}\Phi, \tag{15}$$

$$\rho_{11} = \rho_{22} = \rho_{33} = 1, \quad \rho_{23} = \rho_{32} = \cos\vartheta \tag{16}$$

(the remaining coefficients ρ_{jk} being zero),

$$h_{jk} = -2\frac{\partial^2}{\partial v^j \partial \dot{\alpha}^k}(\vec{K}_1, \vec{\omega}), \tag{17}$$

$$s_j = -\frac{2}{c}\frac{\partial}{\partial \dot{\alpha}^j}(\vec{K}_2, \vec{\omega}) \tag{18}$$

2° If the following notations are introduced

$$q^0 = x^0, \quad q^i = x^i, \quad q^{i+3} = \alpha^i \quad (i = 1, 2, 3) \tag{19}$$

togather with the variable τ, as defined by

$$dS = c d\tau \tag{20}$$

one is led, on the basis of equation (12), in the ordinary way, to equations of the type

$$\frac{d^2 q^A}{d\tau^2} + \Gamma^A_{BC}\frac{dq^B}{d\tau}\frac{dq^C}{d\tau} = 0, \quad A, B, C = \overline{0, 6}. \tag{21}$$

If the variable t is used instead of the variable τ, then the equations [7] are to be employed

$$\frac{d^2 q^A}{dt^2} + \Gamma^A_{BC}\frac{dq^B}{dt}\frac{dq^C}{dt} - \frac{1}{c}\Gamma^0_{BC}\frac{dq^A}{dt}\frac{dq^B}{dt}\frac{dq^C}{dt} = 0, \; A, B, C = \overline{1, 6} \tag{22}$$

After completing some somple calculations, the following equations, of type (22), are obtained:

$$\frac{d^2 x^j}{dt^2} + \frac{\partial}{\partial x^j}\left(\Phi + \Psi + \frac{2}{c^2}\Phi^2\right) + \frac{1}{c^2}\left(\frac{\partial \Phi}{\partial x^j}\delta_{lp} - 2\frac{\partial \Phi}{\partial x^p}\delta_{jl} - 2\frac{\partial \Phi}{\partial x^l}\delta_{jp}\right)\dot{x}^l\dot{x}^p +$$

$$+ c\left(\frac{\partial \xi_j}{\partial x^k} - \frac{\partial \xi_k}{\partial x^j}\right)\dot{x}^k = 0, \tag{23}$$

$$\ddot{\vartheta} + \sin\vartheta\dot{\varphi}\dot{\psi} - \frac{5}{4}A_1 = 0 \tag{24}$$

$$\ddot{\varphi} + \operatorname{ctg}\vartheta\dot{\varphi}\dot{\vartheta} - \frac{1}{\sin\vartheta}\dot{\vartheta}\dot{\psi} - \frac{5}{4\sin^2\vartheta}(A_2 - \cos\vartheta A_3) = 0, \tag{25}$$

$$\ddot{\psi} - \frac{1}{\sin\vartheta}\dot{\varphi}\dot{\vartheta} + \operatorname{ctg}\vartheta\dot{\vartheta}\dot{\psi} + \frac{5}{4\sin^2\vartheta}(\cos\vartheta A_2 - A_3) = 0 \tag{26}$$

where

$$A_l = -\frac{3}{r^2} h_{jl} x^k \dot{x}_k \dot{x}^j - h_{jl} \frac{\partial \Phi}{\partial x^j} + c \frac{\partial s_l}{\partial x^k} \dot{x}^k - \frac{2}{c} s_l \frac{\partial \Phi}{\partial x^k} \dot{x}^k + \\ + \left(\frac{\partial h_{jl}}{\partial \alpha^k} - \frac{\partial h_{jk}}{\partial \alpha^l} \right) \dot{x}^j \dot{\alpha}^k + c \left(\frac{\partial s_l}{\partial \alpha^k} - \frac{\partial s_k}{\partial \alpha^l} \right) \dot{\alpha}^k. \quad (27)$$

The terms which do not belong to the second order approximation have been omitted from the calculus

3° On the basis of the above results, the following conclusions may be drawn

a) The translational motion of the test body may be described on the basis of the expression for ds^2 given under (13), which leads to equations (23).

b) The rotational movement of the test body may be described with the aid of the $d\sigma^2$ expression given under (14), which leads to equations (24), (25), (26)

c) The facts that the translational movement of the test body is not influenced by the mass m_0, and the rotation of the same body is not influenced by $m_0 a^2$ (i e by the moment of inertia) are consistent with the validity of a generalized principle of equivalence.

d) The effects which produce variations in the translational and rotational movements of the test body may be considered as curvature and torsion effects, respectively By adopting this language, one may state that the curvature effects can be described with the aid of the quantities Φ, Ψ, $\vec{\xi}$, while those of torsion, with the quantities h_{jk}, s_j.

e) The $\vec{\Omega} - \vec{v}$ coupling leads to curvature effects, while the $(\vec{x} \times \vec{v}) - \vec{\omega}$, $\vec{\Omega} - \vec{\omega}$ couplings lead to torsional effects.

f) The use of expression (12) has be advantage that it does not make use of the theory elaborated for nonholonomic systems and that one need not employ antisymmetric transport coefficients

REFERENCES

1. M Mathison, *Acta Phys Polon*, **6**, 163 (1937)
2. I G Fichtenholtz, *JETF*, **20**, 233 (1950)
3. A. Papapetrou, *Proc Roy. Soc.*, **A 209**, 248 (1951).
4. F A E Pirani, *Acta Phys Polon.*, **15**, 389 (1956).
5. L D Landau, E. M. Lifşitz, „Teoria cîmpului", Editura Tehnică, Bucureşti, 1963, p. 363.
6. L I Schiff, *Phys. Rev Lett*, **4**, 215 (1960)
7. S Weinberg, „Gravitaţia i kosmologia", Moskva, 1975, p 251—257.
8. W. Adamovitz, A Trautman, *Bul Acad. Polon. Sciences, Math, Phys, Astr.*, **23**, 339 (1975)
9. Z Gábos, J. Szén, *Studia Univ Babeş—Bolyai, Physica*, **29**, 46 (1984).

STUDIA UNIV BABEŞ—BOLYAI, PHYSICA, XXXII, 2, 1987

STRUCTURE STUDY OF INTERMETALLIC OF THE COMPOUNDS $Tb_2Ni_{17-x}Al_x$ BY X-RAYS

V. CRIŞAN*, C. HĂGAN* and I. POP*

Received September 17, 1987

ABSTRACT. — The intermetallic compounds $Tb_2Ni_{17-x}Al_x$ ($x = 0$; 0.15; 0.25; 0 40; 0.60; 1; 1.5; 2; 3; 4; 8, 10, 12; 14; 15; 15.50, 16; 16.25; 16.50; 16.75; 17) were investigated by X-ray diffraction. The compounds are isostructural. Using these data for the investigated series of intermetallic compounds we have proposed the structural models which allow us to explain the variation of the lattice parameters and the c/a ration by the rare earth-atoms occupied positions in the unit cell.

1. **Introduction.** The intermetallic compounds of the transition metals with rare earth crystallize into two structure types:

Rhombohedral R3m (of the Th_2Zn_{17} type) or hexagonal $P6_3/mmc$ (of the Th_2Ni_{17} type) depending on the rare earth or on the thermic applied treatment [1]

The intermetallic compound Tb_2Ni_{17}, prepared by us, has a hexagonal structure of the Th_2Ni_{17} type, with the lattice parameters: $a = 8.190$ Å and $c = 8\,482$ Å We have also prepared the intermetallic compound Tb_2Al_{17}, which is a new compound, isotypic with Tb_2Ni_{17} It was interesting to see, if there is a mutual solid solubility between these two compounds.

Our structural investigation have shown that there is a large range of solid solubility, with the general formula $Tb_2Ni_{17-x}Al_x$. This means that the Ni atoms in the Tb_2Ni_{17} compound are easily replaced by the aluminium atoms.

From the positions and the intensities of the diffraction lines we have determined both the lattice parameters and the structural parameters z_e, z_f and z_k, which fix the atom positions in the unit cell. This allows to elaborate a crystalline model for every investigated intermetallic compound

2. Experimental. The compounds were prepared by arc melting stoichiometric amounts of the elements in a pure argon atmosphere The purity of the starting materials was Tb 99 9% and Ni 99.9%.

The X-ray diffraction investigations were performed on TUR—M—62 equipment, using the Cr K_α radiation. The density of the samples was determined both from X-ray data and directly, using a pyknometric method.

3. **Results and discussions.** The $Tb_2Ni_{17-x}Al_x$ series of intermetallic compounds represents only a single phase; the diffraction patterns for each compound being indexed in accordance with the hexagonal structure type. There were no lines which could be attributed to pure elements or to other phases.

* *University of Cluj-Napoca, Faculty of Mathematics and Physics, 3400 Cluj-Napoca, Romania*

Table 1

Calculated and observed $1/d^2$ values and observed intensities of the X-ray diffraction lines for the compound $Tb_2Ni_1Al_{17}$ (Cr K_α radiation, $\lambda = 2.28962$ Å)

2θ	$1/d^2$ (obs)	*hkl*	$1/d^2$ (calc)	The intensity
17 50	0.0177	100	0 0167	vw
22 50	0 0290	101	0.0279	vw
27 65	0 0436	002	0.0436	w—m
29 60	0 0498	110	0.0508	vw
31.60	0 0566	102	0 0608	m
33.60	0 0637	111	0 0617	w
36 35	0 0742	201	0 0787	m
42 20	0.0989	112	0.0944	vs
43 20	0 1034	003	0 0981	vs
44 90	0 1113	103	0 1150	vs
46 40	0 1184	210	0.1186	vs
48 40	0 1282	211	0 1295	vw
52.10	0 1472	113	0.1489	vs
53 70	0.1556	212	0.1624	m
57 20	0 1748	004	0 1743	m
58.20	0 1805	104	0 1913	vw
60 40	0 1931	302	0 1961	vw
63.00	0.2083	220	0 2034	s
64.70	0.2185	310	0.2203	m
66.90	0.2318	311	0 2312	vw
68.80	0.2435	204	0 2421	m
70 10	0.2516	303	0 2506	w
71 80	0 2623	400	0 2712	w
73 70	0 2744	005	0.2724	vw—w
74 50	0 2796	401	0 2821	vw—w
76 00	0 2892	105	0 2894	vw—w
77 40	0 2983	223	0 3014	vw—w

Table 2

Calculated and observed $1/d^2$ values and the observed intensities of the X-ray diffraction patterns for the compound $Tb_2Ni_2Al_{15}$ (Cr K_α radiation, $\lambda = 2.28962$ Å)

2θ	$1/d^2$ (obs)	*hkl*	$1/d^2$ (calc)	The intensity
14.90	0 0128	001	0.0114	w
16.90	0 0165	100	0.0171	vw
22 20	0 0283	101	0.0285	vw
28 30	0.0456	002	0 0455	vw
30 60	0 0531	110	0 0514	m
32 40	0 0594	102	0 0627	vw
33 50	0.0634	111	0 0628	m
35 20	0.0698	200	0 0686	m
38 00	0 0809	201	0 0799	m
42 10	0.0984	112	0.0969	vs
43.80	0 1062	003	0 1024	vs
44.80	0 1108	202	0 1141	vs
46 50	0.1189	103	0 1195	vs
47 95	0 1260	210	0.1200	vw
48 80	0 1302	211	0 1314	vw
53 80	0 1562	300	0 1543	m
55.50	0 1654	212	0 1655	vw
57.35	0 1757	203	0 1710	s—vs
58.70	0 1833	004	0 1820	s—vs
60.20	0.1919	104	0 1992	s—vs
61 70	0.2006	302	0.1998	vw
62 95	0 2080	220	0.2057	vw
64 40	0.2167	221	0 2171	vw
66 80	0.2312	114	0.2335	m
68.80	0 2435	204	0 2506	m
71.80	0.2623	303	0.2567	v—m
72 90	0.2693	312	0 2683	vw
76.00	0.2892	401	0.2856	w—m
77.30	0.2976	214	0.3020	w—m
79 60	0 3126	223	0.3081	w—m

The experimental results for the compounds $Tb_2Ni_1Al_{16}$ and $Tb_2Ni_2Al_{15}$ are given in Tables 1 and 2, which include the observed and calculated $1/d^2$ values and the experimental determined intensities The very good agreement of these values confirms the existence of a hexagonal single-phase structure for these compounds

Similar results were obtained for all the compounds. The lattice parameters and densities of the whole series of the compound are given in figures 1 and 3. The continous solubility of the compounds Tb_2Ni_{17} and Tb_2Al_{17} can be also revealed from the concentration dependence of the lattice parameters (Fig. 1) and of the density (Fig 3). As one can see, the lattice parameter *a* decreases linearly as the number of Ni atoms per unit formula increases, while the parameter *c* decreases non-linearly and remains almost constant when the number of the Ni-atoms is greater than approximately ten [2]

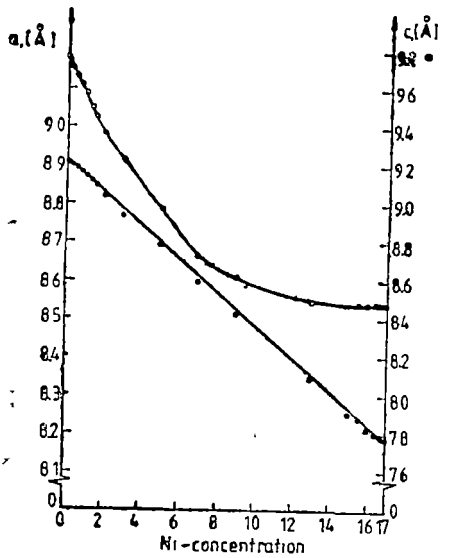

Fig 1.

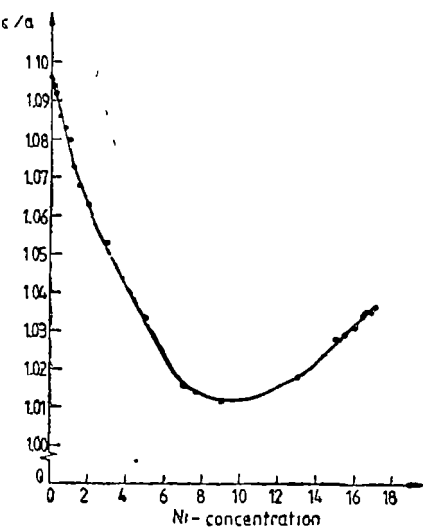

Fig 2

The ratio c/a (Fig. 2) decreases as the number of Ni atoms increases and has a minimum value at approximalety nine Ni atoms per unit cell, and then it increases till the number of the Ni atoms is 17 The region where the minimum appears, i e for $x \in (8, 11)$ is the same with the region where the dependence of the c parameter versus Ni atoms concentration changes his slope.

The experimental density of the compounds increases linearly with the Ni content, in good agreement with the variation of the a lattice parameter The difference (shown in the Fig 3) between the density values determined by the X-ray and pyknometric method may be due to cavities in the bulk samples

The structural parameters z_e, z_f and z_k were determined by fitting the experimental intensities of the diffraction patterns with the intensities calculated using the formula

$$I_{hkl} = m \quad L \quad p \quad A(\mu)|F_{hkl}|^2, \qquad (1)$$

where m represents the repeted factor, L is the Lorentz factor, p is the polarization factor and $A(\mu)$ is the absorption factor

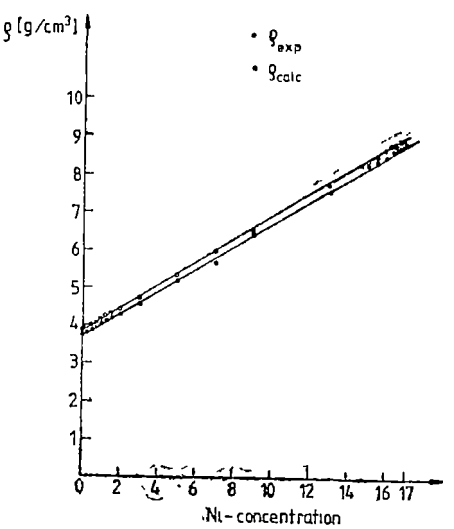

Fig. 3.

Table 3

The experimental and calculated intensities for the (00*l*) lines of $Tb_2Ni_1Al_{16}$

001		002		003		004		The structural parameters used for the calculated intensities (c. units)		
Calculated intensity (arbitrary units)	Experimental intensity (arbitrary units)	Calculated intensity (arbitrary units)	Experimental intensity (arbitrary units)	Calculated intensity (arbitrary units)	Experimental intensity (arbitrary units)	Calculated intensity (arbitrary units)	Experimental intensity (arbitrary units)	z_e	z_k	z_f
8,00285	6,15859—	19,71437	16,42291—	9,13462	8,21146—	2,53291	2,05286—	0,08	0 48	0 30
7,79139	10,26432	20,52864	20,52864	8,60629	12,31784	2,59641	6,15859	0 08	0 48	0 32
8,00285	6,15859—	19,71437	16,42291—	9,13462	8.21146—	2,53291	2,05286—	0 08	0 52	0 30
7,79139	10,26432	20,52864	20,52864	8,60629	12,31784	2,59641	6,15859	0 08	0 52	0 32
10,02051	6,92371—	16,35298	16,34527—	9,23718	8,74433—	3,07675	3,04367—	0 32	0 04	0 26
10,29278	10,72415	17,97171	20,14565	8,94523	12,54477	3,56256	6,92371	0 32	0 04	0 27
7,05577	5,66315—	14,86494	14,57892—	8,76369	7,44630—	2,56327	2,09684—	0 34	0 00	0 26
7,28452	9,22946	16,38982	18,14524	8,47938	11,01263	3,02601	5,66315	0 34	0 00	0 28
6,90495	6,92371—	18,08936	14,99158—	10,88020	7,73344—	4,24353	2,28954—	0 32	0 02	0 36
6,34477	10,72415	16,59782	18,62065	11,22123	11,36257	3,99239	5,91867	0 32	0 02	0 38

Table 4

The experimental and the calculated intensities for the (00*l*) patterns of $Tb_2Ni_2Al_{15}$

001		002		003		004		The structural parameters used for the calculated intensities (c units)		
Calculated intensity (arbitrary units)	Experimental intensity (arbitrary units)	Calculated intensity (arbitrary units)	Experimental intensity (arbitrary units)	Calculated intensity (arbitrary units)	Experimental intensity (arbitrary units)	Calculated intensity (arbitrary units)	Experimental intensity (arbitrary units)	z_e	z_k	z_f
8,50785	5,13264—	1,22698	0,32507—	20,94194	19,55529—	18,31998	17,15151—	0 00	0 48	0.28
8,46679	9,94014	1,03449	5,13264	21,32481	24,36284	18,67063	21,95907	0.00	0 50	0 28
8,50785		1,22698		20,94194		18,31998		0 00	0 52	0 28
8,23106	4,80186—	1,13997	0,32507—	18,41916	18,23224—	16,51144	15,99385—	0 02	0 48	0 26
8,46650	9,27865	1,22698	4,80186	20,22585	22,70903	16,01554	20,47064	0 02	0 48	0 28
8,42493		1,03449		20,60310		17,22685		0 02	0 50	0.28
8,23106		1,13997		18,419616		16,51144		0.02	0.52	0 26
8,46650		1,22698		20,22585		16,01553		0.02	0 52	0.28

From the X-ray diffraction patterns we have determined the positions of the planes on which the atoms are situated, namely the parameters z_k, z_e and z_f for which we needed only the (00*l*) lines intensities)

The intensity of this type of the lines were divided, as usually, by five classes very week, week, medium, strong and very strong

The position of the atoms in the unit cell is determined starting from the positions of the Th_2Ni_{17} structure ($P6_3/mmc$) From the view point of the symmetry, the most favourable positions were earlier analysed [2], pointing out that, usual the rare-earth atoms occupy the 2b and 2d positions, the Ni atoms, and the Al atoms respectively, occcupy the 4*f*, 6*g*, 12*j* and 12*k* positons The X-ray measurements performed for the $Gd_2Ni_{17-x}Al_x$ compounds and interpreted with a simplified formula point out this distribution [2, 3].

But if we consider the formula (1) for the calculated diffraction patterns intensities, where the absorption factor is determined, it is seen that the above rule is applicable only to some of the intermetallic compounds of the series, namely for $x \in (9, 17)$ For the other compounds with $x \in (1; 8)$ the rare-earth atoms occupy the 4*e* positions, in accordance with [4]

The distribution of the atoms, obtained from the intensity of the diffraction ines using the formula (1) is given in Table 5

Table 5

The crystallographic positions of the atoms

The intermetallic compound	Tb	Ni	Al
Tb_2Ni_{17}	2b 2d	4f 6g 12j 12k	—
$Tb_2Ni_{16}Al_1$	2b 2d	4f 4e 12j 12k	2c
$Tb_2Ni_{15}Al_2$	2b 2d	6g 12j 12k	4e
$Tb_2Ni_{13}Al_4$	2b 2d	2c 12j 12k	4e 4f
$Tb_2Ni_6Al_8$	2b 2d	6g 12k	4f 12j
$Tb_2Ni_7Al_{10}$	4e	2c 12k	2b 2d 4f 12j
$Tb_2Ni_5Al_{12}$	4e	4f 6g	12j 12k
$Tb_2Ni_3Al_{14}$	4e	2c 4f	2b 2d 12j 12k
$Tb_2Ni_2Al_{15}$	4e	4f	6g 12j 12k
$Tb_2Ni_1Al_{16}$	4e	2c	4e 4f 12j 12k
Tb_2Al_{17}	4e	—	4f 6g 12j 12k

As one can observe in table 5, the Ni atoms occupy in the Tb_2Ni_{17} and $Tb_2Ni_{16}Al_{15}$ compounds the 4*f* positions, namely the so called „dumb-bell" positions responsable for the magnetic properties. Nevertheless in the $Tb_2Ni_2Al_{15}$; $Tb_2Ni_3Al_{14}$ and $Tb_2Ni_6Al_{12}$ intermetallic compounds the nickel atoms occupy the 4*f* positions, due to the 4*e* positions occupied by the Tb atoms these compounds show different magnetic properties in comparison with the Tb_2Ni_{17} compound. The same magnetic behaviour have the other compounds with the 4*f* positions not occupied by the nickel atoms, i e Tb_2Al_{17}; Tb_2NiAl_{16}; $Tb_2Ni_7Al_{10}$.

In comparison with the ideal positions of Th_2Ni_{17} compound [5], in the investigated by us compounds the positions 2*c* and 4*e* are occupied.

The distribution of the atoms given in Table 5 explains the Ni concentration dependence of the c/a ratio and of the c parameter of the studied compounds.

At small concentrations of the nickel atoms when the occupied positions for the rare earth atoms, are $4e$, the dependence is linear, the curve has a negative slope. When the rare-earth atoms occupy the $2b$ and $2d$ positions the variation of the ratio c/a has a positive slope The variation of the parameter c is monotonous, but the slope is different in function of the occupied positions of the Tb atoms

The parameters z_f, z_k and z_e determined from the (00*l*) patterns have not a single well determined value, but a large range of variation In Tables 3 and 4 are presented the values z_f, z_k and z_e obtained for the $Tb_2Ni_1Al_{16}$ and $Tb_2Ni_2Al_{15}$ compounds The (00*l*) patterns intensities calculated with these parameters are in good agreement with the experimental intensities

3 **Conclusions.** From the X-ray investigations results that there is a continous solubility of the Tb_2Ni_{17} compound in the Tb_2Al_{17} compound with the general formula $Tb_2Ni_{17-x}Al_x$

This is suported by the a and c lattice parameters dependence on the nickel atoms concentration and by the structural model proposed for the X-ray intensity values of the compounds.

In spite of this, the used method does not allow the study of the statistic atoms distribution, but it points out clearly that the rare-earth atoms positions change from the $4e$ positions to the $2b$ and $2d$ positions — according with the other previous reported results [4]

REFERENCES

1 B E Warren, "X-Ray Diffraction", Addison—Wesley, Reading, Mass, 1969.
2 I Pop, V Crişan, M Coldea, G Borodi, *Physica*, **130 B**, (1985) 504—507.
3 V Crişan, I Pop, N Dihoiu, *Revista de Chimie*, **35** (1984) 174
4 H Figiel, K. Lemanska, A. Lemanski, A Kulac, A Semkowicz, *Acta Phys. Polonica*, **A 61** (1982) 99
5 W. B Perason, "A Handbook of Lattice spacings and Structures of Metals and Alloys", Nr 2, Pergamon Press, Oxford, 1967.

STUDIA UNIV BABEŞ—BOLYAI, PHYSICA, XXXII, 2, 1987

EFECT OF CRYSTALLINE FIELD ON THE MAGNETIC PROPERTIES OF DIAMAGNETIC IONIC CRYSTALS

I. GH. POP* and I. POP**

Received October, 12, 1987

ABSTRACT. — In order to study the radial influence of the crystalline field on the magnetic properties of the ionic crystalline systems we have introduced the anionic and cationic radial correction functions, the radial deformation coefficients for positive and negative ion and the overall radial correction coefficient. Thus, we obtain a method which correlates the radial deformation and the orbital overlap of the radial deformable ions.

1. **Introduction.** The magnetic properties of the ionic crystalline systems are determined by a Langevin diamagnetic susceptibility χ_d^L and a Van Vleck paramagnetic susceptibility χ_p^{VV} [1]. The radial deformation of the ions (cation and anion) in the presence of the crystalline field must be taken into account. The crystalline potential effects are of opposite signs for the cations and anions, thus there is an increase from free ions values of χ_d^L for the cations and a decrease for the anions [2] Because of the radial deformation of the ions there is an overlap of the radial deformable ions, this fact being the origin of the Van Vleck paramagnetism [3]. The reconsideration of this contribution to the magnetic susceptibility of the ionic systems [4] and a correct evaluation of the radial effect of the crystalline field on the free ion Langevin susceptibility allow us to make a more objective analysis on the magnetic behaviour of the ionic crystalline systems.

2. **Theoretical remarks.** The free state ion magnetic susceptibility of the diamagnetic systems given by

$$\chi_{d,l}^{[A^+][B^-]} = \chi_{d,l}^{[A^+]} + \chi_{d,l}^{[B^-]} \tag{1}$$

is modified in the presence of the crystalline field in the form

$$\chi_{cr}^{[A^+B^-]} = \chi_{d,cr}^{[A^+,B^-]} + \chi_p^{[A^+B^-]} \tag{2}$$

where $\chi_{cr}^{[A^+B^-]}$ is the measured χ magnetic susceptibility of the ionic diamagnetic crystalline system, and $\chi_{d,cr}^{[A^+,B^-]}$ represents the radial corected diamagnetic susceptibility of the ionic system given by (1).

* *Polytechnical Institute of Cluj-Napoca, Physics Departement, 3400 Cluj-Napoca, Romania*
** *University of Cluj-Napoca, Departmen of Mathematics and Physics, 3400 Cluj-Napoca, Romania*

In order to calculate the diamagnetic Langevin susceptibility in crystal system, $\chi_{d,\,\mathrm{cr}}^{[A^+,\,B^-]}$, we have introduced the radial anionic and cationic radial correction functions [5] defined by

$$g_{\mathrm{anion}}(r_C) = A - \frac{B}{r_C^2}, \quad g_{\mathrm{cation}} = \frac{r_C}{\mathrm{cr}_C - D} \tag{3}$$

with A, B, C, D coefficients given for each ionic system In such a way we can write

$$\chi_{d,\,\mathrm{cr}}^{[A^+,\,B^-]} = \sum_{\tau=A,\,B} \{\chi_{d,\,\mathrm{core}}^{\tau} + \chi_{d,\,\mathrm{outer}}^{\tau}\} = \chi_0 \sum_{\tau=A,\,B} \{\overline{(r_{nl}^2)}_{\tau}^{\mathrm{core}} + \overline{(r_{nl}^2)}_{\tau}^{\mathrm{outer}} g_{\tau}(r_C)\} \tag{4}$$

with $g_\tau(r_C)$ given in Fig 1. for alkali halides crystalline systems

The radial deformation coefficients for cations and anions can be obtained in the form:

$$k_{i,\tau} = \frac{\overline{(r^2)}_{\tau}^{\mathrm{crys}}}{\overline{(r^2)}_{\tau}^{\mathrm{free}}} = \frac{\overline{(r^2)}_{\tau}^{\mathrm{core}} + \overline{(r^2)}_{\tau}^{\mathrm{outer}} \cdot g_{\tau}(r_C)}{\overline{(r^2)}_{\tau}^{\mathrm{core}} + \overline{(r^2)}_{\tau}^{\mathrm{outer}}} \tag{5}$$

and the overall radial correction coefficient of the ionic crystalline system is defined by

$$k_i = \frac{k_{i,\,\mathrm{an}} \overline{(r^2)}_{\mathrm{an}}^{\mathrm{free}} + k_{i,\,\mathrm{cat}} \overline{(r^2)}_{\mathrm{cat}}^{\mathrm{free}}}{\overline{(r^2)}_{\mathrm{an.}}^{\mathrm{free}} + \overline{(r^2)}_{\mathrm{cat}}^{\mathrm{free}}} \tag{6}$$

represented for alkali halides crystals *versus* r_+/r_- ratio in Fig 2

Thus, the crystalline Langevin diamagnetic susceptibility of the ionic system, $\chi_{d,\,\mathrm{cr}}^{[A^+,\,B^-]}$, can be expressed in the form

$$\chi_{d,\,\mathrm{cr}}^{[A^+,\,B^-]} = k_i \chi_{d,\,i}^{[A^+,\,B^-]} \tag{7}$$

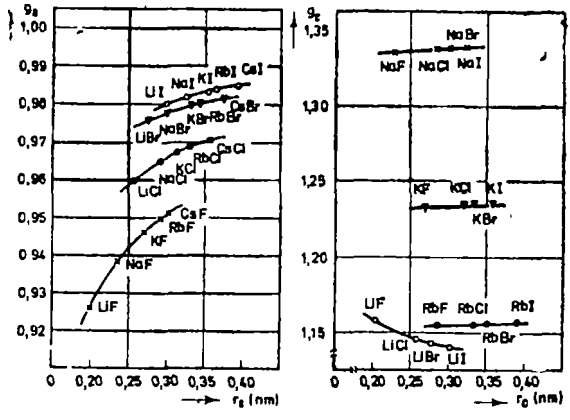

Fig. 1. Radial anionic and cationic correction functions for alkali halides crystals.

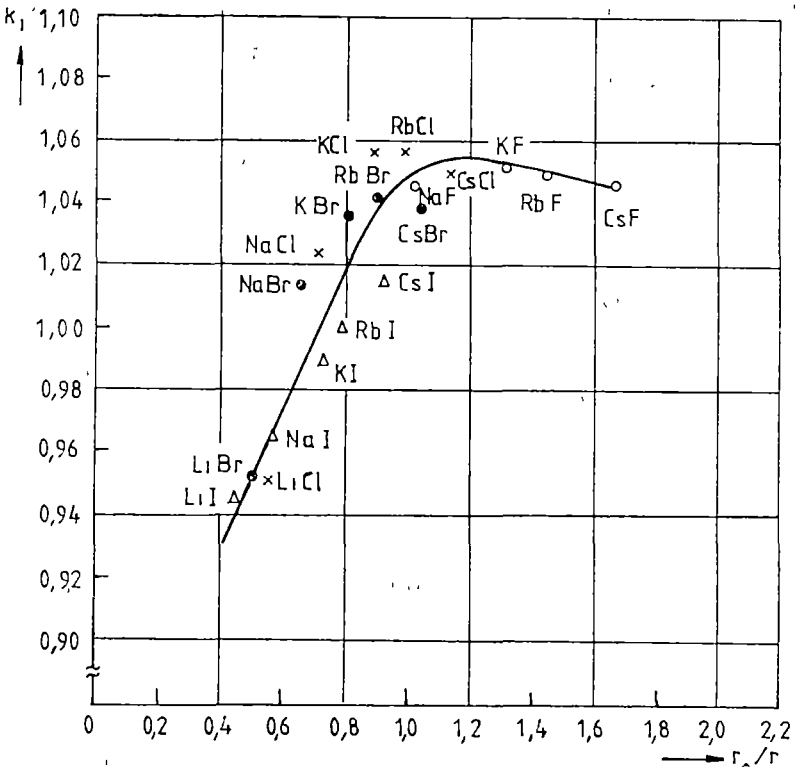

Fig 2 The overall radial correction coefficient for alkali halides crystals.

the overall effect of the crystalline field on the charge distribution of the ions in crystal resulting from diagram $\chi_{d,cr} - \chi_{d,i}$ (Fig. 3), for alkali halides, amonium halides and alkali earth oxides.

The magnetic measured susceptibility of the ionic crystalline system can be written in a Pascal scheme form [4, 6], thus

$$\chi = \sum_{ions}^{ions} \chi_{d,i} + \lambda_i \tag{8}$$

where λ_i is a correction term of positive sign, which contains the diamagnetic and paramagnetic contributions to the susceptibility, due to the radial deformation and the orbital overlap of the radial deformable ions [3, 4] From Fig 4, it is evident that the ionic crystalline systems have different magnetic properties than the same free ions systems

3. **Discussions and conclusions.** The effect of the crystalline field on the magnetic properties of diamagnetic ions in the ionic crystals can be studied using the radial correction functions, the increase of the cations and the decrease of the anions being well represented in isoanionic and isocationic series. The influence of the crystalline neighbourhood on the anion and cation is impor-

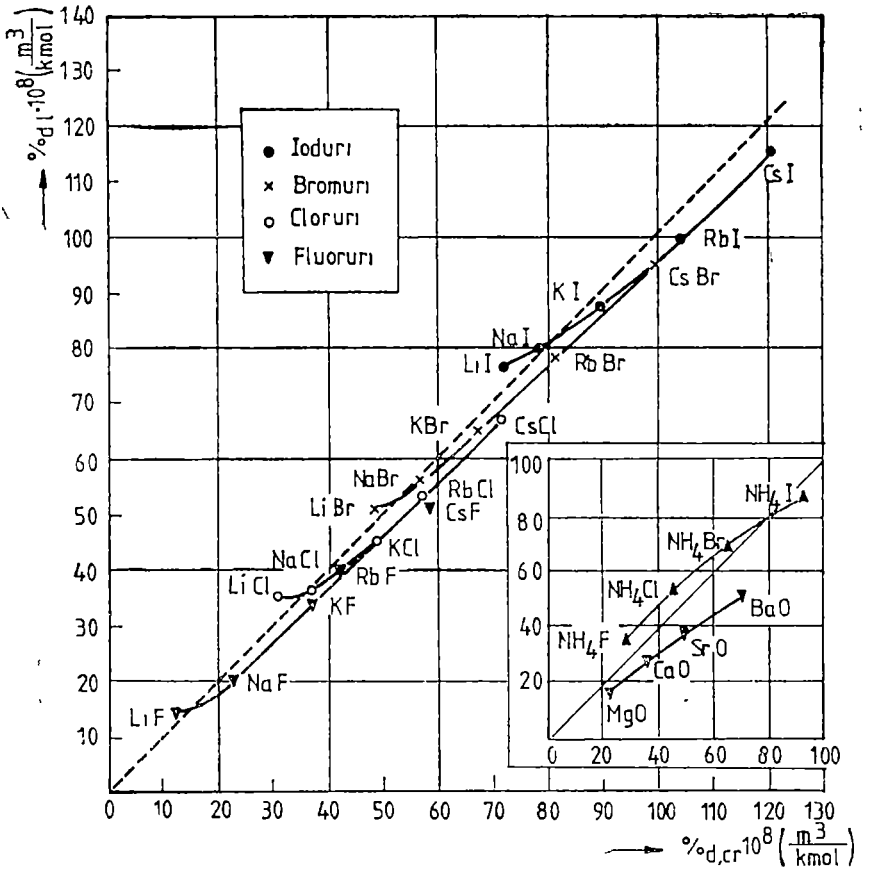

Fig 3. The radial crystalline field effect on the diamagnetic susceptibility for alkali halides, amonium halides and alkali earth oxides.

tant. In an isocationic series, the cationic radial deformation is constant and important, except the lithium halides where because of the small size of the lithium ion, the second order interaction in crystal becomes significant. In an anionic serie the deformation of the anion is increased in the same serie, the most significant increase being presented by F^-, Cl^- anions.

Values $k_i < 1$ correspond to systems with ratio $r_+/r_- < 1$, where the cationic radial deformation is negligible in relation to that of the anion partner (LiI, LiBr, LiCl, NaI, KI) A $k_i = 1$ value does not mean an absence of a radial deformation of ions, but a compensation of anionic and cationic radial deformation in crystal. The $k_i > 1$ values correspond to a radial deformation of the anion and cation too

The amonium halides and alkali earth oxides have a little different behaviour than alkali halides Thus the ammonium halides present a specific radial deformation (T_d group symetry of NH_4^+ ion), and the alkali earth oxides have a much greater cohesive energy than alkali and ammonium halides.

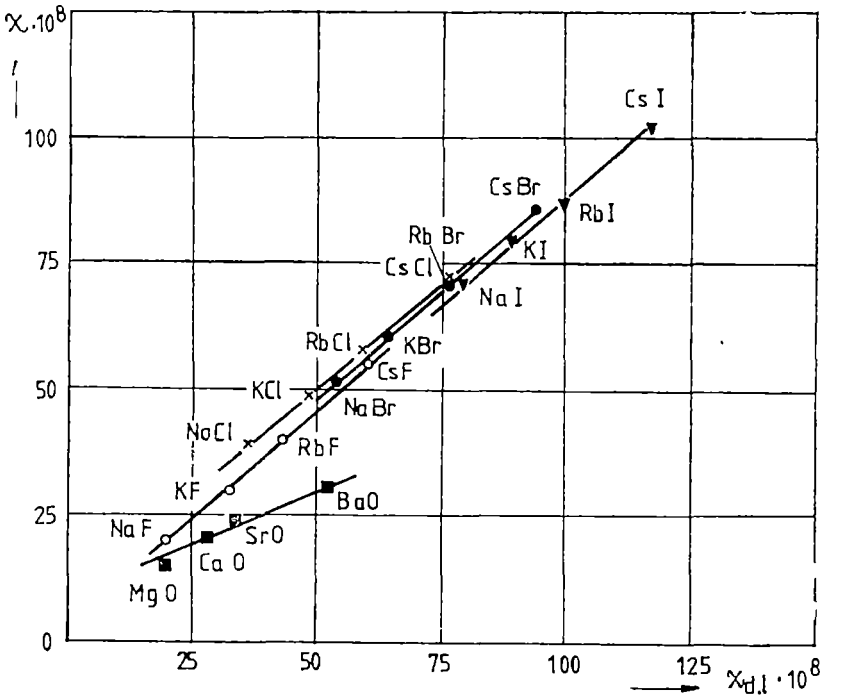

Fig. 4. The Pascal scheme for ionic crystalline systems.

The evaluation of radial crystalline field effect on magnetic properties of ionic systems, proposed by us, is more complet and practical than other methods known [7, 8], being correlated with orbital overlap of the radial deformable ions.

BIBLIOGRAPHY

1. Van Vleck, J. H., "The theory of electric and magnetic susceptibilities", Univ. Press., Oxford, 1932.
2. Schmidt, P. C., Weiss, Al., "Dass T. P.," *Phys. Rev*, **B 19**, 5525 (1979)
3. Pop, Gh. I., Pop I., "Imbroane Al. M.," *Studia Univ. Cluj-Napoca, Physica*, **XXX**, 61 (1985).
4. Dorfman, Ya. G., "Diamagnetizm i himiceskaja svjaz, Gos izd.," Moskva, 1961
5. Pop, Gh. I., Pop, I., Toşa, V., „Progrese în fizică", Iaşi, 1985, pag. 368.
6. Pop, Gh. I., *Thesis*, Univ. of Cluj-Napoca, 1987.
7. Petrasen, M. J., Abarenkov, J. V., Kristofel, N N, *Vestn. Len Univ* **16**, 7 (1960).
8. Sachs, L. M., *Phys. Rev.*, **124**, 1283 (1961).

STUDIA UNIV BABEŞ—BOLYAI, PHYSICA, XXXII, 2, 1987

OBTAINMENT OF MAGNETIC FIELD GRADIENTS AND ANALYSIS OF SPATIAL RESOLUTION IN EPR IMAGING

AL. NICULA*, S. AŞTILEAN*, M. TODICĂ* and S. NICULA*

Received November 18, 1987

ABSTRACT. — New developments of EPR imaging is presented and the general method for processing spin images is discussed A method for obtaining magnetic field gradients in the cavity of JES-3B spectrometer is also discussed. We contribute to a generalization of the expression for spatial resolution in EPR imaging in the case of nonlinear gradient superimposed in cavity

Introduction. Magnetic resonance imaging, both EPR and NMR, is concerned with the spatial distribution of electron or nuclear spins in heterogeneous samples and is performed to measure them, generally using magnetic field gradients. In reality, EPR imaging has some additional requirements although it is basically similar to NMR imaging First, the linewidths of samples are considerably broader compared to those of NMR Second there may be a hyperfine structure and this imposes the most severe requirement and finally, in investigating samples having magnetic anisotropy, an undesirable extrashift of resonant lines takes place [1] These requirements are all far from being completely resolved today On the other hand, EPR imaging has developed only of late and in the last few years it has begun to prove itself its application to various fields the knowledge about spatial distributions of paramagnetic species is available for studies on transport phenomena in solid films, biological systems and reactions of radiation products [2, 3, 4]. The first description concerning EPR imaging was made by Lauterbur [5]. Two reviews have been published which describe papers published to date in view of applications and give a perspective on the state of the art in EPR imaging and also discuss the future development of the field [1, 6]

1. **Interpretation of the EPR spectrum in magnetic field gradients.** We can show that the power absorbed by an elementary volume of the sample which exists at the resonance is:

$$P(x, y, z)\, dv \sim \chi''(x, y, z)\, H_m^2(x, y, z)\, dv \tag{1}$$

where: P(x, y, z) is power density, $\chi''(x, y, z)$ is the imaginary part of the local dynamic susceptibility and H_m is the amplitude strength of the microwaves field. We should bear in mind the fact that between $\chi''(x, y, z)$ and $\chi_0(x, y, z)$

* *University of Cluj-Napoca, Department of Mathematics and Physics, 3400 Cluj-Napoca, Romania*

there is a connection Introducing a normalized distribution function $c(x, y, z)$ of paramagnetic centres, we can define a generalized filling factor.

$$\overline{\eta} = \frac{\int\limits_{\text{sample}} c(x, y, z) \cdot H_1^2(\vec{r})\, dv}{\int\limits_{\text{cavity}} H_1^2(\vec{r})\, dv} \tag{2}$$

Thus, beside the classical expression of the filling factor, we have introduced a general filling factor through the normalized distribution function of paramagnetic centres $c(x, y, z)$. In EPR, the maximal absorbed power takes place providing the Larmor condition is fulfilled.

$$\omega = \gamma \cdot H_0 \tag{3}$$

In spatial nonlinear magnetic field gradients, in the most generla case, the local value of the resonant field is

$$H_0 = [(H + H_z(\vec{r}))^2 + H_y^2(\vec{r}) + H_x^2(\vec{r})]^{1/2} \tag{4}$$

were H is the variable homogeneous field directed along the z axis, and $H_{x,y,z}(\vec{r})$ are the components of the field which is superimposed in the cavity, dependent on the position r of the elementary volume. So the Larmor condition is fulfilled for a value of the H homogeneous magnetic field only in a certain sample, or only in a sample when we have more samples spatially distributed in the cavity We will deal with the most general case, that is of a tridimensional sample having a heterogeneous distribution $n(x, y, z)$ of paramagnetic centres.

The mathematical problem in EPR imaging is that of the reconstruction of the distribution $n(x, y, z)$ from the distribution $n(H_x, H_y, H_z)$, i e reconstruction from projections Let us consider first the distribution function $n(\vec{H})$. We can establish the relation.

$$n(\vec{H})\, dH = \frac{1}{N} \int\limits_{V(H)}^{V(H+dH)} n(x, y, z)\, dv = \frac{1}{N} \int \frac{n(x, y, z)}{|grad\, \vec{H}|}\, dS_H \cdot dH \tag{4}$$

$$H = -H_z(\vec{r}) + [H_0^2 - H_y^2(\vec{r}) - H_x^2(\vec{r})]^{1/2}$$

For a variation of the magnetic field H, we will obtain an overlapping of local spectra.

The EPR spectrum can be expressed mathematically as a convolution integral:

$$s(u) = \int\limits_{-\infty}^{+\infty} n(u') \cdot f(u - u')\, du' \tag{5}$$

where the variable u denotes the relative magnetic field, $u = H - H_0$, while H and H_0 stand for external magnetic field and the peak resonant field, respectively. The expression $n(u)$ corresponds to the distribution function $n(H)$ which one attempts to measure and $f(u)$ is the response function (or instrumental broadening plus lineshape function) A number of methods have been developed to solve Eq. (5) for $n(u)$, observing $s(u)$ and $f(u)$

The most widely used method is the Fourier method [7, 8] Since Eq (5) is the convolution integral, its Fourier transform is discribed as.

$$S(\omega) = F(\omega) \cdot N(\omega) \tag{6}$$

where $F(\omega)$ and $N(\omega)$ are the Fourier transforms of $f(u)$ and $n(u)$, respectively. Then, since $s(u)$ and $f(u)$ can be determined experimentally as follows

1) $s(u)$ — the EPR spectra in magnetic field gradients,

2) $f(u)$ — the EPR response spectra in a homogeneous magnetic field, finally $n(u)$ can be calculated by

$$n(u) = (2\pi)^{-1} \int_{-\infty}^{+\infty} \frac{S(\omega)}{F(\omega)} \quad exp\ (i\omega u)\, d\omega \tag{7}$$

Next, as we have pointed out, the distribution function of the paramagnetic centers $n(x, y, z)$ is to be derived from the distribution $n(H_x, H_y, H_z)$. The reconstruction of the function $n(x, y, z)$ has not been solved yet But, the overpassing of this difficulty is made using constant magnetic field gradients

$$\begin{aligned} H_0 &= H + \left(\frac{\partial H_z}{\partial z}\right) \cdot z + \left(\frac{\partial H_z}{\partial y}\right) \quad y + \left(\frac{\partial H_z}{\partial x}\right) \cdot x = \\ &= H + G_z \quad z + G_y \quad y + G_x \cdot x \end{aligned} \tag{8}$$

There are few published results which use non-constant magnetic field gradients [9, 10] in EPR imaging and we are not dealing here with use time dependent gradients.

2 **Obtainment of the magnetic field gradient.** There are many methods to obtain magnetic field gradients A simple configuration is the Maxwell pair, which is a pair of circular coils each with radius a, more likely a Helmoholtz system, but with opposing currents This system gives zero field in the midplane. The magnetic field in the M point situated at the z distance from the midplane, on the symetry axis, is

$$H_z(z) = \frac{NIa^2}{2} \quad \{[a^2 + (b + z)^2]^{-3/2} - [a^2 + (b - z)]^{-3/2}\} \tag{9}$$

where $2b$ is the distance between the two coils, and N is the number of turns

Eq (9) can be expanded as a Taylor series and we find this expression in the first order of aproximation

$$H_z(z) = \frac{NIa^2}{2} \cdot [-6b(a^2 + b^2)^{-5/2}] \cdot z \tag{10}$$

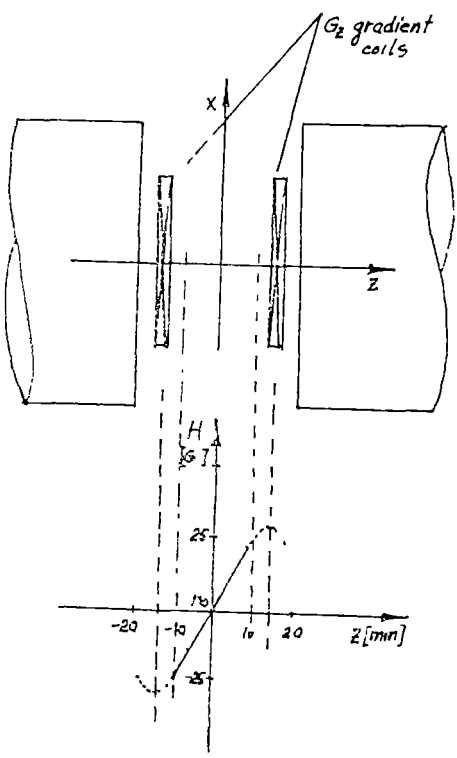

Fig. 1. The arrangement of gradient coils

Thus, for $z \in [-z_0, z_0]$ and $z_0 \ll b$, in cavity a constant gradient is superimposed along the homogeneous magnetic field The value of the magnetic field gradient is·

$$G_z \equiv |\, grad\, H_z| = \frac{NIa^2}{2}\,[-6b(a^2 + b^2)^{-5/2}] \tag{11}$$

The optimum magnetic field gradient is obtained when $2b = a\sqrt{3}$, [11] In our preliminary calculations, we have observed the condition imposed by the JES-3B spectrometer, i e the avaiable space for the arangement of coils (see Fig 1). In this case we estimate the minimal practical value at about 25 G/cm.

3. The spatial resolution in EPR imaging. In a pioneering experiment many workers [1] achieved one-dimensional EPR imaging using simple constant gradient coils on a standard EPR spectrometer and they performed experiments on a phantom sample or spatially separated samples. Most recently, EPR imaging by using nonconstant magntic field gradient, i.e. dipolar fields [10], has been developed for also a phantom sample consisting of four capillary tubes containing DPPH substance The theoretical study of spatial resolution on a constant magnetic field gradient has been discussed and a resolution of about 10 μm has been estimated [12] (if linewidth is of 1 G and a magneticfield gradient of 10^3 G/cm)

In this part, the aim of our study is to derive a general mathematical formulation of spatial resolution, when a nonlinear magnetic field is used in EPR imaging Let two volume elements, with signals just barely detectable separately, have the distance Δz In the presence of the nonlinear magnetic field parallelly applied to the laboratory homogeneous variable field H, the EPR spectra spatial shift of the two volume elements is·

$$H_1 = H_0 - H_z(z_1) \;\; and \;\; H_2 = H_0 - H_z(z_2) \tag{12}$$

where $H_z(z)$ is the gneral form of the nonlinear magnetic field superimposed in cavity We write the expansion function $H_z(z)$ using Taylor's formula

$$H_z(Z_2) = H_z(z_1) + \Delta Z \;\; \frac{dH(z)}{dz}\bigg|_{z=z_1} + \ldots \tag{13}$$

Spatially separated volume elements can be detected as separate peaks if their „distance" in variable field is $\Delta H = \sqrt{2\ln 2} \cdot \Delta H_{1/2}$, for a Gaussian lineshape. Then using Eq. (12) and Eq. (13) ΔH is given by

$$\Delta H = \Delta z \cdot \frac{dH_z(z)}{dz} \tag{14}$$

and, therefore, *spatial resolution* Δz, can be reprezented by the expression:

$$\Delta z = \frac{\Delta H_{1/2}}{\sqrt{2\ln 2}\left(\frac{dH_z}{dz}\right)} = \frac{\Delta H_{1/2}}{\sqrt{2\ln 2} \cdot |grad_z H(z)|} \equiv f(\Delta H_{1/2}, z) \tag{15}$$

Discusions Admitting $H_z(z) = Cz^k$, as the general form of a nonlinear magnetic field

1) If $k = 1$, we find $G_z \equiv |grad_z H(z)| = constant$, and the spatial resolution, first proposed in [12], is

$$\Delta z = \frac{\Delta H_{1/2}}{\sqrt{2\ln 2} \cdot G_z} \tag{16}$$

This expression is well-established in EPR imaging with constant magnetic field gradient.

2) If $k = -3$ and $C = -|\vec{m}|$ (the magnetic dipole moment of a permenent magnet) we have a magnetic field with dipolar structure [10] and the spatial rezolution Δz can be reprezented by:

$$\Delta z = \frac{\Delta H_{1/2}}{\sqrt{2\ln 2} \cdot 3m} \cdot z^4 \sim z^4 \tag{17}$$

Thus, using nonlinear magnetic fields, we shall not lobtain the same resolution in the whole volume. This fact will complicate the obtaining of the distribution function of paramagnetic centers, but the problem can be solved and it stands in our view.

However, if the number of paramagnetic spins Δn involved in a volume fraction defined by Δz in the sample, and $\Delta n/\Delta H$ is less that the sensitivity of EPR spectrometer, then the resolution depends upon the concentration of the spins rather than upon the field gradient Evidently the narrower the line, the higher the resolution becames and also the more advantageous its signal-to-noise ratio is. We note that the spin-spin exchange phenomenon is another limit of resolution for high concentrated paramagnetic spins.

4. Conclusions. In the first part of our paper we have presented, according to the reference literature, the problems of processing spins images in EPR imaging. We have directed our attention toward the Fourier transform — a method which we will device in the avaiable technique at the University of Cluj-Napoca Laboratory.

In the second part, referring to our previous results [10] we have analysed the spatial resolution in EPR imaging in nonconstant magnetic field gradients,

i.e. dipolar field. We have presented the advantages and disavantages of this method compared with the use of constant gradients. In this paper a method for obtaining the constant magnetic field gradient in the cavity of JES-3B spectrometer has been discutssed. According to our laboratory conditions a gradient of about 25 *G*/cm has been estimated.

REFERENCES

1. K. Ohno, *Applied Spectroscopy Rev*, **22** (1), 1—56 (1986) and *Magn. Reson Rev*, vol 11, pp. 275—310, 1987.
2. L. J. Berliner and H Fujii, J *Magn Reson*, **69**, 68—72 (1986).
3. K. Ohno, *J. Magn. Reson*, **64**, 109—114 (1985).
4. F. Demsar, P. Ceve and M Schara, *J. Magn. Reson*, **69**, 258—263 (1986)
5. P. C. Lauterbur, *Nature (London)*, **242**, 190 (1973)
6. S. S. Eaton and G. R. Eaton, *Spectroscopy I*, **32** (1986).
7. L. C. Alen, et al., *J. Chem Phys.*, **40**, 3135 (1964)
8. T. Inoue, *Nucl. Instrum. Methods*, **104**, 541 (1972)
9. O. E. Yakimehenko, et. al., *Dokl. Akad Nauk SSSR*, **268**, 384 (1983).
10. Al. Nicula, S. Nicula, L. Giurgiu and I Ursu, *Studia, ser Physica*, **XXXI**, 1 1986.
11. I. A. Tanner, *Rev. Sci. Instrum*, **36**, 1086 (1965).
12. W. Karthe and E Wehrsdorfer, *J Magn Reson*, **33**, 107—111 (1979)

STUDIA UNIV BABEŞ—BOLYAI, PHYSICA, XXXII, 2, 1987

MAGNETIC SUSCEPTIBILITY STUDIES OF $x Cr_2O_3 \cdot (1 - x)[2P_2O_5\ Na_2O]$ GLASSES

I. ARDELEAN*, GH. ILONCA*, O. COZAR* and IL EANA ARDELEAN*

Received September 18, 1987

ABSTRACT. — Magnetic susceptibility measurements have been performed on $x Cr_2O_3\ (1 - x)[2P_2O_5 \cdot Na_2O]$ glasses with $0 < x \leqslant 20$ mol % Data suggest that in the glasses with $x \geqslant 10$ mol % the chromium ions undergo negative exchange interactions From Curie constant and atomic magnetic moment values we have established that in these glasses both Cr^{3+} and Cr^{5+} ions are present, the latter being in small proportion

Introduction. Several experimental results suggest that the valence states and distribution mode of the transition metal ions in the network of the oxide glasses depend on the matrix structure [1], preparation conditions [2] and nature of the transition metal ions [3]. Up to now, the EPR [4—8] studies of the oxide glasses with chromium ions have suggested the presence of Cr^{3+} ions only, which may be magnetically isolated or coupled by negative super-exchange magnetic interactions In [9] we have evidenced that in the lead-borate glass matrix both Cr^{3+} and Cr^{5+} ions are present, the latter being in small proportion, in agreement with the atomic magnetic moment values, $\mu_{at} = (3\,82 \pm 0\,07)\mu_B$ In these glass system, for concentrations $x \leqslant 20$ mol% Cr_2O_3, the isolated Cr^{3+} ions coexist with those coupled by negative super-exchange magnetic interactions, the isolated ones prevailing only for $x < 3$ mol% Cr_2O_3

In order to provide further information on the chromium in oxide glasses, results of magnetic susceptibility studies of chromium ions in soda-phosphate oxide glasses are reported in the present paper.

Experimental. $x Cr_2O_3 \cdot (1 - x)[2P_2O_5 \cdot Na_2O]$ glasses, with $0 < x \leqslant 20$ mol% were studied, maintaing the P_2O_5/Na_2O ratio constant, that is keeping the matrix structure unmodified In this way, the glass matrix $2P_2O_5 \cdot Na_2O$ was initially prepared by mixing $NH_4H_2PO_4$ and Na_2CO_3 and melting this admixture in a sintered corundum crucible We used a technique previously reported [10] After cooling, the host glass was crushed and the resulting powder was mixed with appropriate amounts of Cr_2O_3, before final melting at $T_M = 850\,°C$ for 0 5 h The molten glass was poured onto a stainless-steel plate. The structure of these glasses was studied by X-ray diffraction analysis and did not reveal any crystalline phase up to 20 mol% Cr_2O_3.

Magnetic susceptibility data were obtained with a Faraday type balance in the temperature range 80 to 300 K

Results and discussion. The temperature dependence of the reciprocal magnetic susceptibility of the various glasses is presented in Fig 1 For the glasses

* *University of Cluj-Napoca, Department of Mathematics and Physics, 3400 Cluj-Napoca, Romania*

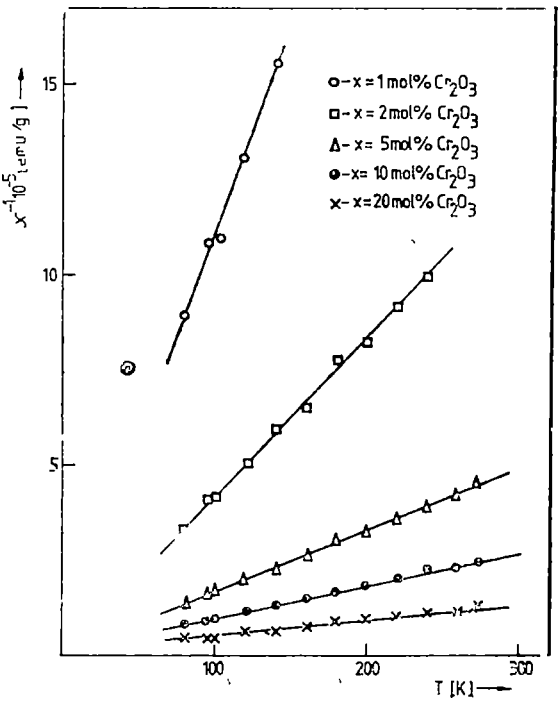

Fig. 1. Temperature dependence of the reciprocal magnetic susceptibility.

Table 1

Curie constants, magnetic moments and paramagnetic Curie temperatures

x [mol% Cr_2O_3]	C_M [emu/mol]	μ_{at} [μ_B]	θ_p [K]
1	0.02722	3.31	0
2	0.07076	3.76	0
5	0.17465	3.74	0
10	0.34060	3.71	−20
20	0.68756	3.72	−45

with a Cr_2O_3 content < 10 mol%, a Curie law is observed. This suggests that the predominant part of chromium ions are isolated and that no magnetic order is present. For a Cr_2O_3 content $\geqslant 10$ mol% the reciprocal magnetic susceptibility obeys a Curie—Weiss law behaviour, with a negative paramagnetic Curie temperature.

For the glasses with $x \geqslant \geqslant 10$ mol% Cr_2O_3, the high-temperature susceptibility data indicate that the chromium ions in the glasses undergo negative exchange interactions and are coupled antiferromagnetically In this case, the antiferromagnetic order takes place only at short-range, and the magnetic behaviour of the glasses can be described by the so-called mictomagnetic [11] type order.

This behaviour is in accord with EPR studies [12] A similar conclusion was reached by Landry *et al* [5] and confirmed by Fournier *et al.* [6] Theoretical calculations [13—15] have shown that negative exchange interaction can occur in amorphous systems.

The composition dependence of the paramagnetic Curie temperature, θp, is presented in Table 1. The absolute magnitude of the values of θp increases when the Cr_2O_3 content increase

To determine accurately the values of the Curie constants, C_M, and atomic magnetic moments, μ_{at}, a correction due to the diamagnetism of the glass matrix and Cr_2O_3 was taken into account The composition dependence of the Curie constants, C_M, is presented in Fig 2 The values of the Curie constant, which is proportional to the ion concentration, vary linearly with the chromium ion concentrations For the glasses with $x \geqslant 2$ mol% Cr_2O_3, the experimental values obtained for the atomic magnetic moment $\mu_{at} = (3.74 \pm 0.03)\,\mu_B$, where μ_B is the Bohr magneton (see Table 1) are very close to the magnetic moment of Cr^{3+} cations in the free ion state:

$\mu_{Cr^{3+}} = 3.87\ \mu_B$ [16], in agreement with the behaviour usually observed in paramagnetic salts [16], containing chromium ions. The smaller values obtained for the atomic magnetic moments of glasses with $x \leqslant 20$ mol % Cr_2O_3 may be attributed to the presence of Cr^{5+} ions, for which the atomic magnetic moment in the free-ion state is $\mu_{Cr^{5+}} = 1.73\mu_B$ [16]. The presence of these ions in the glass with $x = 1$ mol % Cr_2O_3 was evidenced by EPR measurements [12] Except this sample for which $\mu_{at} = 3.31\ \mu_B$, in the other samples the proportion of Cr^{5+} ions is small compared to the proportion of Cr^{3+} ions

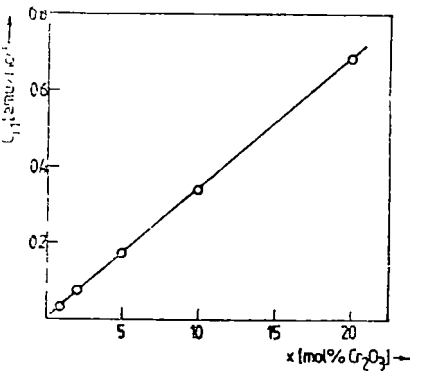

Fig 2. Composition dependence of the Curie constant.

Conclusion. By means of magnetic susceptibility studies, the xCr_2O_3 $(1 - x)[2P_2O_5 \cdot Na_2O]$ glasses with $0 < x \leqslant 20$ mol% were studied, obtaining information concerning the chromium ion distribution in the glass matrix, which explains their magnetic behaviour.

Magnetic properties of $xCr_2O_3 \cdot (1 - x)[2P_2O_5 \cdot Na_2O]$ glasses are dependent on the Cr_2O_3 content. For the glasses with $x \geqslant 10$ mol% Cr_2O_3, chromium ions undergo negative exchange interactions and are coupled antiferromagnetically From atomic magnetic moments values it results that the antiferromagnetic coupling is achieved between Cr^{3+} cations, which are predominant at the whole concentration range

REFERENCES

1 E Burzo, I Ardelean and I Ursu, *J Mater Sci*, **15**, 581 (1980).
2 E Burzo, I Ursu, D Ungur and I Ardelean, *Mater Res Bull*, **15**, 1237 (1980).
3 I Ardelean, Gh Ilonca, D Bărbos and H Adams, *Solid State Commun.*, **40**, 769 (1981)
4. V K Zakharov and D M Yudin, *Soviet Phys Sol Stat*, **7**, 267 (1965).
5 R J Landry, J T Fournier and C G Young, *J Chem Phys*, **46**, 1285 (1967).
6 J T Fournier, R J Landry and R H Bartram, *J Chem Phys*, **55**, 2522 (1971).
7 E I Abdrashitova, R Ya Rhodakovskaya and N I Kharkova, *Inorg. Mater USSR*, **8**, 1966 (1968)
8 I V Chepeleva, E R Zhilinskaya, V V Lazukin and A P Cernov, *Phys Stat Sol (b)*, **73**, 65 (1976)
9 I Ardelean, Gh Ilonca, M Peteanu, D Bărbos and E Indrea, *J Mater. Sci*, **17**, 1988 (1982)
10 O. Cozar, I Ardelean, Gh Ilonca, *Proceedings of the XXIII Congress* AMPERE *on Magnetic Resonance*, Ed by B. Maraviglia, F De Luca and R Companella, Instituto Superiore di Sanita, Roma, September 15—19, 1986, p 248
11. J H Coey, *J Physique*, **35**, C6—89 (1974)
12 O Cozar, I Ardelean, Gh Ilonca, in press
13 A W Simpson, *Phys Stat Sol*, **40**, 207 (1970).
14 S Kobe and K Handrich, *Phys Stat Sol*, **42**, K69 (1970).
15 R Hasegawa, *Phys Stat Sol b*, **44**, 613 (1971)
16 E Burzo, „Fizica Fenomenelor Magnetice", vol 1, Ed Acad RSR, Bucureşti, 1979, p 241.

STUDIA UNIV BABEŞ—BOLYAI, PHYSICA, XXXII, 2, 1987

MAGNETIC BEHAVIOUR OF THE α-Fe_2O_3 OXIDE

LILIANA POP* and IULIU POP*

Received October 2, 1987

ABSTRACT. — The temperature dependence of the magnetic susceptibility was carried out for the α-Fe_2O_3 oxide between 100 and 1.350 K Results show that for the temperature range between 964—1.350 K the magnetic susceptibility is temperature independent, that is very peculiar for a transition element oxide This means that some kind of magnetic order still persists up to 1 350 K, and the paramagnetic state commences at much higher temperature

Introduction. The α-Fe_2O_3 oxide crystallises in the corundum type of structure. The unit cell with the rhombohedral system of crystallisation contains two Me_2O_3 unit formulas and belongs to the $D^6_{3d} - R\bar{3}c$ space group. The cations are distributed along the thernary axis in the 4c seats and the anions in the 6c positions The crystalline parameters are. $a = 5.424$ A; $\alpha = 55°17'$, $u = 0.355$, and, $x = 0\,552$ The corundum type of structure is based on a little deformed compactness of the O^{-2} ions, where half of the octahedral seats are occupied with perfect regularity by Me^{3+} cations. Alternating anionic and cationic layers may be separated in the corundum structure; the cations being distributed along the thernary axis, while the anions are distributed along the $\bar{3}$ axis As a result one obtaines a structure formed of MeO_6 octahedrons disposed in an infinite chain along the direction of the rhombohedral axis. Because of the exchange and electrostatic interactions the anions and the cations are shifted from their ideal seats and the alternating layers are goffered. So the ideally centered anionic octahedrons cationic centered are deformed by the supplemental atractive forces between this cations, but the three oxigen ions diverge, while the corresponding ions from the nearest neighbor anionic layers converge, determining so a high screening of the positive electric charges. These shifts are different for the concrete cases of the compounds and determine different values of the exchange energy interactions and, consequently, different magnetic spin structures [1].

In such-type structure Ishikawa and Akimoto [2] evaluated four types of the exchange intreactions Γ_a, Γ_b, Γ_c and Γ_d The higher values of the exchange energy have the first two interactions Γ_a and Γ_b, because of the cation-anion-cation biggest angle, which allows for larger overlapping of the d-orbitals of the cations over the p-orbitals of the anions The exchange energies Γ_c and Γ_d have less essential role in the direct exchange. From the analysis of the different possible kinds of antiferromagnetic ordering in the corundum structure there results three possible types of ordering with an u-parameter. Shull, Strauser and Wollan [3] pointed out that hematite, α-Fe_2O_3, at

* *University of Cluj-Napoca, Department of Mathematics and Physics, 3400 Cluj-Napoca, Romania*

$T_N = 948$ K passes from the paramagnetic state in the antiferrromagnetic state with the spin magnteic moments oriented perpendicular on the *c*-axis, but at 250 K the spin magnetic moments are oriented antiferromagnetically on the direction of the *c*-axis, the rhombohedron axis as · +——+, in accordance with the first mode of the antiferromagnetic ordering, whence the specific temperature dependence of the magnetic susceptibility

Experimental results and discussion. The temperature dependence of the magnetic susceptibility for α-Fe_2O_3 oxide in the temperature range 100—1.350 K and in the magnetic field of 9 500 G intensity was pointed out using a Weiss—Forrer equipment with 10^{-8} cm³/g sensitivity.

According to the magnetic spin structure pointed out by neutrons diffraction [3], the temperature dependence of the magnetic susceptibility has a particular character, as one can see from Fig. 1

Magnetic susceptibility changes with temperature increase in three stages. Below $T_{sr} = 250$ K when the magnetic spin moments are oriented antiferromagnetically parallel to the *c*-axis of the crystal α-Fe_2O_3, the magnetic susceptibility remaine practically temperature independent at the value of $14\,4 \cdot 10^{-6}$ cm³ g^{-1}, and at T_{sr} jumps up to $49\,4 \cdot 10^{-6}$ cm³ g^{-1} For $T > T_{sr}$ the magnetic spin moments are antiferromagnetically ordered but oriented perpendicular to the *c*-axis, and the magnetic susceptibility remains almost constant up to 780 K and then falls like for a ferromagnetic in the neighborhood of the Curie temperature, up to the value of $18\,8 \times 10^{-6}$ cm³g^{-1}, corresponding to the paramagnetic state. So, this temperature corresponds to the critical temperature for transition from the antiferromagnetic state to paramagnetic state, i.e the Néel temperature, determined from neutronografic measurements to be T_N=948K. From the magnetic measurements it results that the critical temperature is

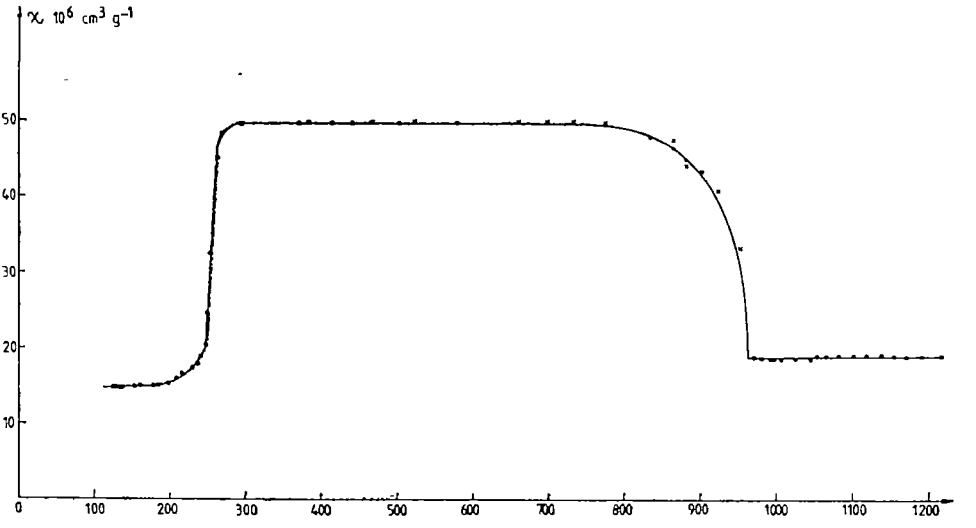

Fig 1.

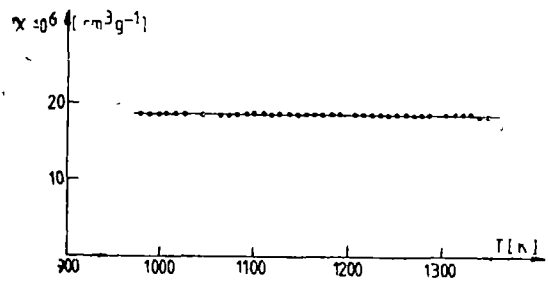

Fig. 2.

situated a little higher, at 964 K, but it is not sure if that is the Néel temperature, because in the paramagnetic region the magnetic susceptibility is not temperature dependent up to 1,350 K, the temperature we could reach

Fig. 2 shows the paramagnetic susceptibility as temperature function between 964 and 1.350 K. As can be seen, the magnetic susceptibility is constant in this temperature range. This result is very peculiar for the transition element oxide with localised magnetic moments. For such kind of materials, in the paramagnetic region the temperature dependence of the magnetic susceptibility must usually fallow the Curie—Weiss law and can not be a Pauli paramagnetism

So, we consider that this experimental result is a new one for α-Fe_2O_3 oxide, not relevated so far. The temperature independent magnetic susceptibility for $T > T_N$, means that the critical temperature obtained from neutron diffraction data at 948 K, or from magnetic measurements at 964 K, is actually a critical temperature for the transition of order-order type, and not order-desorder type, i e it is not a Néel temperature, as it has been considered so far.

The temperature independent magnetic susceptibility in such a large temperature range may show that some kind of magnetic order persists still up to 1,350 K, and the paramagnetic region is situated at much higher temperature.

3. Conclusions. The temperature dependence of the magnetic susceptibility for α-Fe_2O_3 oxide in the temperature range 100—1 350 K changes in three stages, each stage being connected with the specific magnetic spin structure. The last stage considered so far as paramagnetic state for $T > 948$ K, in fact is not a paramagnetic state, but the spin structure has not been determined yet. Between 964 K and 1 350 K the magnetic susceptibility is temperature independent, and can not be a paramagnetic state in this temperrature range. The paramagnetic region is situated at more higher temperatures than 1.350 K. So, the Néel temperature considered so far as $T = 948$ K is not an order-desorder critical temperature, but order-order critical temperature for the α-Fe_2O_3 oxide.

REFERENCES

1 Yu. A Iziumov, R P. Ozerov, "Magnitnaia neitronografia", Izd "Nauka", pp 340—359, Moskva, (1966)
2. Y. Ishikawa, S Akimoto, *J Phys. Soc. Japan*, **12**, 1083 (1957)
3. C. Shull, W. Strauser, E. Wollan, *Phys Rev*, **83**, 333, (1951)
4. Liliana Pop, *Teză*, Universitatea din Cluj-Napoca (1987)

STUDIA UNIV BABEŞ—BOLYAI, PHYSICA, XXXII, 2, 1987

IN SITU EXPERIMENTS ON EGGS RADIOACTIVITY BETWEEN 1-st TO 30-th OF MAY 1986

C. COSMA*, K. KOVÁCS*, T. FIAT*, FELICIA COSMA** and L. MÂNZAT*

Received October 23, 1987

ABSTRACT. — Some aspects on the radioactivity of hen eggs laid between May 1—30, 1986 are presented It is konown fact that eggs behave as radionuclides sepparators as follows: the ^{131}I is concentrated in the egg content and ^{140}Ba in the egg shell.

Introduction. Intense radioactive fall-out between May 1 and 10, 1986 caused by the radioactive cloud passing over Romania was favoured by the rain in some zones during the time [1—4] Our laboratory measurements indicated an initial fall-out of over 10^6 Bq/m^2 (gamma global) because of the torrential rain in the city of Cluj-Napoca on May 10, at 5 p m. (more than 30 l/m^2 = 30 mm) [3] compared with the annual time average of 150.000—200 00 Bq/m^2 [2].

There were prevalent nuclides of ^{132}Te, ^{132}I and ^{131}I in this initial fall-out. The ratio between the activity of ^{132}Te to ^{131}I was of 1.5 in the samples of water from the mentioned zone on May 1. A good fraction from ^{131}I and ^{132}I went back in the atmosphere due to the nice and warm weather that followed after May 1. The measurements carried out on a sample of sediment, which was uncovered, exposed until the May 17 showed that about 2/3 of the total amount of ^{131}I went back to the atmosphere. This fact is sustained by the large radioactive activity of the atmosphere in the city of Cluj-Napoca (40 Bq/m^3) [5]. The great quantity of ^{132}Te discovered in the rain water on May 1 is in a good agreement with the amounts of these nuclides leaked in the atmosphere [6] and also in accordance with measurements made in other laboratories [7]

In the adjacent zones of the city of Cluj-Napoca, where no rain was recorded between May 1—5, the quantity of ^{132}Te decreased for 4 to 5 times, as previously reported [1].

In the order of importance, the following radionuclides: $^{140}Ba + ^{140}La$, $^{103}Ru + ^{103}Rh$, $^{95}Zr + ^{95}Nb$ contributed to the total activity during the month of May. There were identified ^{134}Cs, ^{136}Cs, ^{137}Cs, $^{90}Mo + ^{90}Te$, ^{106}Ru, ^{129m}Te, ^{135}Sb, ^{110m}Ag, ^{141}Ce, ^{144}Ce in the rain water and other samples from the surrounding environment, beside, the mentioned nuclides

There was no evidence in our records of pure beta radionuclides (^{98}Sr, ^{90}Sr etc.) due to used gamma spectrometry method

The grass was mostly contaminated component part of the environment and it contaminated rapidly the great majority of foods The grass radioactive

* *University of Cluj-Napoca, Departament of Mathematics and Physics, 3400 Cluj-Napoca, Romania*
** *Sanitary College of Cluj-Napoca, 3400 Cluj-Napoca, Romania*

contamination has penetrated immediately in all animal products milk, butter, cheese, meat, eggs etc. We are taking in study the external contamination of grass due to the radioactive fall-out during the period of time involved (May 1—15). Some fast rising plants with more intensive substance exchange through leaves as spinach, lettuce, stinging, nettles, presented increased internal contamination.

Experimental method. Identification of the radionuclides was done by a 512 channel analysor of NTA—512 M type, coupled to a GeLi detector of KOVO 327-type The total gamma activity was measured by a 4 channel analysor of NP—424 type coupled to a NaI(Tl) detector of ample size (75 × 45 mm) The measurements were done in an integral regime ($E_\gamma > 80$ keV), with the detector and the sample in a lead tower. The geometry efficiency factor of the apparatus is known with a precision around 30% [8, 9] in this case. Experimental measurements involved the following aspects

a) daily examination of eggs activity;

b) measurements on the activity of two lots of eggs one lot of eggs from hens which were partially fed with contaminated grass and the other one from hens which were fed with uncontaminatedfood, but sitting in open air on a concrete ground;

c) observing the nuclide repartition in the egg shell and the content of the egg,

d) the decreasing of the mostly contaminated eggs activity *versus* time

Results and discussion. Fig. 1 presents the activity evolution (counting speed, imp /10 s) for eggs from hens fed with grass and for eggs from hens not fed with grass.

We can notice in Fig 1 that the eggs activity *versus* time (from the hens fed with no grass) is maintained at a relative low value, corresponding to a counting speed of around 100 imp/10 s, between May 5—15, while the activity of the eggs from hens fed with grass is 5 times greater between May 2—10 The activity of the eggs from hens fed with grass presents two peaks The first is higher on May 5 and 6, due to the massive fall out on May 1 and 2 (rain), and the second peak is higher on May 9 and 10, which corresponds to some new accentuated fall-out in that zone between May 6 and 7

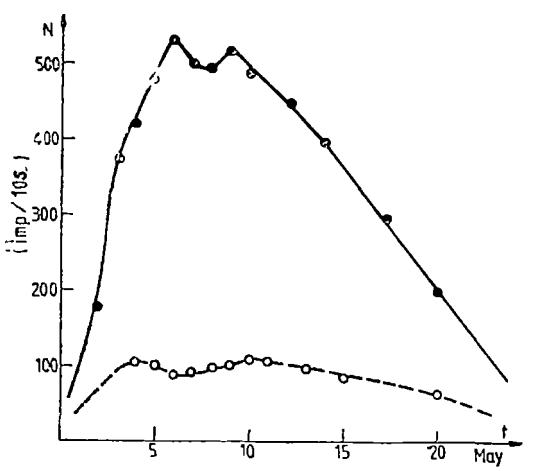

Fig. 1. Time evolution of eggs activity ● — with grass, ○ — with no grass.

Fig 2 represents the gamma spectrum for the egg shell and Fig 3 represents the same for the egg content

Spectra were made for the shells and the content of two eggs, on May 8 The eggs were reaped on May 6

The shells had over 50% from the total gamma activity, concentrating a great amount of $^{140}Ba + ^{140}La$ as can be seen from these spectra This fact can be explained if we consider that the egg shell contains a great quantity of calcium which has a chemical analogy with barium. The fact that the maximum eggs activity is reached after 2 or 3 days, later than the maximum activity of the

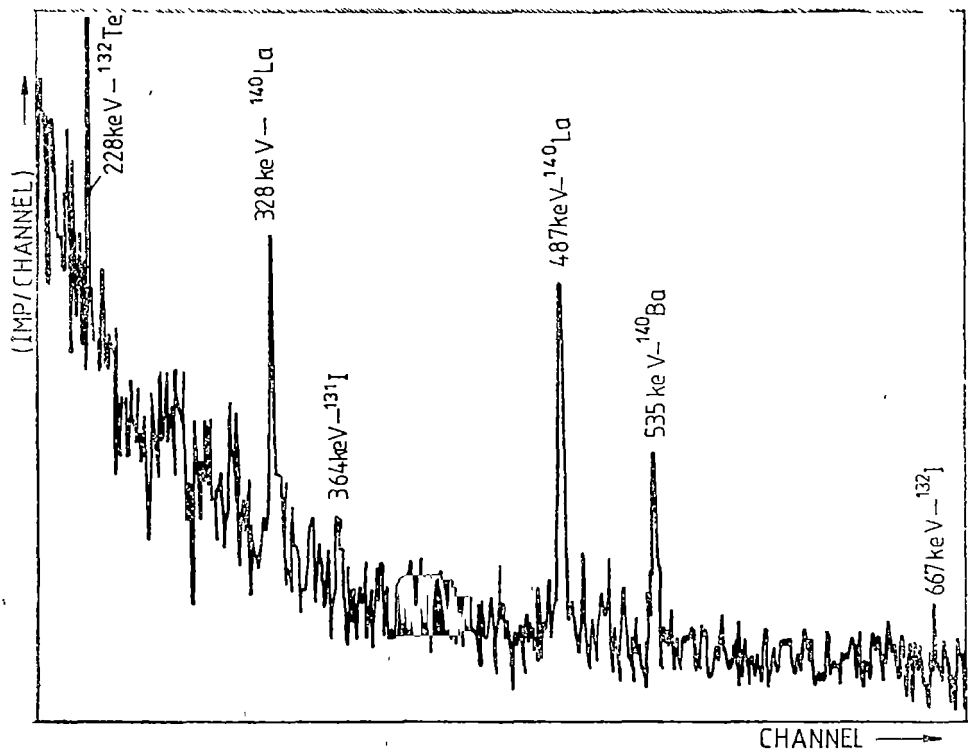

Fig. 2. Gama spectrum of the egg shells.

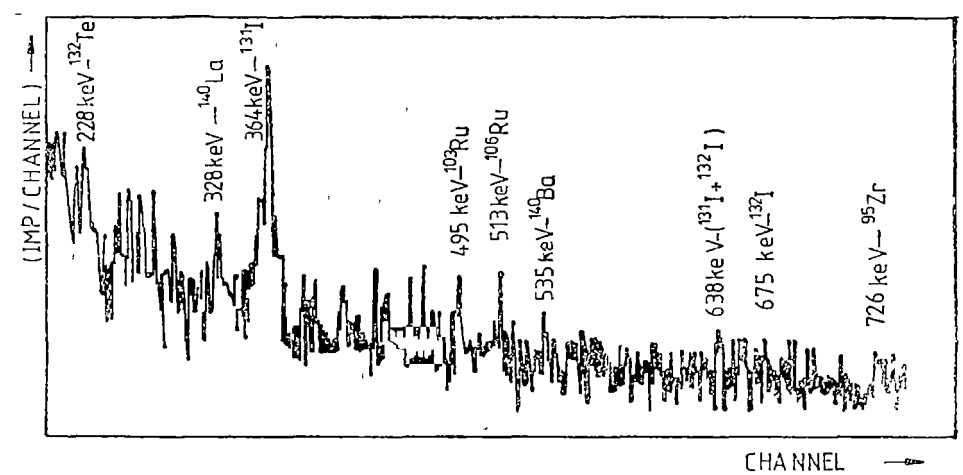

Fig. 3. Gama spectrum of the egg content.

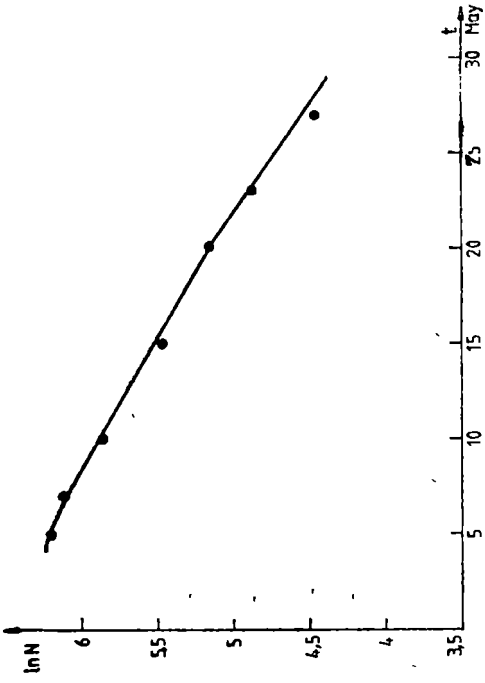

Fig. 5. Evolution of the egg content activity *versus* time

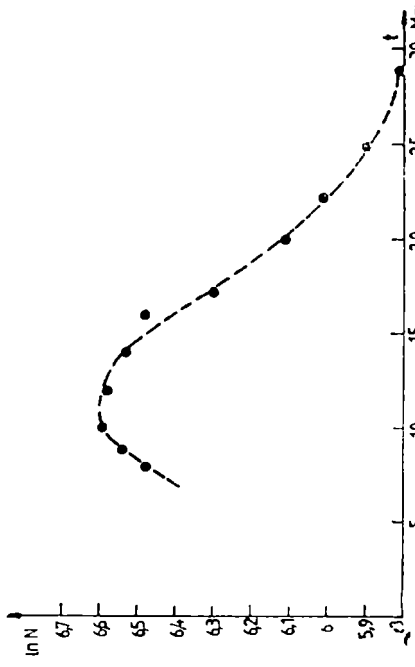

Fig. 4. Evolution of the egg shell activity *versus* time.

environment, is due to the period of the egg formation in final stage. We found in the egg shell some ^{132}Te, too, due to the great contamination with this radionuclide brought in the area by the rain of May 1 Radioisotopes ^{131}I and ^{132}I evinced less pregnant as we can see from the two peak heights, at 364 keV and 672 keV.

The great concentration of ^{131}I and the low concentration of ^{132}Te, ^{140}Ba and ^{95}Zr can be observed on the spectrum of Fig. 3

For the most radioactive eggs reaped on May 5 and 6 we consider the desintegration curves sepparately for the egg shell and for the egg content. Fig 4 shows the egg shell radioactivity evolution *versus* time

In the first instance, the gamma activity increases because of ^{140}La generation. Then, the activity decreases with a medium half life period of approximatively 14 days, which corresponds to the pregnant presence of ^{140}Ba in transit equilibrium to ^{140}La.

Fig. 5 presents the evolution of the egg content activity *versus* time. The sample is desintegrated with a half life period of approximatively 8 days, corresponding to a considerable presence of ^{131}I, as Fig 3 also shows.

Gamma global activity has been calculated, based on measurements in determined geometry and considering that the efficiency of the detection is known in integral regime. It was found the value of 483 Bq/egg, distributed as follows: 301 Bq/egg for the shell and 182 Bq/egg for the content — for the eggs reaped on May 5.

Conclusions. The experiments described above revealed the following aspects

1. Eggs are precious witnesses of vegetable food contamination with fission products, especially with Ba and I

2 Eggs behave as radionuclides separators, acting especially on ^{140}Ba and ^{131}I nuclides ^{140} Ba is separated in the egg shell and ^{131}I in its content.

3 The main part of the initial gamma activity was located in the egg shell.

4. The most of the eggs activity diminished with uncontaminated food—fed hens.

REFERENCES

1 C Cosma *et al*, *Internal Report*, University of Cluj-Napoca, May 1986.
2 M Oncescu, *I R A C '86, Internal Reports*, Bucharest, 1986
3 C Cosma, I Mastan, V Znamirovschi, T Fiat, O Cozar, F Koch and Ana Toderean, *Proc of the Symposium Methods, Models and Techniques in Physics and Related Fields, 26—27 sept, 1986*, pg 160.
4 R. Jahr, W. Kolb, U Lauterbach, *PTB Mitteilungen*, **96,** 240 (1986)
5 I. Chereji, L Dărăban, D Bogdan, C Bratu, S Boşcăneanu, *Proc on the Symposium Methods, Models and Techniques in Physics and Related Fields, 26—27 sept 1986*, pg 209
6 * * * "Information on the Cernobyl APS Accident and Its Consequences Prepared for IAEA", *Atomnaia Energia*, **61,** (5), 301, (1986)
7 A Andraşi *et al KFKI—1986—42/K Report*, Budapest, 1986
8. C Cosma, *Thesis*, University of Cluj-Napoca, 1986
9 C Cosma, I. Mastan, V Znamirovschi, *St. Cerc Fiz*, **33,** 351 (1981).

STUDIA UNIV BABEŞ—BOLYAI, PHYSICA, XXXII, 2, 1987

QUANTUM MECHANIC EFFECTS IN HIGH-SPEED ROTATING FRAMES

O. CRISTEA*

ceived May 29, 1987

ABSTRACT. — The purpose of this paper is to construct the Dirac Hamiltonian in rotating frames and investigate Zeeman-type effects by a general covariant method For completeness, we examine some possibilities of testing the behaviour of Dirac particles in a rotating frame

1. Introduction A possible way to test the results predicted by general covariant quantum mechanical theories is to simulate gravitational fields by rotating frames However, even in the case of high-speed rotating frames, the expected effects are very small For this reason, many researcher argue that we lack all non-ambigous experimental evidence on the behaviour of elementary particles as predicted by general covariant quantum field theories. The development of high-speed rotation techniques, in the last years, has made possible to obtain acceleration fields greater than 100 million times gravity [1]. These techniques lead to a revival of the interest concerning quantum mechanical effects in centrifugal fields in connection with the possibility to test the rules for transforming a quantum mechanical Hamiltonian into a non-inertial frame Actually, promissing results are expected from experiments concerning the decay of radionuclides on centrifugal rotors [2]

As pointed out in some previous papers, the degeneracy of a highly excited state may be removed by a gravitational field (see for instance [3—5]), as well as by a centrifugal field [6, 7] The idea that an inertial field leads to a Stark-type effect can be understood in the framework of customary quantum mechanics [8] On the other hand, in an earlier papar [9], Schmutzer has found an interesting similarity between the angular velocity and the magnetic field which can explain satisfactorily the behaviour of rotating superconductors.

The purpose of this paper is to investigate interference and Zeeman-type effects by means of a general covariant method We are especially interested in obtaining results which are useful from an experimental point of view. The method to derive the one-electron Hamiltonian is a generalization of the one developed by Schmutzer for slowly rotating frames [9].

2 **The general covariant Dirac Hamiltonian.** The quantum field equations may be generalized to non-inertial frames by replacing all derivatives ∂_k by covariant derivatives ∇_k For spin 1/2 particles, ∇_k can be expressed as

$$\nabla_k = \frac{\partial}{\partial x^k} + \frac{1}{4}\gamma^j(\gamma_{j,k} - \gamma_l\Gamma^l_{jk}), \tag{1}$$

* *University of Cluj-Napoca, Department of Biology, 3400 Cluj-Napoca, Romania*

and the general covariant Dirac equation reads as follows.

$$\gamma^k\left(\nabla_k - \frac{ie}{\hbar c} A_k\right)\Psi + \frac{m_0 c}{\hbar}\Psi = 0 \tag{2}$$

The γ_k matrices satisfy

$$\{\gamma_k(x),\ \gamma_l(x)\}_+ = 2g_{kl}(x), \tag{3}$$

which defines a Clifford algebra
It is convenient to our purpose to express the Dirac matrices by means of the Pauli matrices:

$$\gamma^k = i\begin{pmatrix} 0 & -\sigma^{k\alpha\dot{\beta}} \\ \sigma^{k}_{\dot{\alpha}\beta} & 0 \end{pmatrix}, \tag{4}$$

where σ^k obeys.

$$\sigma^{k\sigma\dot{\rho}}\sigma^{l}_{\dot{\rho}\mu} + \sigma^{l\sigma\dot{\rho}}\sigma^{k}_{\dot{\rho}\mu} = 2g^{kl}\delta^{\sigma}_{\mu},\ \delta^{\sigma}_{\mu} = \hat{1},\ \mu,\ \sigma,\ \dot{\rho} = 1, 2. \tag{5}$$

In the case of a rotating frame around $\hat{z}$ ($\vec{\omega}$ = constant), the metrix can be written as.

$$g_{00} = -1 + \frac{\omega^2}{c^2}(x^2 + y^2),\ g_{\alpha\beta} = \delta_{\alpha\beta},\ g_{01} = -\frac{\omega}{c}y,\ g_{02} = \frac{\omega}{c}x,\ g_{03} = 0 \tag{6}$$

Substituting (6) into (3) and solving the system of equations, via (4) we get

$$\gamma^0 = -\overset{(0)}{\gamma^0},\ \gamma^\beta = \overset{(0)}{\gamma^\beta} + g_{0\beta}\overset{(0)}{\gamma^0}, \tag{7}$$

where $\overset{(0)}{\gamma^k}$ represents the Dirac matrices in an inertial frame. Using the notation

$$g^{0\mu}\left(\frac{\partial}{\partial x^\mu} - \frac{ie}{\hbar c}A_\mu\right) = \frac{1}{c}\vec{\omega}\left[\vec{r} \times \left(\nabla - \frac{ie}{\hbar c}\vec{A}\right)\right], \tag{8}$$

the Dirac equation in a rotating frame comes to the form:

$$-\overset{(0)}{\gamma^0}\left(\Psi_0 + \frac{i}{\hbar c}V\Psi\right) + \overset{(\vec{0})}{\gamma}\left(\nabla - \frac{ie}{\hbar c}\vec{A}\right)\Psi + \overset{(0)}{\gamma^0}\frac{\omega}{c}\left[\vec{r} \times \left(\nabla - \frac{ie}{\hbar c}\vec{A}\right) + \frac{i}{2}\overset{(\vec{0})}{\sigma}\right]\Psi + \\ + \frac{m_0 c}{\hbar}\Psi = 0, \tag{9}$$

where $\vec{r} = x^\mu\vec{e}_\mu$ and $\overset{(\vec{0})}{\gamma} = \overset{(0)}{\gamma^\mu}\vec{e}_\mu$.

Writting (9) in the usual manner,

$$i\hbar\frac{\partial\Psi}{\partial t} = \hat{H}\Psi, \tag{10}$$

where $\tau = \frac{x^0}{c}\sqrt{-g_{00}}$ is the proper time of the particle, we finally get

$$\hat{H}_D = \frac{1}{\sqrt{-g_{00}}}\left[c\overset{(0)}{\vec{\alpha}}\left(\vec{p} - \frac{e}{c}\vec{A}\right) + \hbar\vec{\omega}\vec{L} + V + \overset{(0)}{\beta} m_0 c^2\right]. \tag{11}$$

Here, $\vec{L} = \frac{1}{\hbar}\vec{r} \times \left(\vec{p} - \frac{e}{c}\vec{A}\right) + \vec{S}$ is the angular-momentum operator,

$$\vec{S} = \frac{1}{2}\hbar\overset{(0)}{\vec{\sigma}}, \quad \overset{(0)}{\vec{\alpha}} = \alpha^\mu \vec{e}_\mu, \quad \overset{(0)}{\alpha^\mu} = \overset{(0)}{\gamma^0}\overset{(0)}{\gamma^\mu}, \quad \overset{(0)}{\beta} = -i\overset{(0)}{\gamma^0}$$

With the help of the decompositions

$$\Psi = \begin{pmatrix} \xi^\beta \\ \\ \eta_{\dot{\beta}} \end{pmatrix}, \quad \overset{(0)}{\alpha^\mu} = -\begin{pmatrix} \overset{(0)}{\sigma^\mu}_{\alpha\dot{\beta}} & 0 \\ \\ 0 & -\overset{(0)}{\sigma^{\mu\alpha\dot{\beta}}} \end{pmatrix}, \tag{12}$$

and using the weak field approximation,

$$(-g_{00})^{-1/2} \approx 1 + (\vec{r} \times \vec{\omega})^2/2c^2, \tag{13}$$

we find the Pauli Hamiltonian in rotating frame

$$\hat{H}_p \approx \frac{1}{2m_0}\left(\vec{p} - \frac{e}{c}\vec{A}\right)^2 + V + \vec{\omega}\vec{r} \times \left(\vec{p} - \frac{e}{c}\vec{A}\right) -$$

$$- \frac{\hbar}{2}\overset{(0)}{\vec{\sigma}}\left(\frac{e}{m_0 c}\vec{H} - \vec{\omega}\right) + \frac{m_0(\vec{r} \times \vec{\omega})^2}{2}. \tag{14}$$

It is easy to see from (14) that the angular velocity ω operates as an equivalent magnetic field:

$$\vec{H}_e = \frac{m_0 c}{e}\vec{\omega}, \tag{15 a}$$

with respect to the spin angular momentum and

$$\hat{H}'_e = 2\frac{m_0 c}{e}\vec{\omega}, \tag{15 b}$$

with respect to the orbital angular momentum.

3. **Experiments in rotating frames.** Several experiments have been carried out in the last twenty years to test the behaviour of Dirac particles in rotating frames. Because in (14) the corrections to the unperturbed Hamiltonian are very small, we may assume that these effects are linearly superposable. For this reason, we may treat every relativistic correction to the unperturbed Hamiltonian neglecting the other terms In this section, we shall briefly examine three experiments which might be considered as tests of the Hamiltonian (14).

3.1 *Rotational effects on the neutron phase.* Some neutron interferometry experiments were carried out to observe the effect of the earth gravitational potential on the neutron phase [10, 11]. Since these experiments are performed on the surface of the earth we have an opportunity to test the rules for transforming a quantum mechanical Hamiltonian into a rotationg frame. The assumed Hamiltonian in these experiments was:

$$\hat{H} \simeq \frac{p^2}{2m} - G\frac{mM}{r} - \hbar\vec{\omega}\vec{L}_0, \tag{16}$$

where $\vec{L}_0 = \frac{1}{h}\vec{r} \times \vec{p}$ is the angular momentum operator of neutron motion about the center of the earth ($\vec{r} = 0$). The difference in neutron's phase, due to the earth's rotation, can be derived from (16) and reads

$$\beta_{\text{rot}} = \frac{4\pi m}{h}\vec{\omega}\vec{A}, \tag{17}$$

where $\vec{A}$ is the normal area enclosed by the beam paths. The agreement of the experimental results with the theory was better than 99%. The rotational effect on the neutron's spin involves polarized beams and, on the other hand, it was too small to be observed in these experiments.

3 2 *Rotational effects on the superconducting electrons' phase.* The essential property of a superconducting de Broglie wave interferometer is that the maximum supercurrent flow through it is a periodic function of the normalized action, $\frac{1}{2h}\oint pdq$, and in a rotating frame can be expressed as

$$I_{\max} = I_0\left|\cos 2\pi\left(\frac{2m'}{h}\pi r^2\omega + \frac{e}{h}\pi r^2 H\right)\right|. \tag{18}$$

Thus, the difference in electrons' phase due to the rotation of the interferometer is

$$\beta'_{\text{rot}} = \frac{4\pi^2 m'}{h} r^2\omega, \tag{19}$$

the same expression as (17). The experiments performed [12] were in good agreement with the theory. In fact, the interference experiments carried out in rotating frame with spin 1/2 particles are somewhat similar to the Michelson—Sagnac-type experiments with light [13]

3 3 *The rotational Zeeman-type effect* Let us consider a relativistic ion which travels along a closed path in strong magnetic field $\vec{H} = (0, 0, H_z)$. Let ω be the angular velocity and e the electric charge of the ion. In the nonrelativistic limit, ω can be expressed as

$$\omega \simeq \frac{eH_z}{Am_p c}, \tag{20}$$

where A is the relative atomic mass of the ion and m_p is the mass of the proton. If experiments are performed with respect to the rotating frame and when the external field vanishes, the Hamiltonian of the electronic shell of the ion which corresponds to (14) reads:

$$\vec{H} \simeq (1/2m_0)\sum_k \vec{p}_k^2 - \frac{\hbar e}{2m_0 c}\vec{H}(2\vec{S}+\vec{L}) + \hbar\vec{\omega}(\vec{L}+\vec{S}) - (e/2c)\vec{\omega}\sum_k r_k \times$$

$$\times (\vec{H}\times r_k) + (e^2/8mc^2)\sum_k (\vec{H}\times\vec{r}_k)^2. \tag{21}$$

In the first approximation, we may neglect the last two terms and (21) becomes

$$\vec{H} \simeq \frac{1}{2m_0}\sum_k \vec{P}_k^2 - \frac{\hbar e}{2m_0 c}\vec{H}(2\vec{S}+\vec{L}) + \hbar\vec{\omega}(\vec{S}+\vec{L}). \tag{22}$$

Remark The eigenvalues of the Hamiltonian (14) give us the possible energies of the electron with respect to the laboratory frame. The term $m_0(\vec{r}\times\vec{\omega})^2/2$ vanishes when measuerments are performed with respect to the rotating frame. As far we know, this Doppler shift term has been measured in the experiments of Katano and Isozumi [14].

The desintegration of the energy levels corresponding to (22) is given by:

$$\Delta E_{\text{rot}} = -\frac{\hbar e}{2m_0 c}H_z(\bar{J}_z + \bar{S}_z) + \hbar\omega\bar{J}_z, \tag{23}$$

where $\vec{J} = \vec{L} + \vec{S}$ and the symbol „$^-$" denotes average value. From customary quantum mechanics it is known that

$$\bar{S}_z = M_J\frac{\vec{J}\vec{S}}{\vec{J}^2};\ \bar{J}_z = M_z;\ M_J = -J, -J+1, \ldots, J. \tag{24}$$

Substitution of (24) into (23) gives.

$$\Delta E_{\text{rot}} = -\hbar M_J(\omega_L \cdot g - \omega), \tag{25}$$

where $\omega_1 = (e/2m_0c)$ Hz and $g = 1 + [J(J+1) - L(L+1) + S(S+1)]/2J(J+1)$. When the same ion is stationary in the magnetic field ($\omega = 0$), (25) becomes

$$\Delta E = -\hbar M_J\omega_L \cdot g. \tag{26}$$

Thus, the relative shift of the rotational Zeeman (spectral) lines is given by

$$\frac{\nu_{\text{rot}} - \nu}{\nu} = \frac{2}{gA}\frac{m_0}{m_p} \sim \frac{1}{gA}\cdot 10^{-3},\ g \neq 0, \tag{27}$$

independent on $\vec{H}$. It is interesting that when $g = 0$ (for instance for the $^4D_{1/2}$ level) the linear desintegration of the energy level is given entirely by the rotational effect. Generally, a relative frequency variation of about $10^{-3} - 10^{-4}$ might be measured by means of an adequate microwave device.

In our opinion, the Hamiltonians (11) and (12) might be useful to the study of several quantum systems in rotating frames: removal of the degeneracy of Rydberg states, spin movement, transitions amplitudes, CPT theorems etc.

Acknowledgement. I am grateful to Prof. L. Kochbach, University of Bergen, for valuable conversations on the theme of hydrogen-like spectrum in non-inertial frames, in the early phases of the present work.

REFERENCES

1. R. Katano, S Shimizu, *Rev Sci Instrum.*, **50** (1979), 805
2. R Katano, Y. Isozumi, *Nucl. Instrum. Methods in Phys Res*, **222** (1984), 557.
3. L. Parker, L. O. Pimentel, *Phys Rev*, **D25** (1982), 3180.
4. T. K Leen, L. Parker, L. O. Pimentel, *Gen. Relat. Gravitation*, **15** (1983), 761.
5. A. K Gorbatsievich, *Acta Phys Pol*, **B16** (1985), 21.
6. O. Cristea, *Dirac Particles in Accelerated Frames*, presented at the Brasov Int School in Phys (1984), unpublished
7. O Cristea, in *Abstracts of Contributed Papers, 11th Int. Conf on GRG*, Stockholm, 1986, p. 415.
8. M. Piso, O. Cristea, *Rev Roum Phys*, **29** (1984), 625.
9. E. Schmutzer, *Ann Physik*, **29** (1973), 75.
10. D. M Greenberger, A W Overhauser, *Rev. Mod Phys*, **51** (1979), 43
11. S. A Werner, J L Staudenmann, R. Colella, A W Overhauser, in: *Neutron Interferometry*, eds. U. Bonse and H Rauch, Clanderon Press, Oxford, 1979, p 209.
12. J. E. Zimmerman, J. E Merceau, *Phys Rev Lett.*, **14** (1965), 887.
13. W. W Chow, J. Gea Banacloche, L M. Pedrotti, V E. Sanders, W. Schleich, M. O. Scully, *Rev. Mod Phys*, **57** (1985), 61.
14. T. Mukoyama, private communication (1984)

STUDIA UNIV BABEŞ—BOLYAI, PHYSICA, XXXII, 2, 1987

ON THE POSSIBILITY OF DETERMINING A MAGNETICAL FIELD FROM ITS HYPOTHETICAL SOURCES

HUBA SZŐCS*

Received September 22, 1987

ABSTRACT. — The autor determines in this work, by solving the system of equations rot $\bar{H} = \bar{J}$ and div $\bar{H} = g$, the intensity H of a magnetical field, knowing its rotations, represented by the density vector, $\bar{J}$, of the electric current and its sources, represented by function g of the density of magnetical charge.

According to experience, generally the induction lines of the magnetical fields generated by (stationary) electric currents are closed curves, what in fact annuls the divergence of the magnetical induction vector $\bar{B}$·

$$\operatorname{div} \bar{B} = 0 \tag{1}$$

From (1) we deduce the inexistence of the sources (magnetical charge, magnetical monopole, magnetical singlet [1].

However, there are relatively simple lines of current configurations which generate magnetical fildes excepting this rule: their induction lines do not close up [2,3,4]. Obviously, in this case we must admit that the divergence of the magnetical induction vector $\bar{B}$ is not annuled.

I. We set to work out an issue to the system of equations:

$$\operatorname{rot} \bar{H} = \bar{J} \tag{2}$$

$$\operatorname{rot} \bar{B} = g \tag{3}$$

where $\bar{H}$ is the intesity vector of a magnetical field, $\bar{J}$ the current density vector and g a scalar function from the volume V of the physical space.

Supposing the magnetical permeability, μ, is constant in V, we have

$$\operatorname{div} \bar{B} = \mu \operatorname{div} \bar{H};\ \operatorname{div} \bar{H} = g/\mu = g_1 \tag{4}$$

thus without rastraining the general frame, we may consider the system:

$$\operatorname{rot} \bar{H} = \bar{J} \tag{5}$$

$$\operatorname{div} \bar{H} = g \tag{6}$$

Supposing the conditions are satisfied

$$H_n = f(Q) \tag{7}$$

* *Huba Szőcs, Institute of Technical Education, 4800 Baia-Mare, Romania*

were H_n is the component of H, after the normal relation to the separations surface, between the volume V and its exterior V, and

$$\int g \, dV = \oint f \, dS \tag{8}$$

where $f = f(Q)$ is a given function, Q being a point of the surface S; relation (8) working at the same time for the determining of the function $g = g(P)$, as well as

$$\operatorname{div} \bar{J} = 0 \tag{9}$$

The solution of the system (5)—(6) is to be sought under the form of an additive function [5]

$$H(P) = \bar{u} + \bar{v} + \bar{w} \tag{10}$$

when P is a point of the physical space.

1) Vector $\bar{u}$ is obtained as a solution to the system

$$\operatorname{rot} \bar{u} = 0 \tag{11}$$

$$\operatorname{div} \bar{u} = g \tag{12}$$

It results

$$\bar{u} = -\operatorname{grad} \varphi_{\bar{u}} \tag{13}$$

where $\varphi_{\bar{u}}$ is the potential of the vector $\bar{u}$, given by the Laplace-Poissons equation

$$\Delta \varphi_{\bar{u}} = -g \tag{14}$$

$\varphi_{\bar{u}}$ being a regular function in V, annuling itself in infinite.

Green's formula gives us

$$\varphi_{\bar{u}} = -\frac{1}{4\pi} \int_V \frac{\Delta \varphi_{\bar{u}}}{r} \, dV = \frac{1}{4\pi} \int_V \frac{g}{r} \, dV \tag{15}$$

and from (13) it results that

$$\bar{u} = -\operatorname{grad} \frac{1}{4\pi} \int_V \frac{g}{r} \, dV \tag{16}$$

The vectorial function $\bar{u}$ does not fulfill the condition from (7)

2) To determine $\bar{v}$, we consider the system of equations:

$$\operatorname{rot} \bar{v} = \bar{J} \tag{17}$$

$$\operatorname{div} \bar{v} = 0 \tag{18}$$

The condition from (9) must be fulfilled throughout the physical space. In order to make this certain, it is necessary that the normal component J_n

should be continual in the points of the surface S. So the function $\bar{J}$ may be prolonged outside the volume V; at the same time observing the condition that in infinite $1/r^{\lambda+2}$, where λ is a positive number, arbitrarily small, should be annuled.

In consequence, we should have

$$\bar{J} = -\operatorname{grad} \varphi_{\bar{J}} \quad (\Delta\varphi_{\bar{J}} = 0) \tag{19}$$

and

$$\left.\frac{\partial \varphi_{\bar{J}}}{\partial n}\right|_S = J_n \tag{20}$$

The solution of the systems (17) — (18) should be sought under the form

$$\bar{v} = \operatorname{rot} \bar{A} \tag{21}$$

where $\bar{A}$ is a vectorial potential, satisfying the equation:

$$\operatorname{grad} \operatorname{div} \bar{A} - \Delta \bar{A} = \bar{J} \tag{22}$$

on the condition that $\operatorname{div} \bar{A} = 0$, what in fact does not restrain the generality.

Obviously, the condition $\operatorname{div} \bar{v} = 0$ is identically satisfied. Thus, obtaining these results, taking into account that in the outer space V' is satisfied (19), we obtain

$$\bar{A} = \frac{1}{4\pi} \int_V \frac{\bar{J}(Q)}{r(P, Q)} \, dV_Q - \frac{1}{4\pi} \int_{V'} \frac{\operatorname{grad} \varphi_{\bar{J}}(Q)}{r(P, Q)} \, dV_Q \tag{23}$$

and, finally

$$\bar{v}(P) = \operatorname{rot}_P \bar{A} = \operatorname{rot}_P \left(\frac{1}{4\pi} \int_V \frac{\bar{J}(Q)}{r(P, Q)} \, dV_Q - \frac{1}{4\pi} \int_{V'} \frac{\operatorname{grad} \varphi_{\bar{J}} - (Q)}{r(P, Q)} \, dV_Q \right) \tag{24}$$

which concludes that function $\bar{v}$ does not satisfie condition (7), either.

3) We obtain the vectorial function $\bar{w}$ as a solution to the system of equations:

$$\operatorname{rot} \bar{w} = 0 \tag{25}$$

$$\operatorname{div} \bar{w} = 0 \tag{26}$$

with a condition to the limiting value:

$$w_n = f(Q) - (\bar{u} + \bar{v})_n \tag{27}$$

In this case $\bar{w}$ will be the solution of the equivalent equation

$$\bar{w} = -\operatorname{grad} \varphi_{\bar{w}} \tag{28}$$

$\varphi_{\bar{w}}$ being a scalar potential:

$$\varphi_{\bar{w}} = -\frac{1}{4\pi} \oint_S K(P, Q) [f(Q) - (\bar{u} + \bar{v})_n] \, dS_Q \tag{29}$$

At the same time $\varphi_{\bar{w}}$ satisfies the equation of Laplace in volume V

$$\Delta\varphi_{\bar{w}} = 0 \tag{30}$$

and on the surface V it satisfies the condition at the limit

$$\frac{\partial\varphi_{\bar{w}}}{\partial n} = w_n = f(\bar{r}_S) - (\bar{u} + \bar{v})_n \tag{31}$$

where $\bar{r}_S$ is the position vector of a point on the S surface

The function $K(P, Q)$ of the from

$$K(P, Q) = k(P, Q) - \frac{1}{r(P, Q)} \tag{32}$$

is a function — Green of the second degree, k representing the solution of the equation

$$\Delta_Q k(P, Q) = 0 \tag{33}$$

satisfying the condition

$$\frac{k(P, Q)}{n_Q} = \frac{4\pi}{S_0} - \frac{\partial}{\partial n_Q} \cdot \frac{1}{r(P, Q)} \tag{34}$$

where S_0 is the area the surface S

In these condition the equations (5)—(6) are satisfied

$$\text{rot}\,\bar{H} = \text{rot}\,\bar{u} + \text{rot}\,\bar{v} + \text{rot}\,\bar{w} = \bar{J} \tag{35}$$

$$\text{div}\,\bar{H} = \text{div}\,\bar{u} + \text{div}\,\bar{v} + \text{div}\,\bar{w} = g \tag{36}$$

including the condition of the limit

$$H_n = (\bar{u} + \bar{v} + \bar{w})_n \tag{37}$$

II. Interpretation of the results.

1. Taking into consideration the meaning of the divergence of a vector, the scalar function $g(P)$ may be interpreted by an analogy to the corresponding electric terms as the density of the sources of the magnetical fields (magnetical charges) having as a measuring unit Vs/m^3. The function $g(P)$ may be known, then function $f = f(Q)$ (7) results from (8) and *vice versa*, function g being known, it results function f from (7).

2 Given the fact that (2) rot $\bar{H} \neq 0$ the determined magnetical field by the source-function $g(P)$ by means of relation (3), observing conditions (7)—(8)—(9), is equivalent to a magnetical field determined by its rotations (the density of electric current) Thus a magnetical field may be generated by singular sources, too

In conclusion, the statement that the laws of physics do not exclude the existence of the magnetic charge [6] is thoroughly confirmed.

The existence and the uniqueness of the system (5)—(6) is ascertined by the theory of the equation with derivatives and the theory of the potential [7].

BIBLIOGRAPHY

1. T. E Tamm, „Bazele teoriei electricităţii", Ed Tehnică, Bucureşti, 1957.
2 K. Simonyi, „Villamosságtan", Ed. a 2-a, Akadémiai kiadó, Budapest, 1962
3 S Sabba, „Liniile de cîmp magnetic a doi curenţi electrici rectilinii egali", *Studii şi Cercetări de fizică*, **XI**, 3 (1960), pp. 563—685
4 S Sabba, „Nouveaux exemples de lignes de champ magnétique ouverts", *Revue Roumaine de Physique*, Tome 15, nr. 1, 1970, pp 11—25
5. H Szocs, „Unele consideraţii asupra cîmpului magnetic", Presentat sesiunea ştiinţifică I P. Baia-Mare 1974; *Buletin Ştiinţific I I S Baia-Mare*, seria B, Vol VII, 1984.
6 T Toró, „Fizică modernă şi filozofie", Editura Facla, Timişoara 1973
7. A N Tihonov, A A Samarski, „Ecuaţiile fizicii matematice", Editura tehnică, Bucureşti 1956

STUDIA UNIV BABEŞ—BOLYAI, PHYSICA, XXXII, 2, 1987

THE DESIGN OF A SYNTACTICAL ANALYSER FOR AN 8-BIT MICROCOMPUTER USING THE k-CODE ALGORITHM

OVIDIU POP*

Received October 26, 1987

ABSTRACT. — A new implementation of the k-code algorithm is presented, as it was required by the structure of an 8-bit microcomputer. This algorithm was used in order to design the syntactic analyser of an I8048 crossassembler Finally, a few conclusions will emphasize the advantages of this algorithm *vs* speed and efficiency

The k-code algorithm has a French origin and it was initially meant to form the core of a 32-bit computer syntactic analyser As it is well known, the syntactic analyser represents one of the most important part needed in the compiler design The program which first implemented this algorithm was called CHARADE. From the very beginning, it must be pointed out the original algorithm is much more complex than the one that is to be presented further. The requirements of an 8-bit microcomputer crossassembler being somewhat different than those of a 32-bit compiler, the original k-code algorithm has been adapted accordingly. This new ,,face" of the k-code algorithm will be the subject-matter of rohat follows.

The k-code algorithm [1] represents a way of converting the syntax of a programming language in the form of a chained list which together with an adequate analyser performs the functions of a descending syntactic analyser.

By descending syntactic analysis, one should understand the building of a derivation tree, when only the root and the leaves of that tree are given, the direction being from the root to the leaves. The descending syntactical analysis verifies if $S = \Rightarrow X$ (read S derives X), where S represents the starting symbol of that language grammar and $X = (x1, x2, \ldots, xn)$ stands for the word to be analysed

The process of descending syntactical analysis is a recursive process. If we try a derivation like $X = \Rightarrow Y1Y2 \ldots Ym$ in a derivation like $X = \Rightarrow P$, this means that P must be divided in m words P1, P2, ..., Pm and a derivation of the following type must be rebuilt:

$$Yk = \Rightarrow Pk, \quad k = 1, m$$

The descending analysis is a restrictive one: left-recursive grammar rules are forbidden

The k-code algorithm requires a special way of writing the grammar rules and, therefore, it is necessary to explain the significance of the metasymbols that are to be used:

* *Mining Computing Center, 3400 Cluj-Napoca, Romania*

< > delimits the names of the non-terminal symbols,
( ) delimits the compound grammar symbols,
. = means „the left member of the grammar rule is defined by ..."
| has the value of logical OR;
' ' delimits one or more terminal symbols;
; marks the end of a grammar rule;
marks a (possible) repetitive statement.

The formal syntax of the programming language generated with the metasymbol described above is understood as a program that analyses a text source as follows. the left part of each production will represent the name of a procedure and everything that comes next to the „: =" metasymbol (including the „;" metasymbol) is the body of that procedure Each syntactical symbol has its own associated list-word with the following structure:

p	m	v	f

The meaning of the four fields in the list-word are as follows·

a] If the current symbol is a terminal symbol then
p = 0
m contains the ASCII code of that terminal symbol.

b] If the current symbol is a non-terminal symbol then
p = 1
m contains the ordinal number of that symbol, according to the arbitrary code used by the programmer.

c] If the current symbol is the number of an action then
p = 3
m contains the number of the action to be carried out.

d] When the ending rule metasymbol „;" is encountered, that is equivalent with
p = 2
m has no meaning.

„v" and „f" of the last two fields of the list-word come from French and they mean true („vrai") and, respectively, false („faux"). These two fields contain the links to the list-words associated, to the successor and to the alternant of a grammar symbol respectively.

The successor of a given symbol is the symbol that follows the symbol taken into consideration in the current production Every symbol (except „;") must have a successor. So, the v field will contain the offset from the current list-word to the list-word that is its successor.

The alternant of a given symbol is another way of defining the non-terminal symbol, if the examination of the current nonterminal symbol fails

The data structures used by the k-code algorithm are as follows

1] A memory buffer (T) which contains the text source,
2] An index I of the memory buffer. This index points to the current symbol of the text source,
3] An index K that contains the address of the currently examined instruction. Letters p, m, v and f denominate the four already described fields of

the list-word pointed to by the K index. These four parameters (p, m, v, f) will be treated by the main procedure of the k-code algorithm as being of type in, because we will presume that the chained lists which are going to be processed by the k-code algorithm already exist as memory data;
4] A stack of which top address is contained by the PTSP pointer. Each stack element is formed by 3 cells named: I', K', Q'.

The k-code algorithm will be described [2] using the pseudocode:

```
proc k-cod (in p, m, v, f); {the main program}
var i, k: index; ptsp: int; vl: boolean;
begin
    k.=program; {k points to the first grammar rule}
    ptsp  =0; {the stack pointer is set to 0}
    i   = 1, {the I index is set to 1}
    vl: = true;
    while vl=true loop
      case (p)
         p=0 ⇒ st; {calls the procedure dealing with the terminal symbol}
         p=1 ⇒ snt; {calls the procedure dealing with the nonterminal symbol}
         p=2 ⇒ fin, {calls the procedure dealing with the end of a production}
         p=3 ⇒ action, {starts the execution of the given action}
       endcase
    endloop
end

proc st; {terminal symbol}
begin
    if m# t [i] then
                    if f=0 then retur_fals;
                           else k: =k+f;
                                exit;
                    endif
               else
                    i: =i+1;
                    k. =k+v;
                    exit;
    endif
end

proc snt; {non-terminal symbol}
var i', k': index; q': int;
begin
    ptsp: =ptsp+1;
    i': =i;
    k': =k,
    if f#0 then q'=1,
           else q'=0;
    endif
      k: =m;
    exit,
end

proc fin, {end of a production (grammar rule)}
var k': index,
begin
    k: =k';
    k: =k+v,
    ptsp: =ptsp-1,
    exit;
end
```

```
proc retur_fals; {dead end}
var i', k': index; q': int,
begin
    while q'=0 loop
        ptsp: =ptsp−1,
    endloop
      k: =k';
      i. =i';
      k: =k+f;
      ptsp. =ptsp−1;
    exit,
end
proc action,
begin
    k· =k+v;
    starts the execution of the action,
end
```

The next paragraph presents the grammar of the I8048 assembly language using the metasymbols described above:

```
 0] ⟨program⟩ := A0 #(⟨instruction_line⟩ A23 );
 1] ⟨instruction_line⟩ := (⟨label⟩)#(' ')(⟨mnemonic⟩' '#(' ')( A25 ⟨operand1⟩
    (',' A26 ⟨operand2⟩)))#(' ')(⟨comment⟩) ⟨sf⟩;
 2] ⟨label⟩ .= ⟨letter⟩ #( A1 (⟨letter⟩ | ⟨digit⟩ | '$'))':' A2 ;
 3] ⟨mnemonic⟩ := ⟨letter⟩ A1 ⟨letter⟩ A1
                                    (⟨letter⟩ A1
                                    (' '| (⟨letter⟩ A1
                                    (' '|⟨digit⟩ A1 ' ')|
                                    |⟨digit⟩ A1 ' '))|
                                    ⟨digit⟩ A1 ' ') A3 ,
 4] ⟨operand1⟩ ·= ⟨decnb⟩ A10 | ⟨hexnb⟩ | A11 | ⟨'$'('+' A12 |'−' A13 )
                  ⟨decnb⟩ A10 A14 |⟨symb_adr1⟩;
 5] ⟨decnb⟩ := ⟨digit⟩#(⟨digit⟩ A4 ) A5 ,
 6] ⟨hexnb⟨ := ⟨hexdg⟩#(⟨hexdg⟩ A6 )'H' A7 ;
 7] ⟨symb_adr1⟩ :=⟨op_1_rez⟩|⟩symb_user⟩ A15 ;
 8] ⟨symb_user⟩ :=⟨letter⟩≈( A1 (⟨letter⟩|⟨digit⟩|'$') A9 ;
 9] ⟨op_1_rez⟩ := A8 ·
10] ⟨operand2⟩ := ⟨decnb⟩ A16 |⟨hexnb⟩ A17 |'$'('+' A12 |'−' A13 )⟨decnb⟩ A18 |
                  '#'(⟨decnb⟩ A42 | ⟨hexnb⟩ A43 |⟨symb_user⟩ A15 )⟨symb_adr2⟩;
11] ⟨symb_adr2⟩ := ⟨op2_rez⟩| ⟨symb_user⟩ A15 ,
12] ⟨op2_rez⟩ := A20 ;
```

13] ⟨comment⟩ := ';'#(A21);

14] ⟨letter⟩ := 'A' 'B' |.. |'7',
15] ⟨digit⟩ := '0'|'1'| |'9',
16] ⟨hexdg⟩ .= '0'|'1'| |'9'|'A'| |'F',

17] ⟨sf⟩ .= A22 ;

The AO ... A43 symbols denominate a number of 44 actions which are executed immediately when the syntactical analyser encounters the corresponding list-word of the chained list These actions were implemented in the I8080 assembly language, thus ensuring the portability of the written program on any microcomputer built around a I8080 or Z80 microprocessor

The advantages of using the k-code algorithm as the core of a syntactical analyser are.

1] The k-code algorithm is not obviously a large one, so its execution speed is extremely high.

2] The k-code algorithm enables the separation of procedures from the data processed upon and as it is well known, this separation constitutes a main goal in modern programming. Data are representted by the chained list and the procedures are a number of actions implemented by the programmer.

3] Being independent, this syntactical analyser might be used in designing a whole family of assemblers. The designer has to write the proper language grammar and to implement the corresponding actions.

REFERENCES

1. Kahan, B., Dumas Primbault, H., Mise en oeuvre d'une methode d'analyse syntactique descendante.
2. Ovidiu Pop., *M. D. Theses* (1986), Polytechnical Institute of Cluj-Napoca

STUDIA UNIV BABEŞ—BOLYAI, PHYSICA, XXXII, 2, 1987

AN X-RAY DIFFRACTION LINE PROFILE ANALYSIS COMPUTER CODE USING FAST FOURIER TRANSFORM AND TIKHONOV REGULARISATION

D. CIURCHEA*

Received October 3, 1987

ABSTRACT. — The computer code described is essentially fast and may be implemented on small size machines Applications of the program in diffusion studies and in deriving the mean crystallite size and the root mean square strains in the crystallite for pure substances are presented

Introduction. The line profile analysis is an important item in the X-Ray diffraction laboratory, allowing the analyst to separate such microstructural features of the material as the crystallite size distribution, the r.m s. strains and the stacking faults probability in the case of pure substances. In the case of solid solutions, when some dependence of the lattice parameter on concentration is available, the interpretation of the diffusion process involved is possible in terms of the concentration profile at an atomic level.

The code described in this paper was designed to work also on small size, BASIC language machines This makes it adequate for less sophisticatedly equiped laboratories or as a training means for students also The code ran successfully in 2 seconds on a CDC Cyber 72 computer, in 20 minutes on a HP 9830A computer and in 40 minutes on a TI 99/4A computer. All these computers have an internal representation of the real number of at least 60 bits

Unfolding Procedure. Due to instrumental aberrations, the measured X-Ray diffraction profile, $h(\theta)$, is a folding of the pure diffraction profile, $f(\theta)$, and of the resolution function, $g(\theta)$, as follows.

$$h(\theta) = \int g(\theta - z) f(z)\, dz \tag{1}$$

The problem is to unfold $f(\theta)$. $g(\theta)$ is commonly taken as the diffraction line of a well annealed specimen in the same θ range.

The most appealing method for the unfolding of the X-Ray diffraction lines is the method of Stokes (1) which implies the calculation of the Fourier transforms of h, g and f. Eq. (1) becomes.

$$H(n) = G(n)\, F(n)$$

and

$$F(n) = \frac{H(n)}{G(n)} \tag{2}$$

* *University of Cluj-Napoca, Faculty of Mathematics and Physics, 3400 Cluj-Napoca, Romania*

Ordinarily, $f(\theta)$ may be constructed from its Fourier coefficients, Eq (2). These coefficients may also be stored for use in line profile analysis by the methods of Warren and Averbach (2) and Gangulee (3) The reconstruction of $f(\theta)$ is essential in the study of the diffusion process and also proves the reliability of the numerical method used in other cases

The flow chart of the code is unbranched and does not require a special discussion except for the features of the Tikhonov regularisation (4) and the handling of the Fast Fourier Transform (FFT) The unbranched structure allows for the segmenting of the program on small size machines

The experimental data vector is first corrected for background and Lorentz-polarisation

In the case of line profile analysis, one passes from constant 2θ steps to constant s steps.

The FFT subroutine implies that the complex vector to be transformed is defined in the $0-2\pi$ range In order to accomodate the $-s$, $+s$ interval to the FFT, the experimental vector is shifted so that its wheight center approximately lies at the $N + 1$ position of the vector of length $2N$ In the next step the positioning is done accurately by interpolation A scale factor is calculated to account for the equivalence of the $-\pi$, $+\pi$ interval to the $-s$, $+s$ interval. Next, the weight center of the peak is transposed at the beginning of the vector. Then the FFT subroutine is called to compute the sine and cosine coefficients.

The difficulty of the Stokes method lies in the numerical instability at large orders of the Fourier coefficients Although both $H(n)$ and $G(n)$ have small values, their ratio, $F(n)$, may take large, false values yielded by the experimental errors in the original vectors, $h(\theta)$ and $g(\theta)$. A common solution is to smooth the experimental data so that the sum of the squares of the differences (SSD) between the original and the reconstructed function is equal to an evaluation of the global experimental error. Usually, this smoothing is done by series truncation (window filter). Tikhonov and Arsenine (4) provided a more realistic type of filter, defined by:

$$b_n = \frac{1}{1 + \alpha T(n)}$$

where b_n is a factor multiplying the n-th Fourier coefficient; α stands for the Tikhonov regularisation parameter and $T(n)$ is a polinomial in n which was taken by us as $T(n) = n^8$. Moreover, a strategy was provided (4) to iteratively determine α over the vector of the Fourier coefficients In order to set α we have used the secant method. The error per measured point is taken as $\sqrt{I}$, where I is the measured intensity. SSD is then given by ΣI, i e. $F(0)$.

By using the secant method, the number of computer statements is minimized and the convergence is good. Even with poor initial values for α, one obtains the final value with 0.1% precision in SSD after 7 iterations.

Subsequent to finding the regularisation parameter, options may be formulated for. diffusion analysis; Warren-Averbach line profile analysis, Gangulee single line profile analysis.

Diffusion Analysis. The principle for the study of the diffusion process was first stated by Rudman (5). With the substitution $y = x/\sqrt{t}$ in the second Fick's law, one obtains,

$$-\frac{1}{2} y \frac{\partial c}{\partial y} = D \frac{\partial^2 c}{\partial y^2}$$

By integration after y and using Fick's first law, one obtains,

$$y_1 = \sqrt{t} \int_0^{c(y_1)} \frac{\partial m(c)}{\partial c} \, dc = \text{const} \int_0^{c_1} N(c) \, dc \tag{4}$$

where $N(c)$ denotes the number of unit cells with the concentration between c and $c + dc$. When some dependence of the lattice parameter on concentration is available, such as the Vegard's law, $N(c)$ is directly related to the diffracted intensity (6):

$$f(\theta) = K |F_{hkl}(\theta)|^2 A(\theta, \mu) LP(\theta) N(c) \tag{5}$$

where K is a constant; $F_{hkl}(\theta)$ is the structure factor; $A(\theta, \mu)$ is the absorbtion factor; $LP(\theta)$ is the Lorentz polarisation factor. Further on, penetration y_1 is scaled to unity,

$$y(c) = \frac{\int_0^c N(c) \, dc}{\int_0^1 N(c) \, dc} \tag{6}$$

The scaled penetration (6) is called effective penetration. Thus, the plot of $c = c(y)$ is possible

Fig 1 presents an example of such an analysis performed with Cu Kα radiation on the (311) peak of a poorly sintered mixture of Thoria-Urania.

It must be noted that the diffusion process screens the effects of crystallite size and microstrains on the line breadth. Moreover, the process analysed takes place at an atomic level

The Warren—Averbach and Gangulee Analysis of the Line Profile. Both these methods use the factorisation of the Fourier coefficients of the pure diffraction profile.

$$F_L(n) = F^P(n) F_L^S(n) \tag{7}$$

where L denotes the order of the reflexion and n the order of the Fourier coefficient.

The Warren-Averbach (2) method is based on the equations:

$$\left.\frac{dF^P(n)}{dn}\right|_{n=0} = -\frac{1}{D_{\text{eff}}} \tag{8}$$

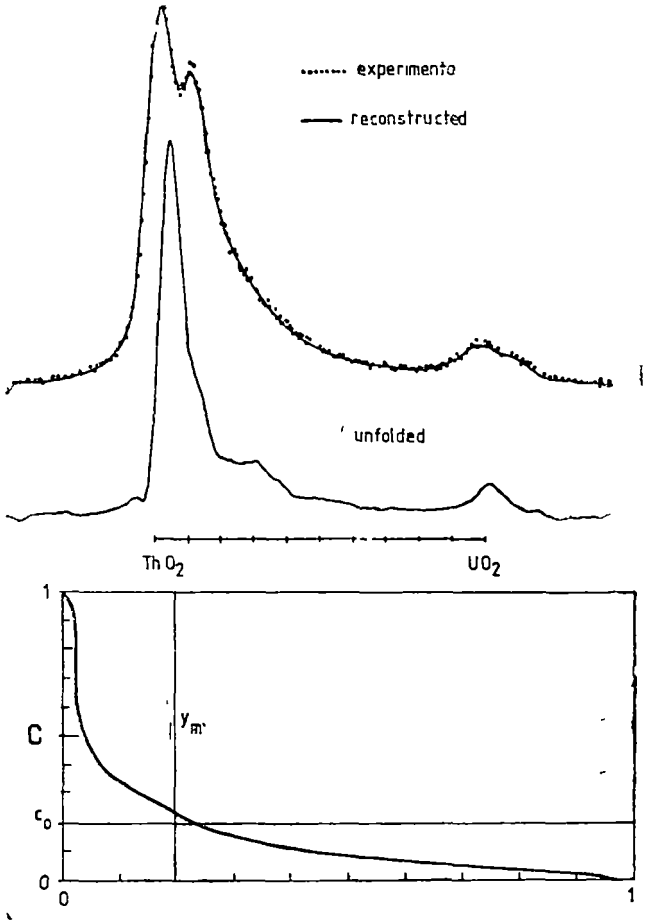

Fig. 1. Data processing example for diffusion analysis on a sintered mixture of Thoria—Urania.

and

$$F_L^S(n) = \exp\left(-2\pi^2 L^2 n^2 \langle \varepsilon_n^2 \rangle\right) \tag{9}$$

where D denotes the mean crystallite size expressed as a number of lattice spacings.

By taking two orders of a reflexion, e.g. (002) and (004),

$$\ln F_1(n) - \ln F_2(n) = 6\pi^2 n^2 \langle \varepsilon_n^2 \rangle \tag{10}$$

$$4\ln F_1(n) - \ln F_2(n) = 3\ln F^P(n)$$

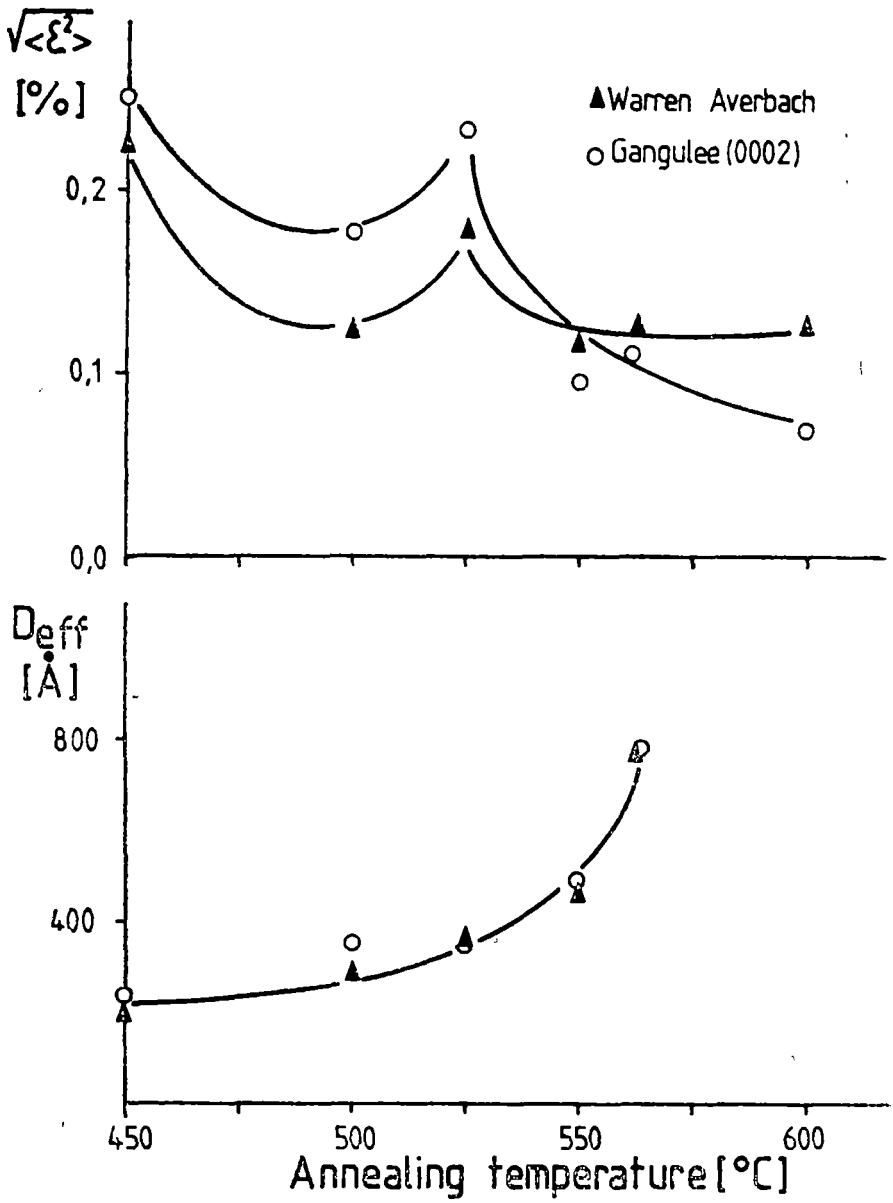

Fig. 2. The microstructural parameters derived by the methods of Warren and Averbach (2) and Gangulee (3) for Zircaloy-4 tubes as a function of the annealing temperature.

If more than two peaks are considered, it is further possible to separate the true crystallite size and the stacking faults contribution to the D_{eff} value (7)

$$\frac{1}{D_{\text{eff}}(hkl)} = \frac{1}{D(hkl)} + \sum_T C_T J_T g(hkl) \tag{11}$$

where D stands for the true crystallite size due to incoherent boundaries, T is a particular type of fault such as deformation fault or twin fault; C_T is the broadening coefficient of a fault of type T; J_T represents the probability of a fault of type T; g is the magnitude of the reciprocal lattice vector Equation (11) was ignored in our code

The analysis of Gangulee (3) relies on approximations of Eqs (8) and (9):

$$F^P(n) = 1 - \frac{n}{D_{\text{eff}}} \tag{12}$$

$$F^S(n) = 1 - 2\pi^2 n^2 \langle \varepsilon_n^2 \rangle \tag{13}$$

Thus, the method by Warren and Averbach implies the measurement of two peaks and two first degree regressions. The method by Gangulee implies the measurement of a single peak and a second degree regression

The illustrative example chosen is the evolution of the microstructural parameters D_{eff} and $\sqrt{\langle \varepsilon^2 \rangle}$ of the Zircaloy-4 tubes by annealing The measurements were performed in 2θ steps of 0 025° for the (0002) and (0004) reflexions The resolution function was taken as the diffraction peaks of a well sintered UO_2 pellet. No caution was taken to avoid the hook effect. The values of D_{eff} and $\langle \varepsilon^2 \rangle$ were calculated on various n intervals and the minimum D value was chosen as representative. The variation of $\langle \varepsilon^2 \rangle$ with n was ignored. $\langle \varepsilon^2 \rangle$ was taken as an average over the interval where D_{eff} is minimum.

The results are presented in Fig 2 It is seen that both methods were able to resolve a lack of monotonousity at 525 °C for the microstrains but not for the crystallite size. The effect is real and was confirmed by the creep properties of the tubes and will be discussed in detail elsewhere (8) The values obtained for D_{eff} are in excellent agreement with those found by others (9, 10).

REFERENCES

1 A R Stokes, *Proc Phys Soc London*, 61 (1948) 382
2 B E. Warren and B L Averbach, *J Appl Phys*, 23 (1952) 497.
3 A Gangulee, *J Appl Cryst*, 7 (1974) 434
4 A Tikhonov and V Arsenine, „Méthodes de résolution des problèmes mal posés", Mir, Moscow, 1974
5 P. S Rudman, *Acta Cryst*, 13 (1960) 905
6 H P. Klug and L E Alexander, "X-Ray Diffraction Procedures", J Wiley and Sons, 1974
7. R. L Rothmann and J B Cohen, *Adv X-Ray Anal*, 12 (1969) 208
8 D. Ciurchea and V Gheaţă, in preparation.
9. J. H Mogard and B L Averbach, *Acta Metall*, 6 (1958) 552
10. A Hapaleţ and M Popovici, *Annual Meeting of INPR* (1985)

STUDIA UNIV BABEŞ—BOLYAI, PHYSICA, XXXII, 2, 1987

ON THE PHOTOCONDUCTIVITY OF PbSe FILMS OBTAINED BY CHEMICAL "ANORGANIC" DEPOSITION

D. DĂDĂRLAT*, RODICA TURCU*, M. CHIRTOC*, RODICA M. CÂNDEA* and CAMELIA FULEA*

Received: October 30, 1987

ABSTRACT. — Electrical conductivity and photoconductivity properties were measured for PbSe films prepared by chemical "anorganic" deposition High activation energy (0 3 eV) for the conductivity was found. The spectral distribution of the photoconductivity was found to be shifted towards lower wavelengths region, as compared with PbSe films obtained by other methods. Experimental data can be explained by a "number" type model for the mechanism of the photoconductivity.

Introduction. It has already been shown that the PbSe films obtained by chemical „anorganic" deposition — CAD — (which uses sodium selenosulfate to generate the Se ions) present optical gap [1], mechanical [2, 3] and structural [4, 5] properties similar to those of the PbSe films obtained by chemical organic deposition — COD — (the Se ions are furnished by seleno-ureea by hydrolysis in alkaline solutions). However, some peculiarities have also been found for films prepared by CAD: spectral distribution of the photoconductivity is shifted towards lower wavelengths region, and conductivity high activation energies [4, 5].

In this paper we focus on these particular properties of CAD PbSe films. A "number" type model for the photoconductivity is considered in order to explain in a consistent manner the experimental data for our PbSe films.

Experimental. PbSe films of an average thickness, between 0 4 μm and 2.5 μm, were obtained by CAD [5]. The films present a good adherence, chemical stability and polycrystalline structure. The phase composition of the films was determined to be PbSe, by X-ray diffraction analysis (4)

All films investigated show *p*-type conductivity, as determined by the "hot point" method and by Hall effect measurements

The electrical resistance ($R_{\square}$) of the films, at room temperature, ranges between 0.5 and 500 MΩ.

The electrical conductivity (σ) was measured by standard d.c. procedure (with a Keithley 616 electrometer) in the 150—330 K temperature range, using a "cold finger" refrigerator system.

The photoconductivity measurements were performed in the 1—4 μm spectral range, with a standard setup [5] The radiation source was the Globar source of a Perkin Elmer 125 spectrophotometer. The modulation frequency of the radiation was 100 Hz. The photoconductive signal from the PbSe film was processed with an Unipan 232B lock-in nanovoltmeter. The same „cold finger" system was used for low temperatures photoconductivity measurements.

Resultsand discussions. A typical behaviour of the electriual conductivity *vs.* temperature, for the PbSe films obtained in our laboratory by CAD, is presented in Fig. 1.

* *Institute of Isotopic and Molecular Technology, 3400 Cluj-Napoca 5, P O. Box 700, R—3400, Romania*

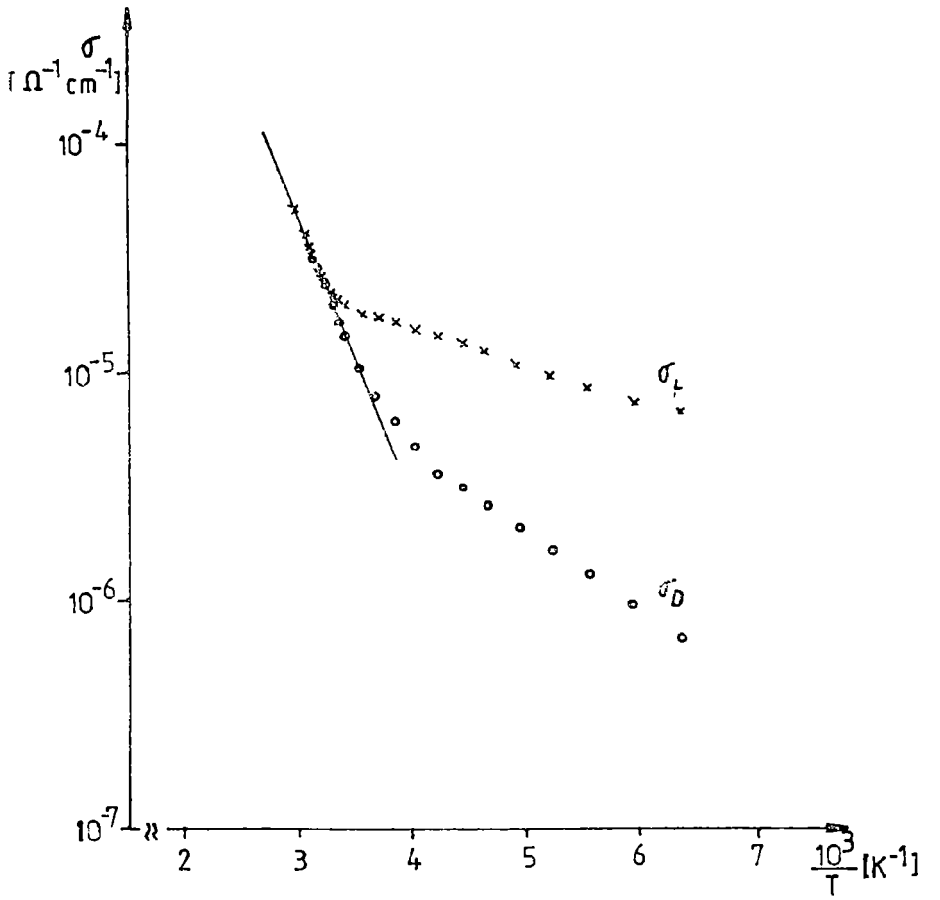

Fig. 1 Typical behaviour of the electrical conductivity *vs.* temperature, in the dark (σ_D) and under illumination (σ_L) for the CAD PbSe films.

These measurements were performed in the dark and under illumination with a tungsten lamp placed at a standard distance from the film.

As one can see from Fig. 1 that a high thermal activation energy for the conductivity has been found and this energy is not affected by the illumination

In order to explain these data, we consider that, in the temperature range investigated, the carrier concentration (p) remains constant [6] and the mobility of the holes is reduced, due to the intercrystalline barriers, by an exponential factor, as compared with the single crystal mobility [7]. Then we can write.

$$\sigma = ep\mu \exp\left(-\frac{E_b}{KT}\right) \tag{1}$$

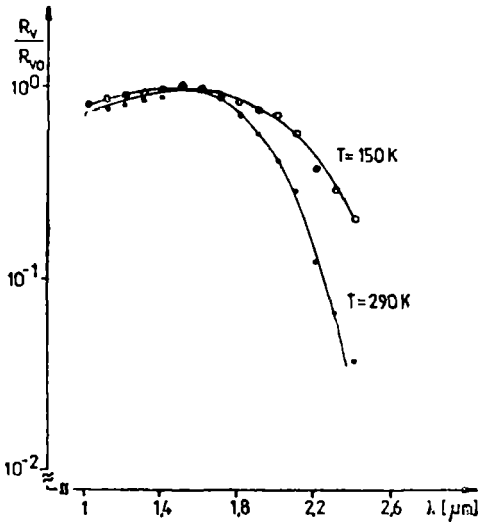

Fig 2 Typical spectral distribution of the photoconductivity for two temperatures of the CAD PbSe films.

Assuming also a temperature dependence of the mobility of the holes in the crystallites of the type $\mu \sim T^{-5/2}$ [6, 8], we can write.

$$\sigma(T) \sim T^{-\frac{5}{2}} \exp\left(-\frac{E_b}{KT}\right) \qquad (2)$$

Extracting the $T^{-5/2}$ dependence from the plots Fig. 1, we find $E_b = 0.32$ eV Having in mind the assumption made on the constance of the carrier concentration, we identified E_b with the thermal activation energy of the carriers over the intercrystalline barriers.

Typical spectral distribution of the photoconductivity, normalised at its maximum value, at constant incident radiation energy, for two temperatures of the film are present in Fig. 2 The results plotted in Fig 2 indicate an anomalous spectral distribution of the photoconductivity of the PbSe films obtained by CAD (with a maximum around 1 5 μm), as compared with the films obtained by COD. We extended our investigations up to 4 μm but no other maximum in photoconductivity was observed We identified the energy corresponding to $\lambda_{1/2}$, with the activation energy for the photoconductivity (E_a), [9] From spectral response measurements (Fig. 2), we found $E_a = 0.63$ eV at room temperature and $E_a = 0.58$ eV at 150 K

These large values for E_a can be correlated with the values of the thermal activation energy, (E_b), obtained from electrical conductivity measurements, if we consider the „number" model [8], for the mechanism of photoconductivity of our CAD PbSe films According to this model the photoconductivity is due to the increase in the number of carriers, no barrier modulation occurs in the films under illumination and the activation energy for the photoconductivity is given by

$$E_a = E_b + E_g \qquad (3)$$

where E_g represents the band gap of PbSe With the values for E_b and E_a determined from our measurements we found $E_g \cong 0.31$ eV, in rather good agreement with the values reported in the literature [10]

In order to check the model we also performed photoconductivity measurements with different background illuminations We found no change in $\lambda_{1/2}$ with the intensity of the background illumination of the film

From photoconductivity measurements performed at different temperatures (Fig 2), we computed a thermal variation of E_a, $dE_a/dT = 6 \times 10^{-4}$ eV/K, closed to that determined for the band gap of PbSe ($dE_g/dT \cong 4 \times 10^{-4}$ eV/K), [10] This also supports the validity of the model

Conclusion. The PbSe films obtained by CAD in our laboratory present large activaton energies (for conductivity and photoconductivity) as compared with the PbSe films obtained by other methods These particular properties can be explained by assuming a „number" model for the mechanism of the photoconductivity We can imagine the CAD PbSe films as a system of crystallites separated by high (0.3 eV) intercrystalline barriers, which are not modulated by the light. The photoexcited carriers need high activation energies in order to pass over the barriers and to participate in conduction.

Acknowledgements. The authors express their gratitude to their colleagues P. Fitori, A Darabont and L Biro for the preparation of the CAD PbSe films and to Dr. D Ristoiu for technical assistance.

REFERENCES

1 I N Glistenko, I. N Sramcenko, A N Kosilova, *J Prikl Khim*, **45**, 1356 (1972).
2. R C Kaithala, D K Pandya, K L Chopra, J *Electrochem Soc*, **127**, 277 (1980).
3 G M Tofanov, G A Kitaev, *J. Neorg Khim*, **14**, 616 (1969)
4 Rodica M Cândea *et all, Phys Stat Sol* (to appear)
5 Rodica M. Cândea *et all, Stud Cerc Fiz* (to appear)
6. U. Schlichting, K H Gobrecht, J *Phys Chem Solids*, **34**, 753 (1973).
7. R. L Petritz, *Phys Rev*, **104**, 1508 (1956)
8 D. H. Roberts, J. E Baines, *J Phys. Chem Solids*, **6**, 184 (1958)
9. D. H. Roberts, *J. Electron Control*, **5**, 256 (1958)
10. See, for example, T. S. Moss, *Proc IRE*, **43**, 1869 (1955)

STUDIA UNIV BABEŞ—BOLYAI, PHYSICA, XXXII, 2, 1987

TEMPERATURE DEPENDENCE OF THE ELECTRICAL RESISTANCE OF Y-TYPE SYNTHETIC ZEOLITES

V. CRISTEA*, ELEONORA TRIF*, NIŢA IUGA* and DORINA STRUGARU*

Received October 31, 1987

ABSTRACT. — Temperature dependence of the electrical resistance for Y-type zeolites is presented Pellets behaviour depends on the history and the degree of hydration of the sample. For parent hydrated pellets the temperature variation of the resistance is of Arrhenius type, with many values of the activation energy in the investigated temperature range, i e. $\Delta T = 20-580°C$. Calcination of the sample to 850°C destroys the zeolitic structure and hence the conduction mechanism is changed. Samples calcined to 900°C behave as an amorphous semiconductor.

Introduction. The scientific interest in properties of zeolites has grown up during last years in regard to the great variety of their application in industry.

In an early study, Freeman and Stamires [1] investigated the electrical conductivity of anhydrous synthetic zeolites, and the effect of various adsorbed phases on their electrical conductivity.

We have shown in a previous work [2] that the resistance of the Y-type zeolite is strongly dependent on the pressure of the ambient atmosphere.

The aim of the present study is to characterize the electrical properties of the Y-type zeolites.

2. **Sample preparation.** The synthetic Y-type zeolites with SiO_2/Al_2O_3 mole ratio of 5.1, containing cations as 10.1% Na^+, 0.49% Ca^{2+}, 0.34% K^+, 0.28% Fe^{3+}, 0.16% Ti^{2+}, 0,16% Mg^{2+} and 0.01% Mn^{2+} were investigated.

The resistance measurements were performed on compact cylinders with a diameter of 12 mm and a thickness between 0 45 and 1.5 mm. The standard pressure of 3000 $kg \cdot cm^{-2}$ has been adopted in the preparation of all pellets. Ag electrodes with a diameter of 10 mm were attached by evaporation in vacuum.

Three kinds of pellets were prepared

a) pellets of parent hydrated powder with indicated composition;

Table I gives the thickness of four a-type pellets, their history and the conditions in which measurements were performed,

b) pellets obtained from powder submitted to a previous heat treatment during 4 hours at 850°C, in air;

c) pellets of type (b) which were submitted to a heat treatment for 1 hour in air at 900°C before the deposition of Ag contacts. As a result of calcination, these pellets contracted themselves in a percentage of about 25%.

3. **Results and discussion.** The resistance variation with temperature for pellets of type (a) is shown in Fig 1.

* *University of Cluj-Napoca, Faculty of Mathematics and Physics, 3400 Cluj-Napoca, Romania*

Table 1

Data on (a) type pellets

Number	Thickness l (mm)	History	Ambient medium and measurement conditions
1	0 55	Submitted to heat treatment in vacuum 24 hours and maintained in vacuum	Vacuum increasing temperature
2	1 23	Maintained in vacuum for a weak	Air, decreasing temperature
3	1.14	Maintained in vacuum for 24 hours	Vacuum Increasing temperature
4	0 45	Maintained in vacuum for eight days	Vacuum Decreasing temperature

For all four pellets of type (a) there are certain temperature ranges where the temperature dependence of the resistance can be described by relations of the Arrhenius type

$$R = R_0 \exp\left(\frac{W_t}{kT}\right) \tag{1}$$

where W_t is activation energy. Within the explored temperature range the samples evidenced one or two values of activation energy, and the highest one corresponds to the highest temperature interval.

In the same temperature range, the values of the activation energy differ from pellet to pellet. It can be observed that the value of the resistance depends upon the history of each pellet That is the explanation of the fact that in contrast with pellets 2, 3 and 4 whose resistance increases with increasing their thickness, the first pellet does not conform to the general rule.

We note that pellet number 1 was previously dehydrated by heating in vacuum for one day and then the resistance measurements were performed in higher vacuum.

We mentione that the plotted values of the resistance include also the contact resis-

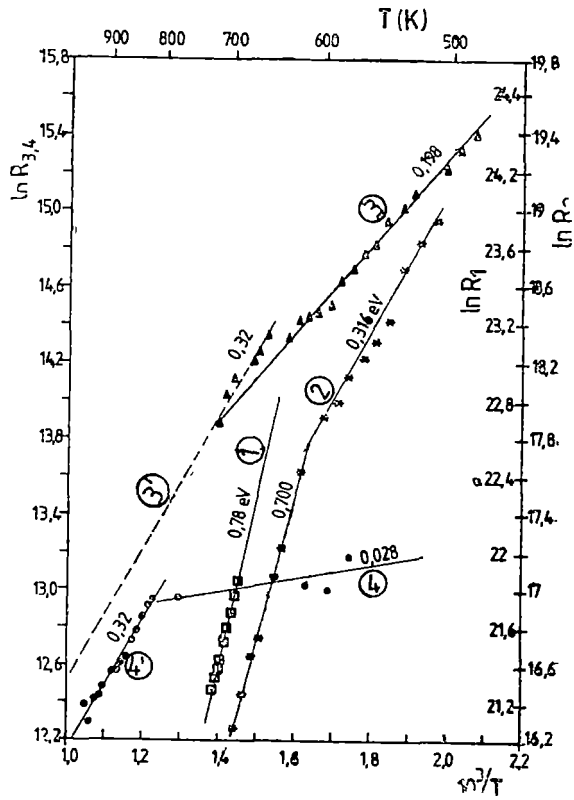

Fig. 1. Temperature variation of the electrical resistance for parent hydrated zeolites (a).

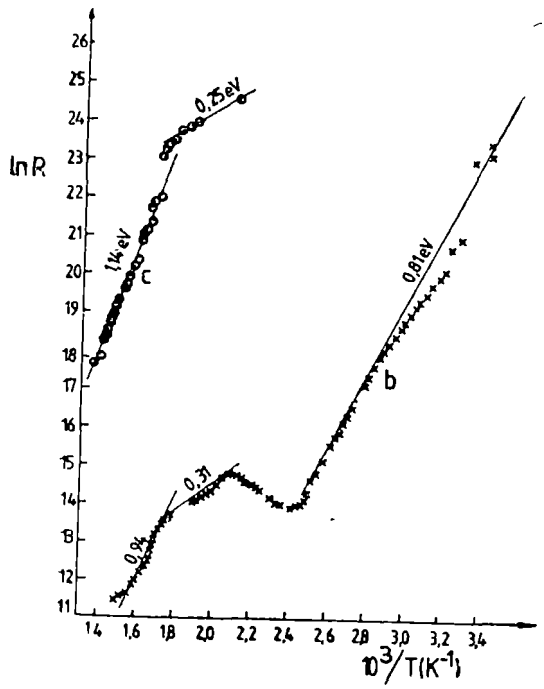

Fig 2 Temperature variation of the electrical resistance for pallets obtained from calcined powder in air to 850°C (b) and for pallets calcined in air to 900°C (c).

tance, R_c, of the pellet with the Ag electrodes We estimated the value of this resistance using the data concerning pellets 3 and 4 One can observe that the extrapolation of high temperature data (3') of pellet 3 is a straight line which is parallel to (4') straight line corresponding to pellet 4 If we assume that at a given temperature say $T = 833$ K, samples 3 and 4 have the same value for electrical conductivity, the value of the measured resistance is of the form

$$R = \frac{1}{\sigma S} l + R_c \qquad (2)$$

By allowing of pellets 3 and 4 to have the same contact resistance, R_c, we obtained $R_c = 259724\ \Omega$ and $\sigma = 4\,885 \quad 10^{-7}\ \Omega^{-1}\ \mathrm{cm}^{-1}$

We note that such a value for σ is in good agreement with values mentioned in the references [1, 3, 4], for different types of zeolites.

In Fig. 2 we have plotted the experimental values of the resistance obtained for the pellets of type (b) and (c), respectively One can note that the tempertture variation of the resistance does not follow a dependence of type (a), and in the temperature range 416—476 K there is a negative slope of the function $\ln (R) = f\left(\frac{1}{T}\right)$. It is known fact that for semiconductor materials this type of behaviour corresponds to the exhaustion region of the impurity levels. In this case, temperature variation of the resistivity is determined by temperature variation of the charge carriers mobility It seems that the zeolite structure was affected during the high temperature calcination before the preparation of pellets There is no resemblance of curve (b) with the curves in Fig. 1.

For pellets of type (b) the low temperature range ($T < 400$ K) is characterised by a high value of activation energy ($W_1 = 0\,815$ eV). In the transition range, 476—580 K, the activation energy is smaller, i e , $W_2 = 0{,}314$ eV We assume that this activation energy is related not to the binding of the carriers to the zeolite framework but rather to the steric effects At higher temperatutes, $T > 580$ K, there is probably, an intrinsic behaviour of the zeolite lattice.

In the case of pellets (c), calcined to 900 °C, when the zeolite structure collapses [5], the curve $\ln R = f\left(\frac{1}{T}\right)$ is typical for semiconductor compounds. Taking into account that the zeolite structure is already destroyed, we consider that the collapsed structure behaves as an amorphous semiconductor.

4. **Conclusions.** The studied Y-type zeolites behave as ionic conductors their resistance being strongly dependent on temperature and the degree of hydration.

The temperature dependence can be described by an Arrhenius equation, while the degree of hydration is determined by the history of each sample.

The heating of powder to 850 °C destroys the zeolitic structure, and the calcination of the sample to 900 °C leads to formation of an amorphous semiconductor compound.

REFERENCES

1 Freeman, D C., Jr , and Stamires D N, J. Chem Phys 35, 799 (1961).
2 V Cristea, E Trif and Al Nicula, Studia Univ Babeş-Bolyai, in press (1987)
3 Schoonheydt R. A and Uytterhoeven J B., Advances in chemistry series 101 « Molecular Sieve Zeolites I, p. 456, Washington DC 1971.
4 Felicia Iacomi, I. D. Bursuc, Gh. I. Rusu and I Bedeleanu, Lucrările Simpozionului „Zeoliţii în tehnologia modernă", p. 431, Iaşi 1983.
5 D Ştugaru, I Ivan, R. Russu, G. Gheorghe, Al Nicula and E. Trif, Proc. of the Symp. on Methods, Models and Techniques in Physics and Related Fields. sept. 1986, Cluj-Napoca 1987, p. 80.

STUDIA UNIV BABEŞ—BOLYAI, PHYSICA, XXXII, 2, 1987

ROTATIONAL SPLITTING OF CH_4 ANALYSED WITH IRREDUCIBLE INVARIANT TENSOR OPERATOR COMBINATIONS

V. TOŞA*, M. GULÁCSI* and ZS. GULÁCSI*

ceived November 16, 1987

ABSTRACT. — The k-rank tetrahedrally invariant tensor operator (T^k) combinations are used in the analysis of CH_4 rotational splittings The amount of T^4, T^6 and T^8 contributions in the combination is derived in order to give for $^{12}CH_4$ a minimum root-mean-square (rms) deviation from the experimental data.

Introduction. The rotational splitting of the spherical top molecules can be described using k-rank irreducible tensor operators (T^k) which prove to be invariant to the subgroup of the tetrahedrylly or octahedrally rotations [1].

In this paper we analyse the rotational splitting of the $^{12}CH_4$ triply degenerate ν_3 fundamental, using T^4, T^6, and T^8 tensor operators. Our method is based [2] on the observation that in almost all previous models, the hamiltonian consists of a linear combination of the T^k operators up to a given rank. The eigenvalue spectra of these operators up to T^8 as well as the eigenvalue spectra of their possible combinations were calculated by us [3], and have been used in this paper in order to describe the rotational splitting of CH_4. The spectra measured by Pine [4] and by Gray *et al.* [5] were used in the minimisation of the rms differences between the experimental and the theoretical results.

Method. Since the odd k terms cannot contribute to the vibration-rotation energies, the perturbation hamiltonian can be written as:

$$H = \Sigma a_{2i} T^{2i} \tag{1}$$

However, the lowest rank tensor component in Eq (1) is four [6] since the reduction of the representation of the full inversion-rotation group does not contain the A_1 term for $J = 2$ In this way we used a hamiltonian of the form:

$$H = C[(T^4 \cos\varphi + T^6 \sin\varphi) \cos\theta + T^8 \sin\theta] \tag{2}$$

where C is a global coupling constant which enlarge the theoretical eigenvalue intervals to the widths imposed by the experimental spectra In Eq (2) φ and θ take values between $-\pi/2$ and $\pi/2$, the T^4 and T^6 expressions are given in [7] and T^8 is given in [8] The contributions of T^4, T^6, and T^8 in H will be denoted ba a_4, a_6 and a_8, respectively, and from Eq (2) we can write:

$$a_4 = C \cos\varphi \cos\theta \tag{3a}$$

$$a_6 = C \sin\varphi \cos\theta \tag{3b}$$

$$a_8 = C \sin\theta \tag{3c}$$

* *Institute of Isotopic and Molecular Technology, R–3400 Cluj Napoca 5, PO Box 700, Romania*

We used a computer program originally written by us, which calculates and diagonalises the H matrix for every C, φ, and θ set, and compares the calculated eigenvalue spectra with the CH_4 ν_3 fine structure of a given rotational line. The comparison is made by a standard root mean square procedure The construction and the diagonalisation of H was performed separately for every point in the (φ, θ) domain mentioned above, with an equidistant mesh of $\pi/500$ on each axis. When necessary, the step was decreased to $\pi/1000$.

Results and Discussion. We analysed all P, Q, and R CH_4 rotational manifolds up to a rotational quantum number $R = 10$. Since both sets of experimental data mentioned above gave similar results, we shall give below the specific results obtained by comparison with Pine's data [4]

For each fixed manifold the minimum rms deviations once obtained, the C, φ, and θ parameters are determined, and the contribution of T^4, T^6, and T^8 can be calculated. These contributions are presented in Table 1 for $2 \leqslant R \leqslant 10$ Of course, the $R = 2$ and $R = 3$ cases are treated separately since they cannot be described with T^8 operator.

Table 1

The contribution of T^4, T^6, and T^8 in the H hamiltonian which describe the CH rotational splitting as measured in [4]

R	a_4			a_6			a_8		
	P	Q	R	P	Q	R	P	Q	R
2	0 215	0 196	0 055	0.	0	0.	0.	0.	0.
3	0 643	0.766	0.199	0 022	0 048	−0.006	0.	0	0.
4	1 174	1 687	0 428	−0.022	0 175	−0 027	−0.147	0 106	0.027
5	1.856	2.918	0 741	−0 059	0 368	−0 023	−0 944	0.367	0.093
6	2 727	4.463	1.095	−0 206	0 593	0.	−1.546	0 563	0 275
7	3 725	6.277	1 493	−0 376	0 873	0.066	−2 354	1 193	0.469
8	4.874	8.337	1 930	−0 555	1 213	0 182	−3 706	2 115	0.852
9	6 168	10 648	2.296	−0 819	1 549	0.334	−4 700	2.710	1 168
10	7.717	13.196	2.783	−1 142	1 835	0.334	−5 262	5 866	5 348

As it can be seen from Table 1, the a_4 absolute values are five to ten times greater then the a_6 corresponding values which, on their turn, are greater than the a_8 absolute values It has to be remembered that these values represent the amount of T^k contribution in the hamiltonian.

At first glance, it seems that the T^8 introduction is a complication which brings no significant improvements in the description of the rotational splitting. In order to verify this assumption we have analysed, for each fixed manifold, the particular cases $\theta = 0$ and $\theta = \varphi = 0$ in the hamiltonian. As it can be seen from Eq (2) these cases represent descriptions without T^8 or without T^8 and T^6, respectively. The quality of the description is given by the value of the minimum rms deviation with respect to the experimental data

We obtained (see also [2]) that the minimum rms, in the case in which T^8 is taken in consideration in the hamiltonian, is ten to one hundred times lower as compared with the corresponding rms value obtained in $\theta = 0$ or $\theta = \varphi = 0$ cases This clearly underlines the necessity of the T^8 use in the description, at least for the CH_4 rotational splitting calculation.

REFERENCES

1. W. G Harter and C W Patterson, *J Math Phys*, **20,** 1453 (1979)
2 V. Toşa, Zs Gulácsi and M Gulácsi, submitted for publication
3 M Gulácsi, Zs Gulácsi and V Toşa, *J Mol Spectrosc*, **118,** 424 (1986)
4 A. S Pine, *J Opt Soc Amer*, **66,** 97 (1976)
5 D. L Gray, A G Robiette and A S Pine, *J Mol Spectrosc*, **77,** 440 (1979)
6 H A Jahn, *Proc Roy Soc*, **A168,** 469 (1938)
7 M Gulácsi, Zs Gulácsi and V Toşa, *J Mol Struct*, **142,** 83 (1986)
8 Zs Gulácsi, M Gulácsi and V Toşa, *J Mol Struct*, **142,** 87 (1986).

STUDIA UNIV. BABEŞ—BOLYAI, PHYSICA, XXXII, 2, 1987

ANHARMONIC FORCE FIELD CONSTANS FOR UF_6 MOLECULE

M. GULÁCSI*, ZS. GULÁCSI* and V. TOŞA*

Received November 16, 1987

ABSTRACT. — Starting from recent high resolution measurements on UF_6 molecule, cubic and quartic anharmonic potential force constants are deduced for this system.

The characteristics of UF_6 molecule has attracted much attention in the last few year because of the possible applications in the multiphoton dissociation and isotope separation processes. In these applications, the knowledge of the intramolecular force field is very important, so the study of force field constants was started many years ago both experimentally [1] and theoretically [2]. The developments in the experimental techniques allowed the determination of the harmonic force field constants with sufficient accuracy. [3]. The specific application however also implies anharmonic constants which are only partially known and published.

Using the recent measurements available in the literature [4, 5] in this paper we deduce cubic and quartic bond force constants f_{ijl}, f_{ijkl}, and cubic and quartic potential force constants Φ_{ijl}, Φ_{ijkl} which appear in the expression of the anharmonic intramolecular potential force field for the unrestricted sum over the dimensionless normal coordinate q_i. Beside the starting experimentally measured molecular parameters, for our calculus we also deduced values for the nonzero Coriolis constants ξ_{ij} [6] and relations between different characteristic molecular constants [7, 8]. Before starting the presentation of the results, we have to mention that the f and Φ values, once calculated, other kinds of force constants can be deduced easily (e g symmetrical cubic and quartic force constants F_{ijl}, F_{ijkl}, the K_{ijl} and K_{ijln} constants which appear in the restricted sum over the normal coordinates; the C_{ijl} and D_{ijln} constants of Fox, etc.).

We start from four exactly measured values: $\alpha_1 = 4\,4 \times 10^{-5}$ cm^{-1} [5], $\alpha_3 = 3.8926066 \times 10^{-5}$ cm^{-1} [3, 4]; $\alpha_{220} = 0\,07724$ MHz [3] and $\alpha_{224} = 0.2132$ MHz [3]. From these, four cubic force constants can be exactly determined [7, 8] (the values are given in cm^{-1}).

$$\begin{aligned} \Phi_{111} &= -71.8529 & \Phi_{233} &= -93.0220 \\ \Phi_{133} &= 68.5976 & \Phi_{335} &= -7\,4797 \end{aligned} \qquad (1)$$

Since they are connected to four direct measured quantities, which were determined with high accuracy, the cubic force constants presented in Eq. (1)

* *Institute of Isotopic and Molecular Technology, R-3400 Cluj-Napoca, P O Box 700, Romania*

must be exact up to 10^{-3} cm^{-1} In comparison, we give the correspondent Φ_{ijl} constants deduced many years ago Overend [2] from a stretching force field model $\Phi_{335} = -3\,635$ cm^{-1}, $\Phi_{133} = -66\,904$ cm^{-1}, $\Phi_{233} = -75\,163$ cm^{-1}. It is interesting to note the relatively exact values obtained in [2] at cubic force field level, for that time, when the experimental possibilities for high resolution measurements were not fully developed Starting from this seccess of the stretching force field in the case of UF_6 molecule, we represent the Φ_{133}, Φ_{233}, and Φ_{335} cubic force constants given in Eq (1) with the bond force constants f_{ijk} [7, 8], obtaining the following values (in milidyn/Å^2)

$$f_{rrr} = -18\,6026,\ f_{rrr'} = -0\,5065,\ f_{rrr''} = -0\,3790 \tag{2}$$

Using Eq (2) we recalculated Φ_{111} in the stretching force field model and obtained $\Phi_{111} = -76\,092$ cm^{-1} which is exact up to 5% (see Eq (1)) This result shows, that in the case of the UF_6 molecule, we can use the representation of the cubic force constants Φ_{ijl} with the bond force constants f_{ijk} with an exactity of 5% Using now Eq (2) we can deduce six new cubic force constants which are in this way correct up to five percent (F_{335} in milidyn/Å^2, Φ_{ijl} in cm^{-1})

$$\begin{aligned} \Phi_{122} &= -68\,3402 & \Phi_{234} &= 3\,9174 \\ \Phi_{222} &= -45\,5993 & \Phi_{236} &= 3\,3382 \\ \Phi_{134} &= 8\,8263 & F_{335} &= -0\,10151 \end{aligned} \tag{3}$$

For comparison we mention the two values deduced in [2] $\Phi_{134}=7\,536$ cm^{-1} and $\Phi_{234} = 3\,728$ cm^{-1}. We must mention again the good agreement between our values and the Overend's results

We deduced also the cubic force constants, but their estimated uncertainity is greater (about 10—20%). For exemplification we give below four values (in cm^{-1})

$$\begin{aligned} \Phi_{246} &= 2\,7116 & \Phi_{144} &= -0\,2318 \\ \Phi_{244} &= 0\,2092 & \Phi_{445} &= -7.2590 \end{aligned} \tag{4}$$

Further on, we analyse the quartic force field constants In order to deduce their values we must use, beside the presented data, other experimentally measured quantities. Below we present a possibility which is based on the X_{11}, X_{12}, X_{13}, X_{22}, X_{23}, and X_{33} values [3]

The obtained results are (the Φ_{ijkl} constants are given in cm^{-1})

$$\begin{aligned} \Phi_{1111} &= 9\,1056 & \Phi^{(1)}_{3333} &= 13\,9830 \\ \Phi_{1122} &= 7.7658 & \Phi^{(2)}_{3333} &= 0\,2556 \\ \Phi_{2222} &= 9.9861 & \Phi^{(1)}_{2233} &= 8\,3369 \\ \Phi_{1133} &= 6\,3519 & \Phi^{(2)}_{2233} &= 0\,3855 \end{aligned} \tag{5}$$

The estimated quartic bond force constants are the following (in mili-dyn/Å^3) ·

$$f_{rrrr} = 62\,674 \qquad f_{rrr'r'} = 0\,8780$$
$$f_{rrrr'} = 3\,2108 \qquad f_{rrr''r''} = 3\,6846 \qquad (6)$$
$$f_{rrrr''} = 5\,1049$$

The stretching force field used for the estimation of the constants presented in Eq (2) and Eq (3) give resembling values (for example $f_{rrrr'} = 3\,775$, or $f_{rrrr''} = 9\,023$) However, we must mention that the uncertaintity for the quartic force field values is great (about 40—50%). This is because the starting X_{ij} values are not known with sufficient precision For comparison we give some values deduced in [2]

$$\Phi^{(1)}_{3333} = 20\,620 \qquad \Phi^{(5)}_{3333} = -0\,156 \qquad (7)$$

In conclusion, starting from experimentally measured molecular parameters, we deduced cubic and quartic anharmonic force field constants for the UF molecule. The normal coordinate indices are those of Hodgkinson *et al* [7] Our analysis reveals that complete description of the UF_6 intramolecular force field imposes high resolution measurements on the bending modes Without them it is not possible to build up an exact potential energy surface for the studied molecule, but such measurements were not published yet.

REFERENCES

1 R S McDowell, L B Asprey and R T Paine, *J Chem Phys*, **61**, 3751 (1974)
2 C Marcott, W G Golden and J Overend, *J Chem Phys*, **68**, 2929 (1978)
3 J P Aldridge *et al*, *J Chem Phys*, **83**, 34 (1985)
4 M Takami *et al*, *Jap J Appl Phys*, **23**, L88 (1984).
5 R S McDowell *et al*, *J Mol Spectrosc*, **113**, 7 (1985)
6 For ξ , starting from the ξ_r value measured in [3], we use the relations presented by Hodgkinson *et al* in [7]
7 D P Hodgkinson, R K Heenan, A R Hoy, and A. G Robiette, *Molec Phys*, **48**, 193 (1983)
8 D P Hodgkinson, J C Barret, A G Robiette, preprint TP 1044, 1984.

STUDIA UNIV BABEŞ—BOLYAI, PHYSICA, XXXII, 2, 1987

TABULATED T^8 EIGENVALUES FOR CUBIC SYMMETRY

ZS. GULÁCSI*, V. TOŞA* and M. GULÁCSI*

Received November 16, 1987

ABSTRACT. — The eigenvalue spectra in $|J, M>$ space of the T^8 irreducible, octahedral invariant tensor operator, is tabulated in this paper up to $J = 10$ angular momentum value. Possible applications are also discussed

The eigenvalues of the k-rank octahedral invariant tensor operators T^k are extensively studied This can be explained by the fact that these operators are used in the analysis of the rotational splitting of the spherical top molecules [1], in high resolution spectroscopy [2], or in the description of the crystal field splitting caused in the electronic spectra by the cubic crystal field [3]. The definition of the T^k terms are strongly connected to the irreducible tensor operator (T^k_q) notion The T^k_q operators ($q = k, k-1, \ldots, -k+1, -k$) are sets of $2k+1$ operators which are tranformed in the rotational group R_3 as

$$R(\alpha, \beta, \gamma)\, T^k_q R^{-1}(\alpha, \beta, \gamma) = \sum_{q'} T^k_{q'} D^k_{q'q}(\alpha, \beta, \gamma) \qquad (1)$$

where $D^k_{q'q}(\alpha, \beta, \gamma)$ represents the irreducible representation of the rotational operator $R(\alpha, \beta, \gamma)$ from R_3, α, β, γ are the Euler angles A linear combination of the T^k_q terms at fixed k, which belongs to the totally symmetric irreducible representation of a cubic point group (T_d or O_h), represents a tetrahedral or octaherdal invariant tensor operator T^k

The T^4 operator explains the effects of the centrifugal distortion on the spherical-top molecules which are clearly shown in the rotational fine structure, or characterize the crystal field splitting caused in the d electronic spectra in cubic environment In many cases (heavy spherical top molecules, f electrons in cubic crystal field), the description is poor, so we must take into consideration different amounts of sixth-rank tensor operator (T^6) contributions [3, 4] Because of this reason Fox *et al* [5] perform computer diagonalisation of T^4, and Krohn presents tabulated eigenvaleus of T^4 and T^6 operators [6] up to $J = 100$ angular momentum value

Studies concerning the light spherical tops (like CH_4, SiH_4, GeH_4) revealed that the rotational splitting for these molecules cannot be described satisfactory using only fourth and sixth rank tensor operators [7] The P(10) pattern of CH_4 [4] and the pure rotational transitions in spherical tops [8], clearly claim the T^8 introduction in the theoretical analysis Starting from these

* *Institute of Isotopic and Molecular Technology, R—3400 Cluj-Napoca, P O Box 700, Romania*

observations, in this paper we present tabulated eigenvalues for the T^8 octahedral invariant tensor operator. We use an expression for the T^k operators

$$T^k = \sum_q a_k^q T_q^k \tag{1'}$$

which is normalised to unity:

$$\sum_q |a_k^q|^2 = 1 \tag{2}$$

For $k = 8$, the a_k^q coefficients are given as follows:

$$a_8^0 = \frac{\sqrt{33}}{8}, \quad a_8^4 = a_8^{-4} = \frac{1}{4}\sqrt{\frac{7}{6}}, \quad a_8^8 = a_8^{-8} = \frac{1}{8}\sqrt{\frac{65}{6}} \tag{3}$$

Here we must mention the earliest derivations of the T^k operators Bethe [11] for $k = 4$, von der Lage and Bethe [12] for $k \leqslant 8$, and Jahn [13] for $k \leqslant 10$. Our coefficients given in Eq. (3) coincide with those given by Ozier [8], and differ with a $8/\sqrt{33}$ multiplicative factor from those given by Robiette *et al* [14] (which in our case accomplishes the normation to unity). The matrix elements are made using the Wigner–Eckart theorem

$$\langle JM' | T_q^k | JM \rangle = (-1)^{J-M} \begin{pmatrix} J & k & J \\ -M' & q & M \end{pmatrix} (J \| T^k \| J) \tag{4}$$

Table 1

The eigenvalues of the T irreducible octahedral invariant tensor operator up to J = 10 angular momentum value. The degeneracies (Deg) and symmetries (Sym) are also presented

J	Eigenvalues	Deg	Sym	J	Eigenvalues	Deg	Sym
4	0 122812	1	A1	8	0 053498	2	E
	0 085968	2	E		0 029227	3	T1
	0.000000	3	T2		−0 012580	2	E
	−0.098254	3	T1		−0 070094	3	T2
5	0.104568	3	T2		−0 075991	3	T1
	0.005314	3	T2	9	0 081627	1	A2
	−0 042263	3	T1		0 059528	3	T2
	−0 101430	2	E		0 051876	3	T1
6	0 150017	1	A1		0 008235	3	T1
	0 050006	2	E		0 000332	3	T1
	0 021432	3	T1		−0 059860	2	E
	0 009872	3	T2		−0.076436	3	T2
	−0.078581	1	A2		−0.092511	1	A1
	−0.088453	3	T2	10	0.073149	3	T2
7	0.088519	3	T2		0 060350	2	E
	0.044142	3	T2		0 021457	3	T2
	−0.003887	3	T1		0 012633	1	A2
	−0.026787	2	E		0.011586	3	T1
	−0.077650	3	T1		−0.003038	2	E
	−0 099495	1	A1		−0.004388	1	A1
8	0 070094	3	T2		−0.060498	3	T2
	0.058454	1	A1		−0 086650	3	T1

where the Wigner $3j$ coefficients are symbolised by $\begin{pmatrix} \cdots \\ \cdots \end{pmatrix}$; $(J \| T^k \| J)$ is the reduced matrix element, J and M denote the quantum numbers of the total angular momentum and its projection on the quantification axis

The eigenvalues were determined by computer diagonalisation procedure up to $J = 10$ angular momentum value, and presented in Table 1 The symmetries of the eigenvalues were deduced with standard methods [4]

The presented eigenvalues can be used, for exemple, in the analysis of the rotational splitting of the light spherical top molecules [7], in the study of the pure rotational transitions [8] or in high resolution spectroscopy [10]

REFERENCES

1 A J Dorney, J K G Watson, *J Mol Spectrosc* **42,** 1 (1972)
2 W G Harter, C W Patterson, *J Chem Phys*, **66,** 4872 (1977), *idem* **66,** 4885 (1977).
3 R S McDowell, "in Laser Spectroscopy III" (Edited by J L Hall and J L Carlsten), Springer Verlag, New York, 1977 pp 102
4 K R Lea, M J M Leask, W P Wolf, *J Phys Chem Solids,* **23,** 1381 (1962).
5 W G Harter, C W Patterson, *J Math Phys*, **20,** 1453 (1979)
6 K Fox, H W Galbraith, B J Krohn, J D Louck, *Phys Rev*, **A15,** 1363 (1977)
7 B J Krohn, *Los Alamos Report LA-6554MS/1976*
8 M Gulácsi, Zs Gulácsi, V Toşa, *J. Mol Spectrosc*, **118,** 424 (1986).
9 I Ozier, *J Mol Spectrosc*, **53,** 336 (1974).
10 M Gulácsi, Zs Gulácsi, V Toşa, *J Mol Struct*, **142,** 83 (1986)
11 J Moret-Bailly, *J Mol Spectrosc*, **15,** 344 (1965)
12 H Bethe, *Ann Phys*, **3,** 133 (1928)
13 F C von der Lage, H Bethe, *Phys Rev*, **71,** 612 (1974)
14 H A Jahn, *Proc Roy Soc London, Ser A,* **168,** 469 (1938)
15 A G Robiette, F M Birss, D L Gray, *Mol Phys*, **32,** 1591 (1976).

STUDIA UNIV BABEŞ—BOLYAI, PHYSICA, XXXII, 2, 1987

ELECTRIC PRISM-HOMOGENEOUS MAGNET DOUBLE FOCUSING MASS SPECTROMETER · EXPERIMENTAL SET-UP · AND PRELIMINARY TESTS

C. CUNA*

Received December 30, 1987

ABSTRACT. — An electric prism and an oblique incidence homogeneous magnet were associated in an experimental double focusing mass spectrometer. It was possible to achieve good sensitivity and resolution (11000, 50% valley) simultaneously

The electric prism, device with four ion refracting planes is a powerful energy dispersing ion optical element, without radial angular focusing action [1]. It was combined in a double focusing mass spectrometre with a homogeneous magnetic prism also without radial focusing properties [2]. In order to ensure angular radial focusing the prisms were associated with cylindric electrostatic lenses [3] whose great third order aberrations were resolution limiting or with transaxial lenses [4] build up from complicated electrode systems, dificult to manage This last geometry allowed very high resolutions.

The instrument reported here uses an electric prism and a homogeneous magnetic field sector with oblique entry and exit. The purpose of our studies was to obtain an increased mass dispersion (compared to the double focusing instruments in current use) and a simultaneous small radial magnification. Then a much reduced dispersion and resolution results if the main aberrations are cancelled. The basic ion optical properties of such an instrument were treated in references [5], [6] and [7]. These may be summarized as follows. a) the angular focusing is ensured by the magnetic sector alone, its magnification being that of the whole instrument, b) the high energy dispersion of the electric prism is counterbalanced by the energy dispersion of an oblique incidence and exit magnetic sector, then a high mass dispersion results.

Our experimental set-up uses many components of the instrument described in [8] as: electonic units, ion detection system, vacuum parts and pumps. The experimental instrument has the following main ion optical parameters: field free spaces between source and electric prism of 887 mm lenght, electric prism-magnet 429.1 mm, magnet-colector 373.1 mm, deflexion angles of the electric prism 54.3°, of the magnet 90° (acting in opposite senses), magnet incidence and emergence angle 31.73°, main path radius 254.5 mm, overall radial magnification —0.287, mass dispersion coefficient 429.1 mm; the electric prism is decelerating

* *Institute of Isotopic and Molecular Technology, 3400 Cluj-Napoca, Romania*

The first experiments were performed with the ion source slit set at a width of 0.22 mm. A maximum ion current of Ar^+ of $9\ 10^{-12}$A was transmited with 4 kV ion source accelerating voltage. With some adjustments mass spectra of some representative substances were recorded at rezolutions between 3500 and 5000. For a source slit width of 0 1 mm, 4 5 kV accelerating voltage and with careful adjustments resolutions around 11000 were measured, the calibrating mass difference being given by the $N - C_2H$ doublet (near the well separated CO^+ small peak).

In the present stage of the work an exhausive comparison between experiment and theory (not fully developed) can not be made. However the aberration coefficients must be small because the above related maximal resolution was obtained without severe angular or energy spread limitations

The next step to improve the instrument performance is to use hexapoles, to correct for ion source slit and analyzer median plane tiltness.

REFERENCES

1 V M Kelman, I V. Rodnikova, M. L Uteev, and P. A. Finogenov, *J T.P*, **40**, 535 (1970).
2. V. M Kelman and D. L. Kaminski, *J.E.T.P.*, **21**, 555 (1951).
3 V M Kelman, I. V. Rodnikova and P. A. Finigenov, *J.T P*, **41**, 173 (1971).
4 S B. Bimurzaev, B. M. Voronin, V. M. Kelman, L. M. Nazarenko, B E. Pechalina, N B. Sokolov, G. V. Fridlandski and E M. Yakusev *J.T.P.*, **53**, 2195 (1983)
5. D. Ioanoviciu, C Cuna, G Kalmuţchi and C Toma, *Progress in Physics*, Sibiu, 1984
6 D. Ioanoviciu, C. Cuna, *Progress in Physics*, Iaşi, 1985.
7. D Ioanoviciu, *Advances Mass Spectrom*, **10**, 899 (1986).
8 C. Cuna and D. Ioanoviciu, *Int J Mass Spectrom Ion Phys*, **54**, 333 (1983)

STUDIA UNIV BABEŞ—BOLYAI, PHYSICA, XXXII, 2, 1987

MAGNETIC MOMENT IN Ni-RICH Ni-Cu-Zn ALLOYS

I. COSMA*

Received December 20, 1987

ABSTRACT. — The temperature behaviour of the magnetization of α-Ni—Cu—Zn solid solution has been studied The decrease of the average magnetic moment with increating concentration of copper and zinc is discussed in terms of the valence electron-concentration of the nonmagnetic atoms

Magnetic properties of Ni solid solutions with non-magnetic elements, especially Ni—Cu alloys, have been widely studied. In the Curie point and saturation moment measurements the plots against the atomic concentration of nickel are linear for important content of nonmagnetic atoms. This behaviour has long been taken as an argument for validity of the rigid band model. But this model fails to explain the magnetic behaviour and other properties of the Ni—Cu alloys in the critical range of concentration. The study results of magnetic susceptibility, specific heat, neutron scatering and the effects of heat treatment are in agreement with the cluster hypothesis A model able to explain all the propeties has to consider an environment dependent-moment of Ni atoms on the basis of short range interaction between neighbouring virtual bound states In terms of such a model the dependence of the average magnetic moment of Ni—Cu alloys on the concentration has been discussed [1, 2]. In the model of environment-dependent moments the local atomic topography is characterized by the number of the copper atoms placed into a certain polyhedron of a Ni atom neighbours. But it is well known that in different binary Ni—rich alloys the electronic structure of solute nonmagnetic atoms determines the rate of decrease of magnetic moment per alloy atom. To obtain additional informations on this behaviour we propose to analyse the Ni—Cu—Zn system.

The alloys used in this study were prepared by melting the mixture of constituent metals in evacuated quartz tubes. For all the specimens the concentration was determined by chemical analysis. In most cases the content was in reasonable agreement with those calculated from the weight of quantities of nickel and copper used The concentrations of the samples are listed in Table 1. All alloys are α-solid solutions in the ternary Ni—Cu—Zn phase

Table 1

Metal	Sample								
	1	2	3	4	5	6	7	8	9
Ni at. %	96 3	93 2	90 6	83 2	79 3	69.6	67 9	63 8	60.0
Cu „	2 8	4.8	8 0	9 6	12 9	21 3	19 7	23 2	25.5
Zn „	0,9	2 0	1.4	7.2	7.8	9.1	12 4	13 0	14.5

* *Department of Physics, Polytechnic Institute, 3400 Cluj-Napoca, Romania*

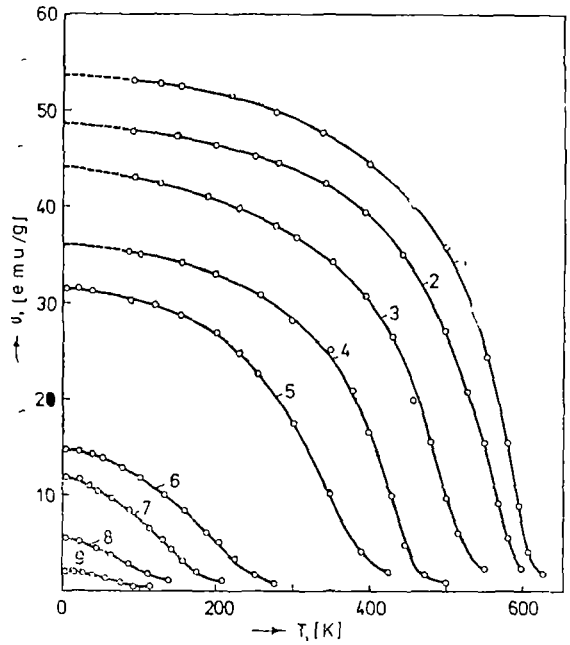

Fig 1 Temperature dependence of magnetization at 14 kOe for $Ni_{1-x-w}Cu_xZn_y$a lloys

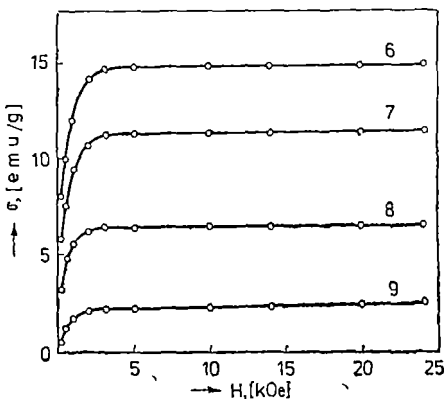

Fig 2 The magnetization isotherms at 4 2 K for samples 6, 7, 8 and 9

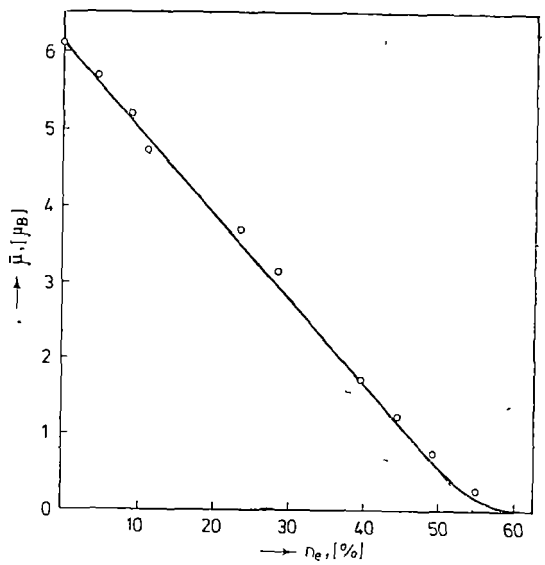

Fig 3 The dependence of saturation magnetic moments for the studied samples (0) as a function of valence electrons of Cu andZn. The solid line presents the data for Ni—Cu alloys [1]

diagram Metallographic examination of all speciment used showed a single-phase structure.

The temperature dependence of magnetization for Ni—Cu—Zn ternary alloys (Fig 1) is a ferromagnetic one

Even for alloys containing lessthan 70 at % Ni the measurements of the field dependence of magnetization at liquid helium temperature clearly indicate that all aloys are saturated in a magnetic field which exceeds 4—5 kOe(Fig 2).

Average magneticmoments μ were obtained from the magnetic saturation values resulting from extrapolation of the graphs σ vs. T to $T = 0$ K at highest field Since for ternary Ni_{1-x-y} Cu_xZn_y alloys it does not make sense to plot the magnetic moment against the Ni concentration, the parameter $n_e = n_x + n_y$ was chosen as a measure for the mean concentration of valence electrons of the nonmagnetic components [3] Values of the magnetic moment per atom alloy against n_e($n_x = 1$ and $n_y = 2$) are shown in Fig. 3 A good agreement beprtween the edictions of the local envionenment model, calculated by Robbins et al, for Ni—Cu alloys and our experimental data is observed.

Finally it is important to notice that all N—rich alloys containing non-magnetic elements, in p articular Cu and Zn, can be characterized by a common parameter n -the mean concentration of valence electrons of nonmagnetic soluteatoms. If the results are discused in terms of a rigid band model it can specify that in Ni—Cu—Zn alloys evry Cu and Zn atom determines itself the decrease of the magnetic moment. If the variation of the average magnetic moment is explained by the model of environment-dependent moments, then the decrease is determined by the number and sort of nearest neighbouring nonmagnetic atoms which suround a nickel atom, or more exactly by their total number of valence electrons

REFERENCES

1. C G Robbins, H Claus and P A Beck, *Phys Rev Letters*, **22**, 1307 (1969).
2 J P. Perrier, B Tissier and R Tournier, *Phys Rev Letters*, **24**, 313 (1970).
3 I Cosma, I Lupşa, O Pop and M Vancea, *Phys Letters*, **49 A**, 87 (1974).

STUDIA UNIV BABEŞ—BOLYAI, PHYSICA, XXXII, 2, 1987

EPR ON SOME SUPERCONDUCTING OXIDE CERAMICS

S. SIMON, I. BARBUR* and I. ARDELEAN*

Received December 30, 1987

ABSTRACT. — The shape and parameters of the EPR spectra obtained at room temperature from high temperature ($T > 80$ K) superconducting and non-superconducting ceramics belonging to the Ba—Y—Cu—O system do not offer a direct correlation with the presence of the high superconducting transition temperature The results of this inverstigation indicate the possibility to use the EPR method in order to appreciate the superconducting quality of the ceramic compounds from the studied system

Introduction One of the main problems in the explanation of high temperature superconductivity, phenomenon which makes further the subject of several scientific works [1—10], is that of the role of the copper ions in the appearance of the superconductivity in perovskite type ceramics from Ba(Sr, Ca)—La(Y)—Cu—O system.

The structural models proposed for these ceramic compounds are based on the results obtained by X-ray analyses In these models one considers that the lattice is made up of perovskite layers of corner-sharing CuO_6 octahedra interlinked with corner-sharing square-planar CuO_4 units In order to understand the high temperature superconductivity, a special importance must be attached to the ratio between the number of Cu^{3+} and Cu^{2+}, ions, considering that transfer $Cu^{3+}—O^{2-} \leftrightarrow Cu^{2+}—O^{-}$ is possible, so that these materials are rather hole than electron superconductors The dependence of the transition temperature on the concentration of the $[Cu—O]^{+}$ units was experimentally established [10]

The electron paramagnetic resonance studies permit of obtaining information on the structure of the Cu^{2+} ions microenvironment and on their magnetic interaction, but the studies carried out up to now [12—14] have been concerned especially with the low-field microwave absorption observed in these materials at temperatures under T_c The characteristic of the EPR spectra of the superconducting ceramic samples at temperatures higher than T_c are only in short presented in these papers.

In this work we present some results obtained by EPR investigation of some ceramic samples from Ba—Y—Cu—O system, prepared by two different techniques Some of the investigated samples exhibit superconducting transition at $T_c < 90$ K

Experimental. In order to obtain samples of composition as near as possible to the perovskite phase $Ba_2YCu_3O_7$, considered to be the superconducting phase in the multiphase ceramic compounds from Ba—Y—Cu—O system, we used both the coprecipitations method from liquid phase [1] and that of the mechanic mixture of the constituent oxides in desired proportion [2], followed by

* *University of Cluj-Napoca, Faculty of Mathematics and Physics, 3400 Cluj-Napoca, Romania*

heating and annealing at temperatures comprised between 900 °C and 950 °C, in air and oxygen flow The samples obtained by the first method are noted with the index *c* and those obtained by the second method are noted with the index *m*

The presence or absence of a superconducting phase with $T > 90$ K in the prepared samples was established by testing the effect of an unhomogeneous magnetic field on the samples cooled under this temperature

The electron paramagnetic resonance measurements were carried out by means of a JEOL spectrometer, in X band, on powder samples, at room temperature For a superconducting sample the EPR spectra were recorded between the room temperature and a temperature below T_c

Results and discussion The EPR spectra recorded at the room temperature on samples which exhibit superconductivity at temperatures above 90 K, and noted with the index *S*, are presented in Fig 1, while the EPR spectra recorded on some samples which are not superconductor up to the mentioned temperature, and noted with the index N, are presented in Fig. 2. One remarks that these spectra are extremely different what regards the shape and the values of their parameters In all the cases the hyperfine structure specific to the EPR spectra of Cu^{2+} ions from polycrystalline systems is not resolved, firstly due to the fluctuations of the microenvironment of these ions, characteristic to the glassy systems, and secondly due to the strong magnetic interactions between the Cu^{2+} ion pairs, which appear in the disordered systems with high concentration of such ions [15—18], hit also between the Cu^{2+} and Cu^{3+} ions present in these ceramic materials

The analysis of the EPR spectra from Fig. 1 indicates that the appearance of the transition to the superconducting state at high temperatures is not conditionated by a certain type of environment of the Cu^{2+} ions, by their concentration and by the type of magnetic interactions between these ions with like or unlike ions Thus, the EPR spectrum of *S* sample, having $g = 2\,11$ and $\Delta H = 260$ Gs, proves that in this sample exists a very high concentration of the Cu^{2+} ions finding in strong magnetic interaction, disposed in clusters, while the Cu^{2+} ions density is smaller in the S_{c1} sample, but the microenvironment and the type of the magnetic interactions are similar. Wholly different is the situation in the case of the sample S_{m2}, wherin the Cu^{2+} ions density is much smaller so that the EPR spectrum becomes alike that of some magnetic dilute vitreous samples, having $g_{\|} = 2\,2$ and $g_{\perp} = 2.04$.

In what regards the samples which do no exhibit transition to the superconducting state above 90 K, their EPR spectra are also very different The spectrum of N_{m1} sample is similar as shape and parameters to the spectra of the samples S_{m1} and S_{c1} The spectrum of N_{m1} samples is much larger, having $\Delta H = 700$ Gs, showing the existence of a CuO phase, while the spectrum of N_{m2} sample is specific to the Cu^{2+} ions, tetrahedral coordinated similar to those recorded from some vitroceramic samples [19] and has the following values for the *g* tensor components. $g_1 = 2\,03$, $g_2 = 2.1$ and $g_3 = 2\,3$

The decrease of the recording temperature, in the case of S_{m1}, determined in the first part of the temperature range only a slight increase of the EPR signal intensity, but at a temperature below T_c it was recorded the EPR signal presented in Fig 3, which presents both low-field microwave absorption and a signal at 3200 Gs If the low field microwave absorption is assigned to the superconductive glassy state, and constitutes an argument that in the sample there are superconductive grains of microns order sized, the signal from 3200 Gs,

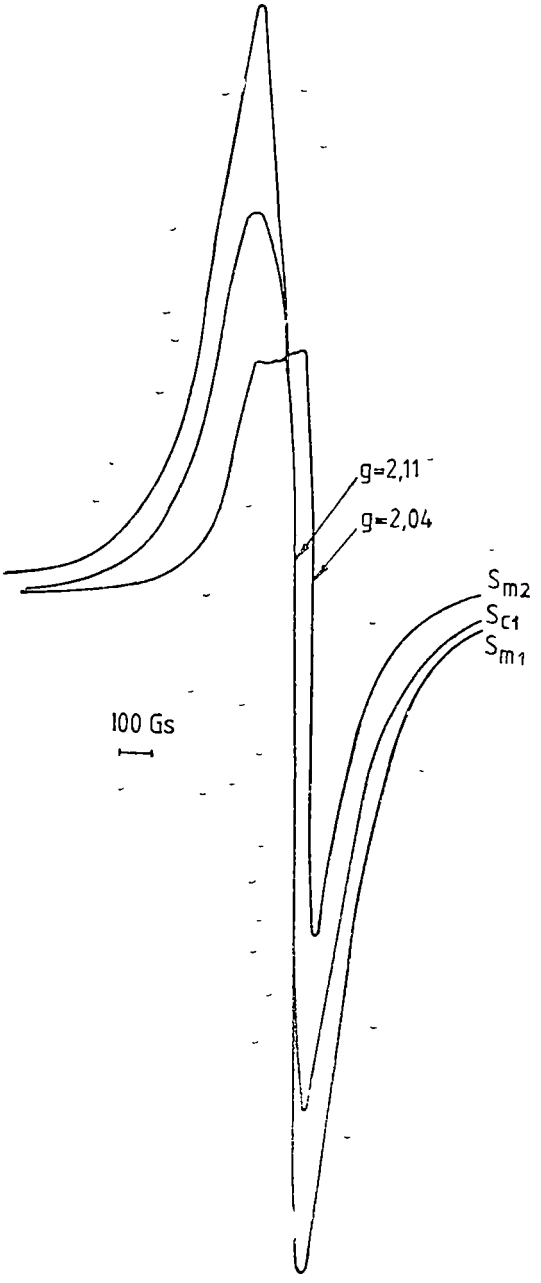

Fig 1 EPR spectra recorded at room temperature from some superconductive oxide ceramics with $T_c > 90$ K

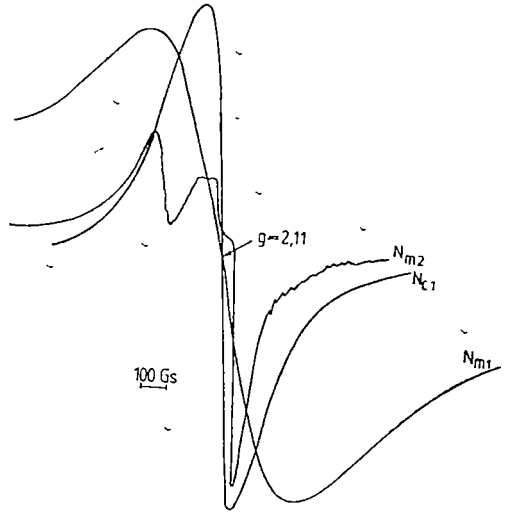

Fig 2 EPR spectra recorded at room temperature from some oxide ceramic non-superconductiveabove 77 K

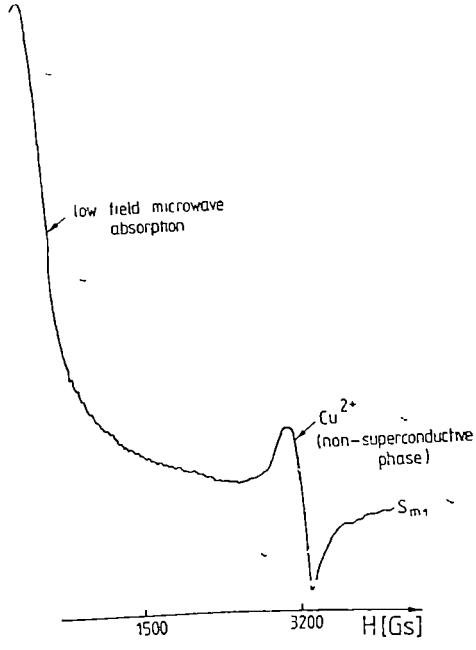

Fig 3 EPR spectrum, recorded at 77 K, from a superconductive ceramics sample with $T_c > 90$ K

much waeker than those recorded at higher temperatures, is assigned to the Cu^{2+} ions from the phase which has not become superconductive The EPR spectra obtained at lower temperature than T_c offer the possibility to estimate the fraction of the non-superconductive phase in this compounds.

Conclusions The EPR results obtained in this work indicated that the appearance of the superconductive state at high temperatures is not essentially determined by the concentration and microenvironment of Cu^{2+} ions It was also revealed that the EPR method may be used to appreciate the superconductive quality of the ceramic compounds from the investigated system

REFERENCES

1 J G Bednorz, K A Muller, *Z Phys B*, **64**, 189 (1986)
2 C W Chu, P H Hor, R L Meng, L Gao, Z J Huang, Y Q Wang, *Rev Lett*, **58**, 4, 405 (1987)
3 R J Cava, B Batlogg, R B van Dover, D W Murphy, S Sunshine, T Siegrist, J P Remeiko, E A Rietman, S Zahurak, G P Espinosa, *Phys Rev Lett*, **58**, 16, 1676 (1987)
4 P H Hor, R L Meng, Y Q Wang, L Gao, Z J Huang, J Bechtold, K Forster, C W Chu, *Phys Rev Lett*, **58**, 1891 (1987)
5 C Politis, J Geerk, M Dietrich, B Obst, H L Luo, *Z Phys B*, **66**, 279 (1987)
6 T Petrişor, A Giurgiu, I Pop, *Studia Physica*, **32**, (1), 74 (1987)
7 I Ursu, E Lăbuşcă, I Mihai, A Novacu, H Petraşcu, M Petraşcu, *A 9-a Sesiune Anuală de Comunicări ICEFIZ*, „Progrese în fizică", Bucureşti, 23—24 oct 1987, p 163
8 L Miu, S Popa, M Popescu, E Cruceanu, *A 9-a Sesiune Anuală de Comunicări ICEFIZ*, „Progrese în Fizică", Bucureşti, 23—24 oct 1987, p 165
9 P Steiner, J Albers, V Kinsinger, J Sander, B Siegwort, S Hufner, C Politis, *Z. Phys B*, **66**, 275 (1987)
10 K A Muller, J G Bednorz, *6-th European Meeting on Ferroelectricity*, 7—11 sept 1987, Poznan, Poland, p 1
11 A Reller, J G Bednorz, K A Muller, *Z Phys B*, **67**, 3 (1987)
12 K W Blazey, K A. Muller, J G Bednorz, W Berlinger, G Amoretti, E Buluggiu, A Vera, F C Matacotta, *Phys Rev B*, (in press)
13 J Stankowski, *6-th European Meeting on Ferroelectricity*, 7—11 sept 1987, Poznan, Poland
14 M V Ştefănescu, S V Nistor, A Novacu, *A 9-a Sesiune Anuală de Comunicări ICEFIZ*, „Progrese în fizică", Bucureşti 23—24 oct 1987 p 232
15 A. R Lusis, J G Kliava, „Fiz Chem Steklo, Sist", Riga (1974) p 68
16 S Simon, V Simon, Al Nicula, vol „Phys Amorf Mat" (Al Nicula and S *Simon*, eds), Cluj-Napoca, 1981 p 47
17 I Ardelean, O Cozar, Gh Ilonca, *Rev Roum Phys*, **28**, 451 (1983)
18 S Simon, V Simon, Al Nicula, *Studia, Physica*, **32**, (1), 56 (1987)
19 S Simon, Al Nicula, *Phys St Solidi (a)*, **81**, K1 (1984)

RECENZII

D Chowdhury, **Spin Glasses and Other Frustrated Systems,** World Scientific, Singapore, 1986

The spin glass (SG) theory has been in the last decade one of the most important field for physicists working in solid stte theory and statistical physics

The book written by Chowdhury startsed (Cap 1) with a presentation of the basic concepts from the spin-glass theory as the frustration of the spin systems as well as the occurrence of the high degeneracy of the ground state due to the frustration In Cps 2—6 the "phase transitions-like" teories are presented, the more sophisticated results obtained by Parisi being the subject of Cap 7 In the Caps 9—10 the author presents the difficult features related to the ergodicity and fluctuations using the formalism of the functional analysis which implies the ultrametricity In the Caps 11—15 the author presents the concret models in the theory of spin glasses discussing the importance of long-range exchange, anisotropy and the external field In the Caps 16—17 the nonlinear susceptibility and the critical behaviour have been discussed The next two chapters, 18—19, are devoted to the dynamics of the spin glass state and, in the Cap 20, the author discuss the frustration in connection with the gange invariance The next two capters, 21 and 22, are devoted to the percolation-like teories based on spin clusters model, and in Cap 23 the author presents the transition in the spin-glass state in analogy with the localization-delocalization tranzition. Cap 24 is devoted to the numerical treatment of the spin-glass state and results are compared with the analytical results obtained in different approximations In Cap 25 the transport properties and the sound attenuation are presented using the perturbation theory methods The next chapter, Cap 26, is devoted to the different special features of the spin-glass state as the local field distribution, the application of the Lee-Yang method for the spin-glass and the occurrence of the spin-glass state in the superconducting materials Cap 27 contains one of the most exciting topics, namely the SG-like-systems The author analysed different systems which present a behaviour similar to the spin-glass state Such systems are electric dipolar and quadrupolar glasses, the electron glas in doped compensated semiconductors, the granular superconductors, the ultradiffusion, and the foramlism of ultrametricity applied at the treatment of the simplest model of the neuron. The last chapter, Caps. 28), contains the conclusions, which in fact show that the spin-glass theory is stil oppen. The book also contains two appendices in which the author has treated the very recent results obtained in the field.

We may conclude that this book provides a good coverage of the recent developments and future directions in the study of the spin-glasses-like systems.

M CRIŞAN

P C W Davies, **The forces of the nature,** second edition, Cambridge University Press, 1986

The book has 175 pages and its contents is arranged in six chapters It is a most interesting story of the major concepts and beautiful ideas introduced by the great physicists of the century, in order to understand the structure of matter and the interactions of particles The book is suitable both for students and those without special knowledge of fundamental physics, because all the essential concepts are explained in an easy language with a minimum of mathematics

All the important concepts of atomic physics, relativity and quantum mechanics are treated in a fine way in the second chapter of the book (quanta, discret levels of energy, the principle of uncertainty, waves and particles, spin, the exclusion principle, etc.).

The nuclear binding force, some important nuclear processes like fission and alpha and beta radioactivity are treated in chapter three.

The main ideas of quantum theory of fields are exposed very clearly in chapter four (strong and weak interactions, virtual particles, etc).

Symmetry and conservation laws are treated in chapter five We appreciate very much the simple and interesting way in which the author explains some very subtle concepts like parity, isotopic spin, strangeness, etc

The last chapter of the book — the road to unification is a most interesting one Here we learn from a master the remarkable progress that has been made in the field of elementary particles, thanks largely to two bold new ideas.

The first is the quark theory of hadrons and the second is the attempt to provide a unified description of the forces of nature The book is very interesting and beautifully written The style is clear and nice The author explains the concepts and ideas very carefully and pay much attention to be as clear and rigorous as possible, using only the possibilities of the human language, without much mathematics It can be read with much intelectual profit and great pleasure The last sentences of the book urges the reader to deep meditation "Mathematics and beauty are the foundation stones of the Universe No one who has studied the forces of nature can doubt that the world about us is a manifestation of something very, very clever indeed "

LAURENȚIU MÂNZAT

W Ebeling, V L Klimontovich, **Selforganization and Turbulence in Liquids,** Teubner-Texte zur Physik, Band 2, Leipzig, 1984, 196 pp

Dr. Werner Ebeling is professor of Theoretical Physics at the Humboldt University in Berlin, and Corresponding Member of the GDR Academy of Sciences He is a specialist in statistical theory of plasmas and in the theory of selforganization and evolution far from equilibrium.

Dr. Yuri Klimontovich is professor at the State University M V Lomonosov in Moscow He is one of the leading specialist in nonequilibrium statistical physics, the author of the well-know monographs on the statistical theory of nonequilibrium processes in plasmas, nonideal systems and of electromagnetic processes

The book Selforganization and Turbulence in Liquids written by Dr W Ebeling and Dr Y. L Klimontovich is devoted to the discussion of certain aspects of the relation between the theory of turbulent flows (which is a quite old discipline of physics) and the theory of selforganization or synergetics (which has been developing with a rapid page in the last 15 years)

By using the methods of thermodynamics and statistical physics the generation of selfsustained oscillations and the formation of stationary concentration patterns are analyzed, as examples for selforganization processes, and the analogy of these processes to turbulent structures is discussed.

The book is a useful contribution to the broad discussion about the nature of turbulence. This book is addressed to researchers in theoretical physics and to those dealing with the fascinating problem of the turbulence

STELIANA CODREANU

W Schultz-Piszachich, **Nonlinear Models of Flow, Diffusion and Turbulence,** near Models of Flow, Diffusion and Turbulence, Teubner-Texte zur Physik, Leipzik, Band 6, 1985, 204 pp

Dr Wolfgang Schultz-Piszachich is specialist in theoretical physics and applied mathematics He is author of a number of publications on potential flows, electron beams, self-consistent fields and flow turbulence

The book *Nonlinear Models of Flow, Diffusion and Turbulence* is devorted to the theory of self-consistent fields with applications to electric space charge distributions, to vortex and turbulent flows

The self-consistent flow field (SCFF) of a statistical vortex distribution represents a novel notion The SCFF serves as a reference quantity for deviation from statistical equilibrium

The fundamental problems of vortex flow and of wall trubulence are treated for flows which are stationary on average The viscous sublayer of the turbulent wall boundary layer is analized in minutely Also studied is a class of homogeneous and isotropic turbulence fields

The diffusion theories of G I Taylor, Smoluchowski and Fokker Planck-Kolmogorov are evaluated Stochastic initial conditions are allowed for in Hopf's theory The influence of additional forces in Navier-Stokes equations of motion is investigated Mathematical supplements are furnished in the Appendices

The book is addressed to theoretical physicists but also to the researcher engineers

STELIANA CODREANU

Jean-Louis Basdevant, **Mécanique quantique,** École Polytechnique, 1986, 574 pag

Le livre ,,Mécanique Quantique" est un manuel d'introduction aux concepts et méthodes élémentaires de cette discipline fondamentale Il est le résultat de la pratique de l'enseignement de la mécanique quantique aquise à l'École Polytechnique depuis plusieurs années

Le matériel est organisé sur vingt chapitres On commence avec les concepts essentiels de la mécanique quantique à partir de la description simplifiée des expériences fondamentales, d'après quoi on introduit la notion de „fonction d'onde" suivie par l'équation de Schrodinger Ensuite, après une toute serie d'applications, riches en contenu physique on abouti à la notion „d'état quantique" et au formalisme de l'espace de Hilbert, permettant la compréhension des divers phénomènes essentiels

On developpe ensuite le formalisme général de la mécanique quantique, en l'appliquant à l'étude d'une série de modèles physiques simples. Sur cette base est ensuite abordé l'étude des phénpoménes physique plus complexes

La dernière partie du cours est destinée aux certains compléments physiques, historique et mathématiques et à un recueil d'exercices et de problèmes

Les chapitres du cours sont, Phénomènes quantiques, Mécanique ondulatoire I Function d'onde, Équation de Schrodinger, Mécanique ondulatoire II Grandeurs physiques, Mesure; Quantification des énergies de quelques systèmes sipmles, Espace de Hilbert, Formalisme de Dirac, Postulats de la mécanique quantique, Système à deux états, Principe du MASER a ammoniac, Commutation des observables, Méthodes d'approximation, Le moment cinétique en mécanique quantique, Première description des atomes, Formalisme du spin 1/2, Résonance magnétique, Lagrangien et hamiltonien, Force de Lorentz en mécanique quantique, Addition des moments cinétiques, Structure fine et hyperfine des raies atomiques, Systèmes de particules identiques, Principe de Pauli, Évolution des systèmes, Physique qualitative Ordres de grandeur de quelques phénomènes microscopiques et macroscopiques, Invariances, Lois de conservation, Premières notions de physique nucléaire, Structure en couches des noyaux atomiques, Mécanique quantique et astrophysique, Historique de la mécanique quantique

Le cours est destiné aux étudiants des écoles polytechniques en ayant pour but une ouverture plutôt générale sur le monde de la microphysique, mais il peut être util aussi pour les étudiants des universités, surtout pour les étudiants en chimie-physique

STELIANA CODREANU

Martin Hartley Jones, University Piess, Martin Hartley Jones, **A practical introduction to Electronic circuits.** University Press, Cambridge, 278p, 1987

The second edition of „A practical introduction to electronic circuits" by M H Jones reprinted in year 1987 at the University Press, Cambridge, offers to the readers an excellent uptodate electronics book It contains 278 pages devided in 14 chapters, characterized by a practical approach of the problems and always kept to real applications

The author presents a full account of the subject, starting with basic concepts such as amplification, thermoionic emission, negative feedback, semiconductor device characteristics, from p-n junctions to field effect transistors, and progressing to analogue and digital integrated circuit chip applications, including a lucid account of microcomputers

In the book are also given circuit diagrams which contain sufficient information to enable the reader to try them out for himself The book also provides computer software listings for some basic experiments involving home computers

The bibliography at the end of the book lists some introductory texts which will fill in the background for the reader with little experience of electrical circuits. The bibliography also lists references which discuss detailed topics to a higher level

I heartily recommande this book to all students and teachers directly interested in electronics and also to those who are workink in other disciplines where electronics is a subsidiary subject It is a reference book

EMIL TĂTARU

R C Barber and V S Venkatasubramanian, H E Duckworth, **Mass spectroscopy** (the 2nd edition), University Press, Cambridge, 1986, 337 p

The authors, having an extensive experience in this field, describe the development of mass spectrocopy, its principles and perfoimances and also its recently applications

In the first part (chapters 1—8), ion optics, ,on sources, detection of positive-ions, deflection type instruments (simple and double focusing instruments, time of flight instruments, cyclotron resonance instruments, quadrupole instruments) and their general applications (determination of isotopic abundances and determination of atomic masses) are presented

The second part (chapters 9—14) consists in special applications of mass spectroscopy in some research fields as nuclear physics, physics of molecules, solid state physics, geology, cosmology and space reasearch, containing the most interesting topics An important application is that in which the reaction products obt a

ined either by fission processes or under accelerated particles bombardment are analysed by mass spectroscopy The ionization and dissociation processes ion-molecule reactions, the molecular structure and the metastability are preseted as applications of mass spectrometry in the physics of molecules. The biomedical and environmental applications are preseted, too The applications in geology and cosmology are referring to age determination of terrestrial and planetary rocks, to isotopic composition determination of meteorites and lunar rocks The mass spectrometry is also successfully used in physico-chemical investigations of the upper atmosphere

We may conclude that the book represents a good coverage of the most recent performances and future directions in the mass spectroscopy field Its scientific content and the clarity of the presentation make it an excelent guide for both students and scientists

V ZNAMIROVSCHI

ÎNTREPRINDEREA POLIGRAFICĂ CLUJ,
Municipiul Cluj-Napoca, Cd nr 578/1988

d e la XXXII-lea an (1987) *Studia Universitatis Babes—Bolyai* apare în specialităţile:

matematică

fizică

chimie

geologie-geografie

biologie

filosofie

ştiinţe economice

ştiinţe juridice

istorie

filologie

In the XXXII-nd year of its publication (1987), *Studia Universitatis Babes—Bolyai* is issued as follows:

mathematics

physics

chemistry

geology-geography

biology

philosophy

economic sciences

juridical sciences

history

philology

Dans sa XXXII-e année (1987), *Studia Universitatis Babeş—Bolyai* paraît dans les spécialités:

mathématiques

physique

chimie

géologie-géographie

biologie

philosophie

sciences économiques

sciences juridiques

histoire

philologie

43 904

Abonamentele se fac la oficiile poştale, prin factorii poştali şi prin difuzorii de presă, iar pentru străinătate prin „ROMPRESFILATELIA", sectorul export-import presă, P. O. Box 12—201, telex. 10376 prsfir, Bucureşti Calea Griviţei nr. 64—66.

Lei 35